Spring 5-15-2016

Regulation of Epithelial Turnover by Host-Virome Interactions

Lulu Sun
Washington University in St. Louis

WASHINGTON UNIVERSITY IN ST. LOUIS

Division of Biology & Biomedical Sciences

Immunology

Dissertation Examination Committee:
Thaddeus S. Stappenbeck, Chair
Marco Colonna
Deborah J. Lenschow
Robert D. Schreiber
William F. Stenson
Herbert W. Virgin

Regulation of Epithelial Turnover by Host-Virome Interactions

by

Lulu Sun

A dissertation presented to the
Graduate School of Arts and Sciences
of Washington University in
partial fulfillment of the
requirements for the degree
of Doctor of Philosophy

May 2016

St. Louis, Missouri

TABLE OF CONTENTS

LIST OF FIGURES AND TABLES

CHAPTER 1

CHAPTER 2

CHAPTER 3

CHAPTER 4

LIST OF ABBREVIATIONS

Ab	Antibody
Apol9	Apolipoprotein L9
AGS	Aicardi-Goutieres syndrome
ANOVA	Analysis of variance
ATP	Adenosine triphosphate
BMDC	Bone marrow-derived dendritic cell
BMM	Bone marrow-derived macrophage
BrdU	5-Bromo-2'-deoxyuridine
BSA	Bovine serum albumin
BV	Bone volume
CBRLuc	Click beetle red luciferase
CD	Crohn disease
cGAMP	Cyclic GMP-AMP
cGAS	Cyclic GMP-AMP synthase
CldU	5-Chloro-2'-deoxyuridine
CRISPR	Clustered regularly interspaced short palindromic repeats
DC	Dendritic cell
DNA	Deoxyribonucleic acid
DS	Double-stranded
EAE	Experimental autoimmune encephalomyelitis
EdU	5-Ethnylyl uridine
EGF	Epidermal growth factor
EGFP	Enhanced green fluorescent protein
ELISA	Enzyme-linked immunosorbent assay
ER	Endoplasmic reticulum
FGF	Fibroblast growth factor
GAPDH	Glyceraldehyde 3-phosphate dehydrogenase
GAS	Interferon-γ activated site
GBP	Guanylate binding protein
GFP	Green fluorescent protein
GM-CSF	Granulocyte macrophage colony stimulating factor
GO	Gene ontology
GTP	Guanosine triphosphate
H&E	Haematoxylin and eosin
HPF	High power field
HSC	Hematopoietic stem cell
IBD	Inflammatory bowel disease
IdU	5-Iodo-2'-deoxyuridine
IFN	Interferon
IFNAR	Type I interferon receptor

IGF1	Insulin-like growth factor 1
IHC	Immunohistochemistry
IL	Interleukin
i.p.	Intraperitoneal
i.v.	Intravenous
IPS-1	Interferon β promoter stimulator 1
IRES	Internal ribosomal entry site
IRF	Interferon regulatory factor
IRGM	Immunity-related GTPase family M protein
ISG	Interferon-stimulated gene
ISRE	Interferon-stimulated response element
JAK	Janus kinase
LCMV	Lymphocytic choriomeningitis virus
LPS	Lipopolysaccharide
LSD	Least significant difference
L-WRN	L cells producing Wnt3a, Rspondin3, and Noggin
mAb	Monoclonal antibody
MAPK	Mitogen-activated protein kinase
MAVS	Mitochondrial antiviral signaling protein
MCMV	Murine cytomegalovirus
MDA-5	Melanoma differentiation-associated protein 5
MEF	Mouse embryonic fibroblast
MeOH	Methanol
MFI	Median fluorescence intensity
MHV68	Murine gammaherpesvirus 68
MicroCT	Micro computed tomography
MiRNA	MicroRNA
MNV	Murine norovirus
MOI	Multiplicities of infection
mRNA	Messenger RNA
NSAID	Non-steroidal anti-inflammatory drug
OAS	2'-5' oligoadenylate synthase
ORF	Open reading frame
PAMP	Pathogen-associated molecular pattern
PBS	Phosphate-buffered saline
PCR	Polymerase chain reaction
pDC	Plasmacytoid dendritic cell
PFU	Plaque forming unit
polyI:C	Polyinosinic:polycytidylic acid
PV	Parasitophorous vacuole
PVM	Parasitophorous vacuole membrane
PYHIN	Pyrin and HIN domain-containing family
qRT-PCR	Quantitative reverse-transcriptase-polymerase chain reaction
RIG-I	Retinoic acid-inducible gene 1
RLR	RIG-I-like receptor
RNA	Ribonucleic acid

ROI	Region of interest
Rspo3	Rspondin3
RT	Room temperature
SD	Standard deviation
SEM	Standard error of the mean
SLE	Systemic lupus erythematosus
SNARE	Soluble NSF attachment protein receptor
SMI	Structure model index
SPENCD	Spondyloenchondrodysplasia
SOCS	Suppressor of cytokine signaling
SS	Single stranded
STAT	Signal transducer and activator of transcription
STING	Stimulator of interferon genes
TLR	Toll-like receptor
TNF	Tumour necrosis factor
TRAP	Tartrate-resistant acid phosphatase
TRIF	TIR-domain-containing adapter-inducing interferon β
TUNEL	Terminal deoxynucleotidyl transferase dUTP nick end labeling
TV	Total volume
µL	Microliter
µm	Micrometer
USP18	Ubiquitin-specific peptidase 18
VEGF	Vascular endothelial growth factor
VSV	Vesicular stomatitis virus
WAE	Wound-associated epithelia
WT	Wild type

ACKNOWLEDGEMENTS

First of all, I would like to thank Thaddeus Stappenbeck for being an exemplary mentor. His enthusiasm for science is contagious, and I have learned a great deal about experimental design, analytical thinking, and clear scientific writing under his guidance. I appreciate all the support and encouragement he has given me these past years.

I would also like to acknowledge the members of my thesis committee. Their broad thinking and rigorous questioning has strongly shaped my project, and I appreciate all of their input during and outside of committee meetings. I am grateful that they have taken so much time to invest in my project an in my development as a scientist.

I thank the past and present members of the Stappenbeck lab, especially Seth Bloom, Gerardo Nava, Hiroyuki Miyoshi, and Kelli van Dussen. I have also had a lot of fun in this lab! It has been a great learning and social environment, and I have made lifelong friends here.

I would also like to thank Darren Kreamalmeyer for his excellence in animal care. This project would not have been possible without his expertise and hard work in breeding and maintaining the many mouse strains that we have used.

I would like to thank the Washington University Medical Scientist Training Program for accepting me into this program and providing funding. Many thanks to the administrative staff of Brian Sullivan, Christy Durbin, Liz Bayer, and Linda Perniciaro for keeping me on track, answering questions, and providing lots of free food throughout the years. Thank you also to Wayne Yokoyama, who has been and continues to be an excellent director of the MSTP program.

I am also grateful for the love and support of my friends. The MSTP class of 2015-ish has been a wellspring of support (and valuable expertise and reagents). It has been wonderful to

work on a PhD at the same time as so many talented and intelligent people. I would also like to thank my friends outside of the program, who remind me that there is a world outside of the lab.

Of course, I would to thank my family. I would not be where I am today if not for my parents and everything they have done for me. My sisters are wonderful, and I know I can always count on them. I would also like to thank my husband, whose patience, love, and understanding have made this all possible.

Finally, funding for this project has been provided by the NIH (AI08488702, P50CA94056), the CCFA Genetics Consortium, and the Shawn Hu and Angela Zeng Graduate Fellowship.

Lulu Sun

Washington University in St. Louis

May 2016

ABSTRACT OF THE DISSERTATION

Regulation of Epithelial Turnover by Host-Virome Interactions

by

Lulu Sun

Doctor of Philosophy in Biology and Biomedical Sciences
Immunology

Washington University in St. Louis, 2016

Professor Thaddeus S. Stappenbeck, Chair

The host immune system must constantly function to maintain chronic commensal and pathogenic organisms in check. These organisms include the virome, which is the viral component of the microbiome. The consequences of immune responses to the virome on host physiology are as yet unexplored, and may have long-term implications in health and disease. Here, I used both genetic and infectious mouse models to investigate how the innate antiviral cytokines Type I interferons (IFNs) modulate epithelial turnover. I first found that mice deficient in Irgm1, a p47 GTPase, had persistently elevated Type I IFNs even in the absence of exogenous viral infection. The *Irgm1*$^{-/-}$ mouse enabled us to study the effects of Type I IFNs on host physiology without the compounding variables imposed by a complex viral infection. I found that Type I IFNs increased epithelial turnover in multiple organs. Chronic viral infection, which induces Type I IFN production, also augmented epithelial turnover, demonstrating the physiological relevance of this process. I discovered that Type I IFNs acted through non-epithelial cells, including macrophages, to promote increased epithelial turnover and wound repair. Downstream of Type I IFN signaling, the highly related IFN-stimulated genes *Apolipoprotein L9a* and *b* stimulated epithelial proliferation through ERK activation. These

findings demonstrate that the host immune response to chronic viral infection has systemic effects on epithelial turnover through a myeloid-epithelial circuit. This work advances our understanding of the mechanisms that modulate proliferation and cell death of epithelial barriers that provide the first line of protection against the environment.

CHAPTER ONE:

Introduction: Epithelial Turnover, Type I Interferons, and Host-Virome Interactions

Proliferation and Turnover of Epithelial Barriers

Epithelial cells make up linings and ducts within many organs in the body, including the digestive and reproductive systems, endocrine and exocrine organs, and also form the surface epidermis (Blanpain et al., 2007). They are continuous sheets of cells joined together by tight junctions, adherens junctions, and desmosomes. The presence of these intercellular junctions maintains epithelial cell polarity, allowing separation of apical and basolateral surfaces (Shin et al., 2006). Epithelial cells can form a single layer (simple epithelium) or multiple layers (stratified epithelium) on top of a basement membrane separating them from surrounding stromal cells and mesenchyme. This highly organized structure is important for the many complex functions that epithelial cells perform, such as glandular secretion, absorption, and transcellular transport.

The epithelium is also the host's first line of defense against the environment. A central part of this protection involves cell turnover, a regulated shedding and regeneration of differentiated tissue cells while maintaining barrier integrity. Different epithelial surfaces and organs have varying rates of turnover at homeostasis, but what regulates these rates is not well understood. For example, the small intestine has a turnover rate of once every 5 days, while the lung epithelium turns over up to once every 6 months (Blanpain et al., 2007). Organs with high intrinsic rates of turnover include the intestine, epidermis, lung, thymus, testis, uterus, and mammary gland (Pellettieri and Sanchez Alvarado, 2007). Other organs may have slower basal rates of epithelial turnover, such as the pancreas, kidney, liver, and cornea (Pellettieri and Sanchez Alvarado, 2007). Amazingly, it has been estimated that we produce and eliminate a mass of cells equal to our body weight in a year (Reed, 1999).

There are three aspects to cellular turnover of adult tissue: generation of new cells, differentiation of newly-generated cells, and cell death. New cells are thought to be generated from adult stem cells that are present in most, if not all, adult organs (Raff, 2003). Stem cells, by definition, are able to self-renew and differentiate into cell lineages from their tissue of origin (Blanpain et al., 2007). In certain organs, such as liver and pancreas, new cells may also originate from division of differentiated cells (Dor et al., 2004; Taub, 2004). Newly generated cells usually undergo a transitional phase of proliferation, known as the transit-amplifying phase, before differentiation (Raff, 2003). It is thought that differentiation involves movement of the precursor cell away from the stem cell niche, where it then receives different extrinsic and perhaps also intrinsic cues for differentiation (Pellettieri and Sanchez Alvarado, 2007). Finally, during homeostatic turnover, differentiated cells undergo cell death, maintaining organ morphology and size. Apoptosis, rather than necrosis, is believed to be the main form of cell death during homeostasis (Pellettieri and Sanchez Alvarado, 2007). During apoptosis, cells undergo programmed cell death in which DNA is degraded and cellular contents are packaged into apoptotic bodies that are phagocytosed by nearby phagocytes. This is in contrast to necrosis, in which cells rupture, releasing their contents and inducing inflammation (Edinger and Thompson, 2004).

A balance between the counteracting processes of cell generation and cell death is necessary to maintain homeostatic turnover. Excessive cell death without regeneration can result in degenerative disorders and could play a role in aging (Sharpless and DePinho, 2004). On the other hand, uncontrolled proliferation without appropriate apoptosis can result in cancerous growth (Green and Evan, 2002). The relationship between cell generation and cell death during turnover is not well understood. It is not known whether dying cells promote proliferation of

nearby cells, or whether proliferating cells promote apoptosis in neighbouring cells. Understanding the mechanisms by which cell generation and cell death are linked and regulated will provide valuable insights into disease pathogenesis.

Epithelial turnover has perhaps been best studied in the intestine, where the three features of epithelial turnover (generation, differentiation, and death) take place in discrete compartments (**Figure 1.1**). The intestinal mucosa consists of a simple epithelial layer forming crypts and, in the small intestine, villus units (Radtke and Clevers, 2005). Four types of differentiated epithelial cells exist: i) Paneth cells, which secrete anti-microbial peptides; ii) enterocytes, which form the majority of intestinal epithelial cells and absorb nutrients; iii) goblet cells, which secrete mucus; and iv) enteroendocrine cells, which secrete peptide hormones. Stem cells are located at the base of intestinal crypts, between Paneth cells, and rapidly divide to produce precursor cells (Blanpain et al., 2007). These cells move upward into the transit amplifying compartment and undergo proliferation. Cells then differentiate as they migrate up the crypt, and in the small intestine, up the villi. Paneth cells are an exception, as they migrate downward to the base of the crypt. Differentiated cells undergo apoptosis at the tips of the villi in the small intestine or at the top of the crypt in the large intestine and are shed into the lumen (**Figure 1.1**) (Creamer, 1967).

The rate of intestinal epithelial turnover is quite high, with regeneration occurring approximately once every 5 days, and can be modulated by different environmental conditions (Blanpain et al., 2007). For example, starvation, malnutrition, irradiation, and drugs have been observed to alter this intrinsic rate (Creamer, 1967). Intestinal epithelial turnover has also been shown to increase during bacterial infection with *Citrobacter rodentium*, a murine model of infectious colitis (Bhinder et al., 2013; Luperchio and Schauer, 2001). In addition, Cliffe *et al*

proposed that increased epithelial turnover acts as an "epithelial escalator" to expel *Trichuris muris*, a murine parasite, from the intestine (Cliffe et al., 2005).

The turnover rate can also be modulated in response to injury, which may be important for proper healing. For example, after physical injury in a wound biopsy system where whole colonic crypts are excised using forceps, crypts adjacent to the wound proliferate to regenerate the intestinal architecture (Seno et al., 2009). In this model, decreased epithelial proliferation was associated with impaired wound healing, demonstrating the importance of this process in repair.

In many of these intestinal models, immune cytokines and signaling pathways have been shown to play an important role in accelerating epithelial turnover. In the wound biopsy system, delayed wound repair was observed in WT mice given neutralizing antibodies against IL-4 and IL-13, and in mice deficient in Stat6 (a downstream mediator of IL-4 and IL-13 signaling) (Seno et al., 2009). Myeloid differentiation factor 88 (Myd88), an adaptor protein downstream of Toll-like receptors, is necessary for epithelial hyperproliferation in response to *Citrobacter* infection in mice (Gibson et al., 2008). The loss of epithelial hyperproliferation and repair in this model resulted in loss of epithelial barrier integrity and bacterial invasion of the crypts (Gibson et al., 2008). *MyD88*$^{-/-}$ mice also showed deficiencies in epithelial proliferation and wound repair in response to dextran sodium sulfate, a chemical that induces an inflammatory colitis (Brown et al., 2007). Finally, in *Trichuris muris* infection, epithelial proliferation was increased by IL-13 signaling and diminished by the chemokine CXCL10 (Cliffe et al., 2005). These findings all support a role for the immune system in modulating epithelial turnover responses to injury and infection.

Host-Virome Interaction

Notably, the role of viruses in the regulation of epithelial turnover is unknown. Since all individuals possess a collection of chronic viruses (a virome) as part of their metagenome, the effects of these microbes on the host should be considered. Research into the virome has lagged behind studies of the bacterial component of the microbiome, as new bioinformatic and sequencing technology has only recently enabled detailed study of commensal and chronic viruses. In a recent review, H.W. Virgin compartmentalized the virome into four components: viruses that infect eukaryotic cells, viruses that infect bacteria (bacteriophages), viruses that infect archaea, and virus-derived genetic elements in the host chromosomes (e.g. endogenous retroviruses) (Virgin, 2014). In contrast to bacteria, which in a healthy individual are generally isolated to mucosal surfaces, viruses can be harbored systemically. It is estimated that a healthy individual possesses at least ten chronic systemic viruses at any given time, including herpesviruses, anelloviruses, adenoviruses, papillomaviruses, and polyomaviruses, among others. (Virgin, 2014; Virgin et al., 2009). Hepatitis B, hepatitis C and HIV are also prevalent in the general population.

Some of these viruses may have little effect on host physiology, while other viruses continuously stimulate the host immune system with increasingly appreciated consequences (Virgin, 2014; Virgin et al., 2009). Stimulation of the immune response can occur during initial infection, continuous replication, or reactivation from latent states. The anti-viral immune response is necessary to keep many of these chronic infections in check. In acquired immunodeficiency, where active surveillance by the immune response is diminished or absent, normally quiescent viruses such as Epstein Barr virus (also known as human herpesvirus 4 (HHV4)), Kaposi's sarcoma virus (HHV8), and human polyomavirus JC virus can reactivate and

cause disease (Bellizzi et al., 2013; Cesarman, 2014). In addition, components of the anti-viral immune response have been linked to complex diseases such as Type I diabetes, inflammatory bowel disease, and asthma, suggesting a role for viral infection in disease pathogenesis (Foxman and Iwasaki, 2011). Viral infection alone is likely not sufficient to induce disease; host genetic predisposition also plays an integral role. For example, persistent murine norovirus infection promoted Paneth cell dysfunction and abnormal response to intestinal injury, but only in genetically susceptible animals (Cadwell et al., 2010). Given the pervasiveness of viral infection and the association of viruses with complex human diseases, the consequences of long-term activation of the antiviral immune system on the host should be explored.

The Type I Interferon Signaling System

The central axis of anti-viral defense is the Type I IFN system. Type I IFNs are a family of innate immune cytokines that are produced in response to viral and other types of infection (Durbin et al., 2000; Muller et al., 1994) . They include multiple IFNαs, IFNβ, and other subtypes, including IFNκ, IFNω, IFNζ, IFNε and two that exist only in pigs and cattle, IFNδ and IFNτ (Hardy et al., 2004; Pestka et al., 2004). The Type I IFN gene locus is located in a cluster on chromosome 9p in humans and on chromosome 4 in mice (Pestka et al., 2004). They are conserved across all vertebrate species, and are an important link between the innate immune and adaptive immune systems (Stetson and Medzhitov, 2006).

Type I IFNs can be induced by three types of recognition sensors that detect viral nucleic acids within their respective compartments: Toll-like receptors (TLRs) that bind foreign nucleic acid in extracellular and endosomic spaces, RIG-I-like receptors (RLRs) that recognize cytosolic RNA, and sensors of cytosolic DNA (**Figure 1.2**). The TLRs are primarily expressed on

macrophages and dendritic cells (DCs), central sentinel cells of the immune system. In particular, plasmacytoid dendritic cells are thought to be the primary producers of high levels of Type I IFNs during infection (Colonna et al., 2004). TLR3 recognizes double-stranded (ds) RNA, found in both DNA and RNA viruses (Alexopoulou et al., 2001). TLR7 and TLR8 bind to single-stranded (ss) RNA, while TLR9 detects unmethylated CpG sequences that are uncommon in vertebrate genomes but are found in the genomes of DNA viruses and bacteria (Diebold et al., 2004; Heil et al., 2004; Hemmi et al., 2000). TLR4 is also able to stimulate Type I IFN production downstream of lipopolysaccharide (LPS) recognition, through the adaptor protein TIR-domain-containing adapter-inducing IFNβ (TRIF) (Yamamoto et al., 2002). TLRs 3, 7 and 9 are localized within the endosomal compartment, while TLR4 is expressed on the plasma membrane surface. This localization allows TLRs to detect viral material originating outside the cell.

In contrast, RLRs are RNA helicases expressed in the cytosol, enabling detection of intracellular viral nucleic acid. The two RLRs, retinoic acid-inducible gene 1 (RIG-I) and melanoma differentiation-associated protein 5 (MDA-5) both detect dsRNA. RIG-I is thought to recognize shorter RNA strands with 5' triphosphate ends, or RNA that assumes complex secondary structures, while MDA-5 recognizes longer RNA molecules (Loo et al., 2008). Both interact with the adaptor molecule interferon-beta promoter stimulator 1 (IPS-1), also known as mitochondrial antiviral-signaling protein (MAVS), found in the outer mitochondrial membrane (Kawai et al., 2005; Seth et al., 2005).

Multiple candidate factors for sensing foreign cytosolic DNA have been proposed, but most are thought to signal through the adaptor protein stimulator of interferon genes (STING) found on the endoplasmic reticulum membrane (Ishikawa and Barber, 2008). Most recently,

cyclic GMP-AMP (cGAMP) synthase (cGAS) has been suggested as a cytosolic DNA sensor (Sun et al., 2013; Wu et al., 2013). Upon binding of foreign DNA, it synthesizes cGAMP from ATP and GTP, which then activate STING (Sun et al., 2013; Wu et al., 2013). Previously proposed candidates include RNA polymerase III, which can transcribe AT-rich DNA (found in some pathogen genomes) into dsRNA that can be recognized by RIG-I (Ablasser et al., 2009; Chiu et al., 2009), and DExD/H box helicases (Kim et al., 2010; Zhang et al., 2011). The pyrin and HIN domain-containing family (PYHIN) protein IFI16 has also been shown to bind dsDNA and trigger STING activation (Unterholzner et al., 2010). It is unclear whether these proposed sensors have distinct roles in particular cell types or whether they act concurrently to recognize foreign DNA and induce Type I IFN production.

Downstream of i) TLR, ii) RLR and iii) STING signaling is the activation of transcription factors called interferon regulatory factors (IRFs) (**Figure 1.2**). Four IRFs can positively regulate Type I IFN production: IRF1, 3, 5 and 7, but only IRF3 and IRF7 have been shown to be key inducers of Type I IFN gene expression in response to viruses (Honda et al., 2006). IRF3 is constitutively expressed, while IRF7 is normally present at low amounts and strongly induced by Type I IFN signaling itself (Marie et al., 1998). Once IRF3 and IRF7 are activated, they dimerize, move to the nucleus and form a complex with coactivators to drive transcription of the Type I IFNs as well as certain other cytokines and chemokines (Honda et al., 2006).

i) The TLRs use the adaptor proteins TRIF (TLR3 and 4) and MyD88 (all TLRs except for TLR3). TRIF signals through TRAF3/TBK1/NAP1 and IKKε to phosphorylate and thereby activate IRF3, while MyD88 activates IRF7 via IKKα (Gurtler and Bowie, 2013; Honda et al., 2006).

ii) Downstream of RLR activation, MAVS interacts with TRAF3 to recruit and assemble a complex composed of TANK/NEMO/IKKε/TBK1, which phosphorylates IRF3 and IRF7 (Belgnaoui et al., 2011). At the same time, MAVS can also interact with TRAF2/TRAF6 to recruit IKKα/IKKβ and NEMO, resulting in activation of NFκB. NFκB also interacts with the IFNβ promoter to drive its transcription (Belgnaoui et al., 2011).

iii) After recognition of cytosolic DNA, STING provides a scaffold to assemble TBK1 and IRF3 in close proximity, allowing for phosphorylation of IRF3 by the TBK1 kinase (Tanaka and Chen, 2012).

Once expressed and secreted from the cell, Type I IFNs all bind to a common Type I IFN receptor, IFNAR (**Figure 1.2**). Despite sharing a single receptor, Type I IFNs can have different cellular effects depending on the IFN subtype (α1 vs β, etc.), the cell type, and the context (i.e. additional cytokine signals). How these pleiotropic effects are mediated is not entirely understood, but it is known that many different signaling pathways can be activated downstream of ligand binding to IFNAR. IFNAR is composed of IFNAR1 and IFNAR2 components, and is expressed on most cell types (de Weerd et al., 2007). IFNAR lacks intrinsic kinase activity, and is constitutively associated with the Janus kinases (JAKs) Tyk2 (interacts with IFNAR1) and Jak1 (interacts with IFNAR2) (Platanias, 2005). Upon ligand binding, the JAKs phosphorylate the receptor components and the signaling transducers and activators of transcription (STATs) molecules (de Weerd et al., 2007). Upon phosphorylation, STATs form complexes that translocate to the nucleus to induce the expression of hundreds of interferon stimulated genes (ISGs) (**Figure 2**). These STAT complexes include STAT1, STAT2, STAT3, STAT4, STAT5 and STAT6 homodimers and heterodimers and a heterotrimer composed of STAT1, STAT2, and

IRF9 that is known as ISGF3 (Gough et al., 2012; Levy et al., 1988; Platanias, 2005). ISGF3 binds to IFN-stimulated response elements (ISREs) present in the promoters of certain ISGs, while other STAT complexes bind to IFN-γ-activated site (GAS) elements present in other ISGs, with some ISGs containing both ISRE and GAS elements (**Figure 1.2**) (Platanias, 2005). IFNAR signaling can also activate the p38 and MEK-ERK mitogen-activated protein kinase (MAPK) cascades (David et al., 1995; Goh et al., 1999), as well as the phosphatidylinositol 3-kinase (PI3K) and NFκB pathways (Uddin et al., 1995; Yang et al., 2005). The multitude of signaling pathways that are triggered by Type I IFNs in turn result in diverse cellular responses to these cytokines.

Further enhancing the complexity of Type I IFN responses are the hundreds of ISGs that can be induced in a given cell type (Schoggins and Rice, 2011). Some ISGs are signaling proteins found in the cytosol, others are transcription factors that act in the nucleus, and still others are secreted molecules (de Veer et al., 2001). Reports that characterize the function of ISGs tend to focus on their role in anti-viral defense. For example, 2'-5' oligoadenylate synthases (OAS) produce 2'-5' oligoadenylates that activate RNase L, which degrades viral (as well as host) RNA (Kristiansen et al., 2011), while the Mx proteins are GTPases that targets viral nucleocapsids even before viral replication begins (Haller and Kochs, 2011). However, ISGs can be involved in a plethora of additional cellular processes. These include mediating apoptosis, transcriptional activation and repression, modulation of immune cells and cytokine expression, protein degradation, and post-transcriptional regulation of gene expression (de Veer et al., 2001). The diversity of ISGs allows for pleiotropic responses and the fine-tuning of host responses to infection. Nevertheless, the functions of many ISGs are yet to be discovered.

While Type I IFNs are strongly induced in response to pathogenic viral infection, there are low constitutive levels of Type I IFNs that are important for homeostasis and to prime the immune system for effective and rapid anti-microbial responses (Gough et al., 2012; Taniguchi and Takaoka, 2001). In the absence of priming by Type I IFNs, cells have diminished responses to Type I IFNs themselves as well as to other cytokines, including IFNγ and IL-6 (Gough et al., 2010) (Mitani Genes Cells 2001). Constitutive amounts of IFNβ maintain high levels of STAT1, IRF9, and IRF7 (which are themselves ISGs) (Gough et al., 2012; Gough et al., 2010; Hata et al., 2001; Taniguchi and Takaoka, 2001). Signaling through the IFNAR complex may also provide a docking site for STAT1, a STAT protein shared with the IFNγ and IL-6 signaling pathways in certain cells (Taniguchi and Takaoka, 2001). With this priming, STAT1 is able to dimerize more effectively upon IFNγ or IL-6 binding to their respective receptors (Mitani et al., 2001; Taniguchi and Takaoka, 2001). The stimuli for constitutive Type I IFN is thought to be the commensal microbiota (Abt et al., 2012; Ganal et al., 2012; Kawashima et al., 2013). Without proper signals from the microbiota, mice are unable to mount an effective response against viruses such as lymphocytic choriomeningitis virus (LCMV) and influenza virus (Abt et al., 2012). The expression of basal Type I IFN is proposed to be IRF-independent, and instead may require AP-1 and NFκB activity (Gough et al., 2012; Gough et al., 2010; Hata et al., 2001).

Because Type I IFNs have so many diverse effects on host physiology, both as a consequence of anti-viral activity and as modulators of immunity, it is important to limit levels of constitutive and induced Type I IFN. Thus, there are many levels of repression of Type I IFN production and signaling. In unstimulated cells, IRF2 and p50 homodimers bind to the IFNβ promoter as repressors, while the transcription factor MafB impairs the interaction of IRF3 with coactivators (Cheng et al., 2011; Harada et al., 1989; Kim and Seed, 2010). In addition,

molecules such as CYLD antagonize upstream pattern recognition receptors to prevent excessive production of Type I IFN, perhaps in response to endogenous nucleic acid (Friedman et al., 2008; Richards and Macdonald, 2011). Together, these pre-infection inhibitors maintain a threshold constitutive level of Type I IFNs. Upon infection, these inhibitors are downregulated and other mechanisms of negative regulation are induced, including control of receptor expression at the cell surface, expression of negative regulatory molecules, and production of microRNAs (miRNAs) (Ivashkiv and Donlin, 2014). Both ligand binding and additional signaling pathways activated by other cytokines and growth factors can promote internalization and degradation of IFNAR (de Weerd and Nguyen, 2012). Many viruses, including Hepatitis C virus, Herpes Simplex virus, and West Nile virus, also subvert Type I IFN signaling by downregulating receptor levels (de Weerd and Nguyen, 2012). In addition, Type I IFNs also provide their own negative feedback by inducing suppressor of cytokine signaling (SOCS) proteins and ubiquitin-specific peptidase 18 (USP18), which compete with STATs for binding to IFNAR and displace JAK1, respectively (Sarasin-Filipowicz et al., 2009; Yoshimura et al., 2007). Finally, miRNAs induced during inflammation can suppress expression of multiple IFNAR signaling components (Gracias et al., 2013). These inhibitory mechanisms prevent the pathology that is associated with increased Type I IFN signaling.

Dysregulation of the Type I IFN system in humans: the Type I Interferonopathies

An emerging group of diseases classified by upregulation of Type I IFNs with inflammation and tissue damage are the Type I Interferonopathies. These disorders are proposed to arise from either i) inappropriate activation of the Type I IFN response or ii) inadequate negative regulation of Type I IFN production (Crow, 2011). The Type I Interferonopathies are

genetically heterogeneous diseases including Aicardi-Goutieres syndrome (AGS), spondyloenchondrodysplasia (SPENCD), and some forms of systemic lupus erythematosus (SLE).

AGS affects the brain and the skin in particular, and can arise from mutations in *TREX1*, *SAMHD1,* the three components of *RNASEH2, ADAR1,* and, most recently discovered, *IFIH1*, which encodes MDA-5 (Crow, 2011; Crow et al., 2006a; Crow et al., 2006b; Rice et al., 2009; Rice et al., 2014b; Rice et al., 2012). Heterozygous mutations in *TREX1* and *SAMHD1* can also cause familial chilblain lupus, a form of cutaneous lupus associated with vasculopathy and painful lesions (Crow, 2011; Rice et al., 2007). TREX1 and RNASEH2 are nucleases that are hypothesized to remove waste nucleic acids from the cytosol. When these proteins are defective, the accumulated host nucleic acids trigger the innate immune response (Stetson et al., 2008; Yang et al., 2007). Specifically, Stetson *et al* showed that TREX1 was important for metabolizing reverse-transcribed single stranded DNA from endogenous retroelements, which then accrued in the cell when TREX1 was absent (Stetson et al., 2008). SAMHD1 has been implicated in the metabolism of nucleic acid from exogenous retroviruses (Laguette et al., 2011). This activity, which could potentially also extend to endogenous retroelements, may be important for limiting immune reactivity. A fourth gene implicated in AGS, *ADAR1*, encodes an adenosine deaminase that acts on RNA. Mutations in this gene could affect editing of specific transcripts important for IFN production or could result in an increase in immunoreactive RNA (Crow, 2011; Wu et al., 2011). Finally, *IFIH1* encodes MDA-5, an RLR that recognizes foreign dsRNA in the cytosol (see above). Mutant MDA-5 bound to dsRNA more avidly than WT, and had baseline activity in the absence of exogenously added nucleic acid, indicating the presence of endogenous dsRNA that could stimulate the mutant receptor (Rice et al., 2014b). These

diverse mutations in AGS all promoted elevations in Type I IFN due to excess and inappropriate recognition of endogenous or exogenous nucleic acid.

SPENCD has some clinical overlap with AGS, and some patients with SPENCD also go on to develop SLE (Crow, 2011). Affected individuals have increased Type I IFN activity thought to be downstream of defects in tartrate-resistant acid phosphatase (TRAP) or osteopontin, a TRAP substrate (Briggs et al., 2011; Lausch et al., 2011). TRAP is expressed in differentiated monocytes, macrophages, dendritic cells and osteoclasts (Hayman, 2008). This expression coincides with the clinical manifestations of SPENCD of autoimmunity and bone dysplasias. Osteopontin has been linked to the production of IFNα in pDCs, but the exact mechanisms of Type I IFN upregulation in SPENCD are unclear (Shinohara et al., 2006).

SLE is a multisystem autoimmune disease associated with elevations in Type I IFNs and autoantibodies against nucleic acids and nucleic acid-binding proteins. However, these autoantibodies can be present before clinical symptoms appear, and the etiology of SLE is still not well understood (Arbuckle et al., 2003). One idea is that in a genetically susceptible individual, induction of Type I IFNs by endogenous nucleic acids or virus can precipitate disease (Crow, 2014). In fact, there are some case reports of patients developing lupus or autoimmunity after receiving recombinant IFNα as therapy for hepatitis C or other disorders (Gota and Calabrese, 2003). Although these findings are merely correlative, the incidence of SLE in IFNα-treated patients is higher than the incidence in the general population, suggesting that IFNs may play a role in SLE pathogenesis (Gota and Calabrese, 2003).

The genetics behind this disease are slowly being elucidated, but findings suggest that SLE is actually a group of genetically distinct disorders with similar clinical phenotypes. The strongest known susceptibility factor for SLE is complement C1q deficiency (Botto et al., 1998;

Botto et al., 2009). Studies show that C1q inhibits IFNα production in pDCs, and that C1q-deficient patients thus have elevations in serum Type I IFN levels (Lood et al., 2009; Santer et al., 2010). Genome-wide association studies (GWAS) and other reports also implicate genes encoding for proteins involved in Type I IFN induction, including IRF5, IRAK1, TYK2, TREX1, IFIH1 and MAVs (Deng and Tsao, 2010; Graham et al., 2009; Pothlichet et al., 2011; Robinson et al., 2011). Based on these discoveries, several anti-IFNα monoclonal antibodies are currently being tested to treat SLE in clinical trials (Kirou and Gkrouzman, 2013; Lichtman et al., 2012). The efficacy of these treatments remain to be seen.

Despite the report of upregulated Type I IFNs in the above disorders, it is unclear whether Type I IFNs are directly pathogenic and what their effect is on host physiology. In this thesis, our findings show that constitutively elevated Type I IFNs can promote systemic epithelial proliferation and cell death. This promotes accelerated wound repair, but may be metabolically expensive and have other unintended consequences.

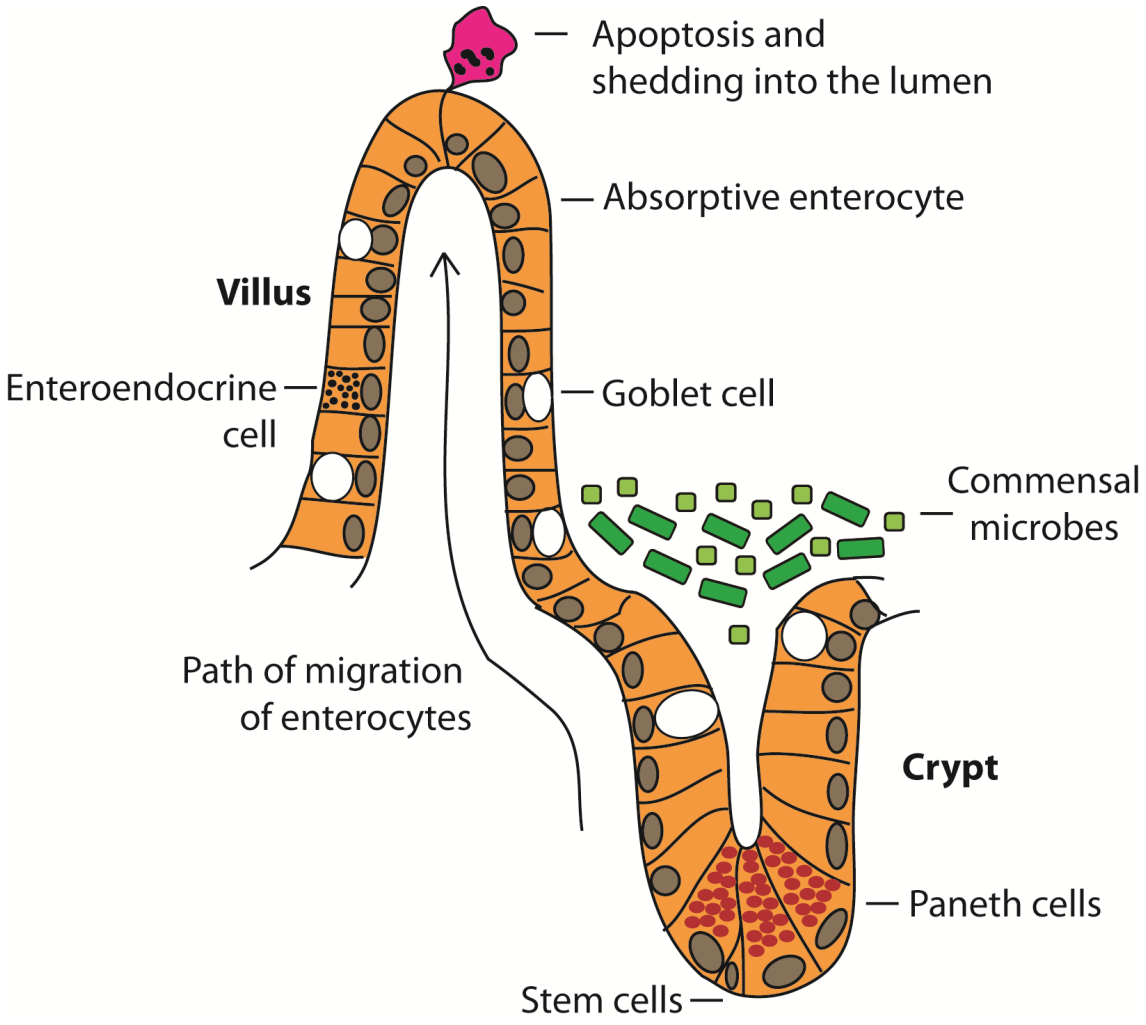

Figure 1.1. Schematic of the structure and turnover of the intestinal epithelium. The intestinal epithelium in the small intestine is formed of crypts and villi. The colonic epithelium lacks villi but has a similar organization of crypts. Stem cells at the base of the crypts differentiate into the 4 types of enterocytes: Paneth cells, goblet cells, absorptive enterocytes, and enteroendocrine cells. As the stem cells differentiate, they migrate up the crypt and villi, eventually undergoing apoptosis and shedding into the lumen.

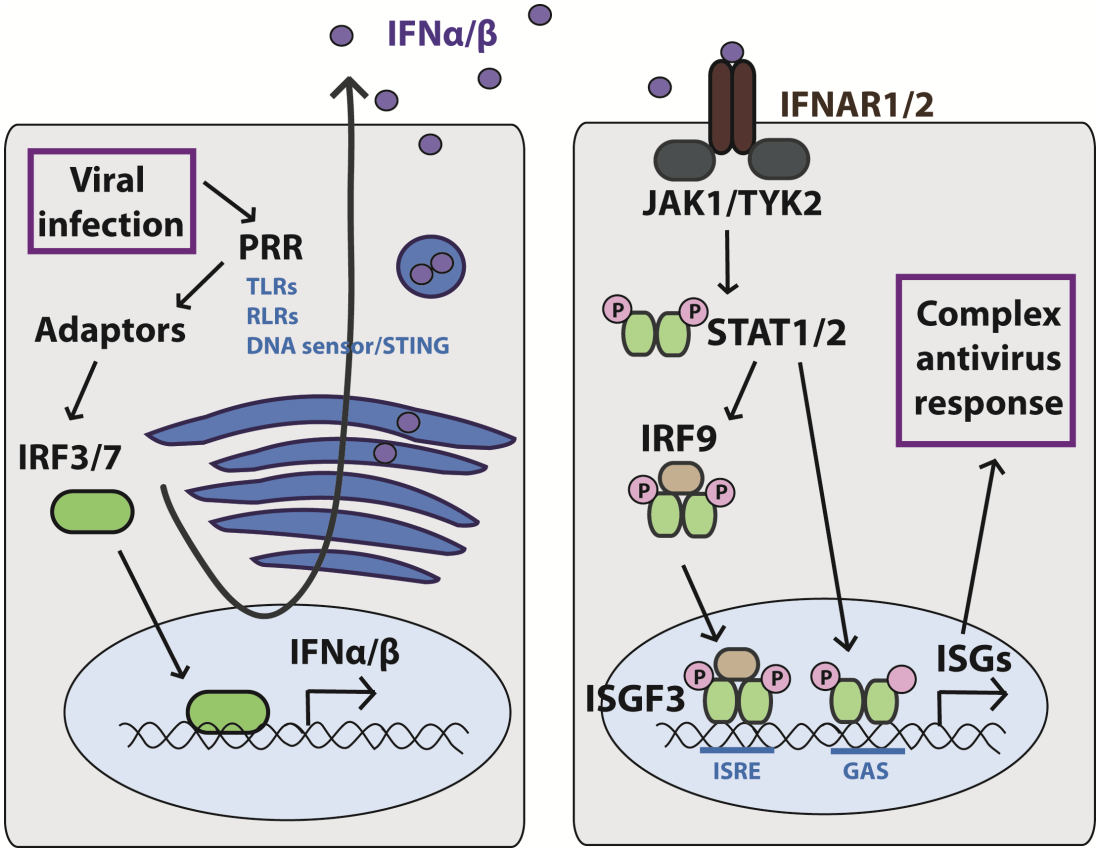

Figure 1.2. The Type I IFN signaling pathway. Viral and other infections are recognized by pattern recognition receptors (PRRs), including Toll-like receptors (TLRs), RIG-I-like receptors (RLRs), and DNA sensors that signal to STING. The PRRs signal through a variety of different adaptors to activate interferon regulatory factors IRF3 and 7, which translocate to the nucleus and promote transcription of Type I IFNs. Once secreted from the cell, all Type I IFNs bind to a common receptor, IFNAR, made of IFNAR1 and IFNAR2 subunits. These are constitutively associated with JAK1 and TYK2 kinases. Upon ligand binding, the JAKs are activated and phosphorylate STAT receptors, which then form stable homodimers. These can then translocate directly to the nucleus and bind IFN-γ-activated site (GAS) elements in the promoter region of interferon-stimulated genes (ISGs), or can bind IRF9 to form an ISGF3 complex that binds to

IFN-stimulated response (ISRE) elements. These regulators activate the transcription of hundreds of interferon stimulated genes (ISGs) to mediate a complex viral response.

CHAPTER 2:

Irgm1 negatively regulates systemic Type I interferon levels

INTRODUCTION

The innate immune system is essential for initial defense against pathogens. Its molecular mediators include secreted molecules that signal to surrounding and distant cell types, as well as intracellular proteins that protect an infected cell from succumbing to or spreading infection. One family of intracellular innate immune proteins is the IFNγ-inducible p47 GTPases. Of these, Immunity-related GTPase family M protein 1 (Irgm1), has been shown to be integral for host defense against multiple intracellular protozoans and bacteria. However, it is unclear whether Irgm1 acts directly in a cell-autonomous manner to protect cells from infection or whether its protection is mediated through effects on immune function.

The Irgm1 knockout mouse was created by Gregory Taylor's group in 2001. They showed that *Irgm1*$^{-/-}$ mice were highly susceptible to infection with *Toxoplasma gondii* and *Listeria monocytogenes* compared to WT mice (Collazo et al., 2001). In short succession, *Irgm1*$^{-/-}$ mice were also shown to be susceptible to *Mycobacterium tuberculosis* (MacMicking et al., 2003), *Mycobacterium avium* (Feng et al., 2004), *Trypanosoma cruzi (Santiago et al., 2005)*, *Salmonella typhimurium* (Henry et al., 2007), and *Chlamydia muridarum* (Coers et al., 2008). Different theories were presented as to how Irgm1 protected mice from these diverse intracellular pathogens. One idea was that Irgm1 aided in the maturation of pathogen-containing phagosomes and their fusion with the lysosome (MacMicking et al., 2003). Further studies built upon this idea, implicating Irgm1 and its human homologue IRGM in autophagosome formation and autophagy-mediated pathogen clearance (Singh et al., 2010). A second hypothesis was that infection in *Irgm1*$^{-/-}$ mice induced lymphopenia and pancytopenia, resulting in death of the mice (Feng et al., 2004; Feng et al., 2008a; Feng et al., 2008b). This defect was associated with impaired expansion of *Irgm1*$^{-/-}$ hematopoietic stem and progenitor cell populations after infection

(Feng et al., 2008a). The mechanism of this was thought to be IFNγ and STAT1-dependent (Feng et al., 2008b; King et al., 2011). In addition, studies showed increased IFNγ-induced autophagy-related cell death specifically in activated CD4+ T cells in *Irgm1*$^{-/-}$ mice (Feng et al., 2008b; Xu et al.). Since CD4+ T cells play an important role in experimental autoimmune encephalomyelitis (EAE), a mouse model of multiple sclerosis, the death of these cells in *Irgm1*$^{-/-}$ mice promoted resistance to EAE (Xu et al.). Another school of thought proposed that Irgm1 played a role in the regulation of macrophage motility (Henry et al., 2007; Henry et al., 2010). Irgm1-deficient macrophages were unable to suppress intracellular growth of *S. typhii*, and had defects in adhesion and motility after stimulation with IFNγ due to decreased actin remodeling (Henry et al., 2007). The different mechanisms of susceptibility in *Irgm1*$^{-/-}$ mice observed by different groups might be accounted for by variance in genetic background, microbiota composition, and/or diverse reagents such as the use of tagged Irgm1 constructs versus antibodies.

The localization of Irgm1 with IFNγ treatment and upon microbial entry also remains somewhat controversial. Irgm1 was found to localize to the Golgi membranes as well as late endosomal and lysosomal compartments in IFNγ-treated cells (Martens et al., 2004; Zhao et al., 2010). Localization to the endolysosomal system required activity of the nucleotide binding site of Irgm1, while localization to the Golgi did not. However, the C-terminal amphipathic helix of Irgm1 was required for localization to both compartments (Martens et al., 2004; Zhao et al., 2010). In addition, palmitoylation of a cluster of cysteines near the amphipathic helix also contributed to appropriate localization to cellular membranes (Henry et al., 2014). Notably, Zhao *et. al.* also found that both N- and C-terminal enhanced green fluorescent protein (EGFP) tags

caused mislocalization of Irgm1, cautioning against the use of these reagents that may have confounded previous studies (Zhao et al., 2010).

Many of the pathogens to which Irgm1 mediates resistance establish intracellular compartments, such as bacterial phagosomes, apicomplexan parasitophorous vacuoles, and chlamydial inclusion bodies. Irgm1 has been shown to translocate to mycobacterial phagosomes in murine macrophages and has been found on *Listeria monocytogenes* vacuoles (MacMicking et al., 2003; Shenoy et al., 2007; Tiwari et al., 2009). Tiwari *et al* showed that this localization was dependent on the recognition of host phosphoinositide lipids phosphatidylinositol-3,4,5-trisphosphate and phosphatidylinositol-3,4-bisphosphate on the nascent phagosome (Tiwari et al., 2009). In this report, the amphipathic helix of Irgm1 was shown to be required for binding to the phosphoinositides. Irgm1 was then found to bind to snapin, a SNARE adaptor protein, and may regulate its assembly activity or phosphorylation to recruit dynein motor complexes(Tiwari et al., 2009). These motor complexes would then allow trafficking of the phagosome along microtubules to maturing autolysosomes, which could then promote membrane fusion and lysosomal destruction of the mycobacteria (Cai and Sheng, 2011).

In direct contrast to these observations, Springer et al did not detect association of Irgm1 with either the listerial or mycobacterial phagosome in mouse macrophages or primary fibroblasts (Springer et al., 2013). They found that there are both a short and a long isoform of Irgm1 that are derived from differential splicing, and developed new anti-serum against these isoforms. They discovered that both isoforms can be found in the Golgi, but the short isoform failed to colocalize with the endolysosomal compartment. Both isoforms were found to weakly associate with mitochondrial membranes as well. Springer et al suggested that reasons for these discrepancies in localization was that in contrast to previous reports, their study distinguished

between extracellular and intracellular organisms and did not use tagged constructs that may have been mislocalized (Springer et al., 2013).

In addition, Irgm1 has not been found to colocalize to parasitophorous vacuoles (PV). Hunn et al proposed that Irgm1 instead regulates other IRG proteins such that they can be recruited to the PV membrane (PVM) (Hunn et al., 2008). There are potentially 23 members of the p47 GTPase (IRG) family in the mouse, 21 of which may be functional and 6 of which have been well-studied (Bekpen et al., 2005; Bekpen et al., 2009) Out of these, three are GMS GTPases (possess a methionine in the conserved P-loop G1 motif of the nucleotide binding site), while the rest are canonical GKS GTPases (have a lysine in that site) (Boehm et al., 1998). The murine GMS GTPases (Irgm1, Irgm2, and Irgm3) are thought to regulate the other GKS GTPases by interacting with GKS proteins in the GDP-bound state and inhibiting GTP binding (Hunn et al., 2008). This would prevent the GTP-dependent oligomerization of GKS proteins and the formation of cytoplasmic aggregates. At the PVM, there is an absence of GMS proteins, which allows for the GKS proteins to take up GTP and be activated at this site (Hunn et al., 2008). These GKS effectors can directly disrupt PV membranes, eventually leading to necrotic death of the infected cell (Ling et al., 2006; Martens et al., 2005; Zhao et al., 2009). A more recent study proposed that the localization of Irgm1 and Irgm3 to host membranes prevented stable association of GKS and guanylate-binding proteins (GBPs), a second family of IFNγ-induced GTPases, to these organelles (Haldar et al., 2013). The absence of GMS proteins on PVs or artificially stripped lipid droplets indicated the presence of "non-self", and resulted in the recruitment and formation of GKS and GBP oligomers to these membranes (Haldar et al., 2013). Based on these most recent studies, it would appear that Irgm1 is not directly involved in cell-

autonomous defense against microbes but instead is a regulator of GTPase activity located on intracellular host membranes.

The human homologue of Irgm1, IRGM, is of clinical interest because of its association with susceptibility to tuberculosis and Crohn's disease, but the two proteins have limited similarity. IRGM is 181 amino acids (aa) in length, while Irgm1 is 409aa long. Out of 174aa that align by protein blast, there is only 57% identity. In addition, human IRGM does not appear to be IFNγ-inducible (Bekpen et al., 2005). Therefore, we recommend caution when extrapolating data from mouse studies to human and vice versa until further knowledge is acquired.

There are 23 p47 GTPases in the mouse, whereas the human genome only has one single full-length gene (IRGC) on chromosome 19 and an expressed, truncated gene on chromosome 5 (IRGM) (Bekpen et al., 2005). Bekpen et al propose that this difference in numbers of p47 GTPase family members is due to differences in the evolutionary history of these genes (Bekpen et al., 2009). The IRG family is at least as old as bony fish but is not present in invertebrates (Bekpen et al., 2005). The genomic sequences and positioning of the mouse genes imply a succession of duplication and divergence over time (Bekpen et al., 2005). In the human lineage, Bekpen *et al* suggest that the IRGM gene became nonfunctional approximately 40 million years ago with the integration of an Alu repeat that disrupted the ORF, and accumulation of stop codons and frameshift mutations, resulting in pseudogene copies in Old World and New World monkeys. However, IRGM was then "resurrected" in perhaps a truncated form about 20 million years ago in human ancestors (Bekpen et al., 2009). At this time, there was an integration of the ERV9 retrotransposon element that serves as the IRGM promoter, the introduction of a new start codon, and the loss of a stop codon (Bekpen et al., 2009). There are 5 splicing isoforms of human IRGM, a-e, but whether these have different functions is unknown. IRGC, on the other hand, was

probably conserved during this time, as it is very similar to murine Irgc; they are both constitutively expressed in the testis and not IFNγ-inducible (Bekpen et al., 2005).

Akin to murine Irgm1, the function of IRGM is still being uncovered. Knockdown studies in human macrophages suggested that IRGM was involved in autophagy and important for autophagy-induced mycobacterial clearance (Singh et al., 2006; Singh et al., 2010). IRGM has also been shown to bind autophagy proteins and the inner mitochondrial membrane lipid cardiolipin to induce mitochondrial fission and autophagy (Gregoire et al., 2011; Petkova et al., 2012; Singh et al., 2010; Tiwari et al., 2009). Four autophagy-related proteins have been found to interact with IRGM: ATG5, ATG10, MAP1LC3C, and SH3GLB1 (Gregoire et al., 2011). In comparison, Irgm1 has been shown to be dispensable in IFNγ-induced autophagy in macrophages (Matsuzawa et al., 2012). Better reagents to study IRGM are necessary to fully characterize its function in human cells.

IRGM polymorphisms have been linked to susceptibility to Crohn's disease (CD), but it is not clear whether risk is due to upregulation or downregulation of expression of IRGM, or change of function of the gene product. CD is a chronic inflammatory bowel disease (IBD) that is characterized by inflammation of the gastrointestinal tract, resulting in damage to the mucosa. Genome-wide association studies have identified dozens of susceptibility alleles that are linked to CD, including IRGM (McCarroll et al., 2008; Parkes et al., 2007). The risk allele rs13361189 is in perfect linkage disequilibrium with a 20kb deletion upstream of the IRGM gene, but this resulted in upregulation of IRGM in some cell types and downregulation of expression in others (Huett et al., 2009; McCarroll et al., 2008). Further complicating the matter, Brest *et al* showed a role for a microRNA (miRNA) that differentially regulated the risk and protective haplotypes (Brest et al., 2011). Their results demonstrated that miR-196 bound strongly to downregulate the

protective haplotype but not the risk haplotype. MiR-196 also had enhanced expression in inflamed tissue. Taken together, these findings suggested a model in which there was upregulation of IRGM in carriers of the risk variant because miR-196 could not effectively bind its target site, especially in inflamed areas (Brest et al., 2011).

In addition, polymorphisms in IRGM have been linked to protection against tuberculosis (Bahari et al., 2012; Che et al., 2010; Intemann et al., 2009). The IRGM variant rs9637876 was associated with increased levels of expression and was protective against *M. tuberculosis* (Intemann et al., 2009). Similar to its murine homologue, IRGM could thus be involved in resistance against mycobacterium. This could also provide an explanation for the evolutionary preservation of gene variants resulting in upregulation of expression that increased the risk for IBD: these variants could be protective against tuberculosis, a widespread infection.

Based on these findings, we were interested in discovering the function of Irgm1, particularly at mucosal surfaces, which would advance our knowledge about why polymorphisms in IRGM influence susceptibility to Crohn's disease in the intestine and tuberculosis in the lung. We found that *Irgm1*$^{-/-}$ mice had systemic elevations in Type I interferons, a family of anti-viral cytokines. Our findings suggest that Irgm1 functions by influencing the innate immune cytokine environment.

MATERIALS AND METHODS

Mice

All experimental procedures were performed under approval by Washington University's Animal Studies Committee. *Irgm1*$^{-/-}$ mice were provided by Dr. Gregory A. Taylor (Duke University, Durham, NC; (Collazo et al., 2001)). *Ifnar*$^{-/-}$ mice are deficient in *Ifnar1* (Muller et al., 1994). These mice were provided by Dr. Robert D. Schreiber and Dr. Herbert W. Virgin (Washington University in St. Louis, St. Louis, MO; (Thackray et al., 2012)). All mice were re-derived into our enhanced barrier facility and were fully backcrossed to a C57BL/6 background. For experiments with knockout mouse lines, heterozygote breeding pairs were used to obtain WT controls.

Micro-computed tomography (MicroCT)

MicroCT of the femur was performed on 12 week-old WT and *Irgm1*$^{-/-}$ mice as previously described (DeSelm et al., 2012).

Toxoplasma gondii infection

Toxoplasma gondii cysts (Type II Prugniaud strain) were obtained from the brains of CBA/J mice injected with *T. gondii* 3-6 months prior. The brains were homogenized, fixed with 3% formaldehyde and cysts were stained with lectin-FITC. The suspension was pipetted onto slides and the number of cysts counted. C57BL/6 and *Irgm1*$^{-/-}$ mice were then infected orally with 7 cysts of *T. gondii*. Weight loss and lethality were monitored daily for 30 days.

Enzyme-linked immunosorbent assay

The mouse IFNγ "Femto-HS" High Sensitivity Enzyme-linked Immunosorbent Assay (ELISA) kit (Affymetrix eBioscience) was used to measure levels of IFNγ in serum (diluted 1:4 in assay diluent) and tissue homogenate (diluted 1:2).

Laser Capture Microdissection and Microarray Analysis

Small intestinal sections were harvested and pinned flat in methacarn fixative (60% absolute methanol, 30% chloroform, 10% glacial acetic acid) for 2 hours. Tissue was then washed and stored in 70% ethanol until blocked in agar. After paraffin embedding, unstained sections were cut onto uncharged slides. Slides were deparaffinized and stained with methyl green for visualization of nuclei. The intestinal epithelium only was captured using a PixCell II LCM system (Arcturus; 7.5μm laser spot) and CapSure HS LCM caps (Arcturus). Total cellular RNA was extracted using PicoPure RNA isolation kit (Arcturus). RNA was amplified and synthesized into cDNA. Microarray analysis was performed on 4x44K mouse whole genome microarrays (Agilent) as previously described (Cadwell et al., 2010).

Type I IFN bioassay

Type I IFN bioassay was performed as previously described (Newby et al., 2007). Briefly, L929 cells were plated at $3.5x10^5$ cells/mL in 12-well plates and rested at 37°C for 4h, then incubated with 1:2 dilutions of serum, tissue homogenate, cell lysates, or plasma and a range of units of recombinant murine IFN-αA (PBL Interferon Source) and IFN-β (PBL Interferon Source) for 24h at 37°C. Neutralizing anti-IFNα (clone TIF-3C5) and anti-IFNβ1 (clone HDβ-4A7) were

pre-incubated with sample or positive control IFN for 1h at room temperature before addition to L929 cells (t0). Neutralizing anti-Ifnar1 antibody (Leinco Technologies, clone # MAR1-5A3) was administered to wells at 3μg/mL at t0 and 1μg/mL at 16-18h after t0. 24h after t0, treatment was aspirated and L929 cells were washed 2X with phosphate-buffered saline (PBS). Green fluorescent protein (GFP)-tagged vesicular stomatitis virus (VSV) (kindly provided by Dr. John Rose, Yale University, New Haven, CT) was added to L929 cells at 10 multiplicities of infection (MOI), and incubated for an additional 10-12h. L929 cells were then trypsinized, washed with FACS buffer (PBS + 3% bovine serum albumin + 0.01% sodium azide) and fixed with BD Cytofix/Cytoperm (BD Biosciences). Cells were run through a flow cytometer and the median fluorescence intensity (MFI) determined. Standard curves with murine recombinant IFNαA were run for each experiment and the level of anti-viral activity was calculated relative to WT samples.

Pan-anti-IFNα and anti-IFNβ antibodies

As will be reported in further detail elsewhere, anti-IFNα (clone TIF-3C5) is an Armenian hamster monoclonal antibody (mAb) that binds to and neutralizes *in vitro* activity of all available murine IFN-α subtypes (IFN-α A, 1, 4, 5, 11, and 13), as assessed by quantitating i) induction of Stat1 phosphorylation; ii) MHC class I induction; and iii) antiviral activity (using a cytopathic effect assay and Vesicular Stomatitis Virus). The TIF-3C5 mAb does not bind murine IFNγ-gamma or IFNβ, nor does it affect functional activity of these IFN species. Anti-IFNβ (clone HDβ-4A7) is a murine IgG2a mAb that binds and neutralizes murine IFNβ but not murine IFNα species or IFNγ using identical assays as described above (Sheehan et al, unpublished observations).

Influenza A infection

For influenza infection, 8-10 week-old male mice were anesthetized with ketamine and infected intranasally with 5000 pfu of influenza A/WSN/33 virus (generated from cDNA as previously described (Neumann et al., 1999), Morales et al, in submission). Mice were weighed and inspected daily. Mice with greater than 30% weight loss were sacrificed as per protocol. Viral titers were determined from lung homogenate of the right lobes by plaque assay (using MDCK cells).

RNA isolation and Quantitative real-time PCR

Tissue was snap frozen in liquid nitrogen and RNA was extracted using the Nucleospin RNA II purification kit (Macherey-Nagel). RNA was extracted from *in vitro* intestinal epithelial cultures by directly adding RA1 buffer from the RNA purification kit and proceeding with the remainder of the protocol. cDNA was synthesized using SuperScript III (Invitrogen). Gene expression was quantified using SYBR Green reagents (Clontech) on an Eppendorf Mastercycler. Δ Ct values were calculated relative to GAPDH.

Histology and immunofluorescence of the lung

For haematoxylin and eosin (H+E)-stained sections of lung, the lung was inflated using 1mL of 10% neutral-buffered formalin through the trachea. Tissue was fixed at room temperature (RT) overnight. Tissue was then washed in PBS, then 35%, 45%, and 70% ethanol for 15 minutes each at room temperature before storage in 70% ethanol at 4°C. Lung tissue was then embedded in paraffin, cut into slides, and then H+E-stained. The area of cellular aggregates and total lung

parenchyma was measured from digital images using ImageJ software. For immunofluorescence, mouse lung was inflated using 2mL of 1:1 PBS:OCT compound (Tissue-Tek). Tissue was then immediately frozen in cassettes surrounded by OCT. Frozen sections were cut on a cryostat and stored at -80°C. When used for staining, slides were dried for 2-3 minutes at RT, then fixed in cold methanol or cold 4%PFA for 5 minutes. After washing with PBS and blocking with 1% BSA and 0.1% Triton X-100 in PBS, slides were incubated with primary antibody for 1hr at RT or overnight at 4°C. Primary antibodies: anti-CD45 Alexa-488 (BD Pharmingen clone 30-F11). FITC-conjugated anti-B220 and unconjugated anti-B220 (Biolegend, clone RA3-6B2). Anti-CD19-PE (Biolegend, clone 6D5). Anti-CD3e Alexa-647 (Biolegend, clone 145-2C11). Anti-CD11c Alexa-647 (Biolegend, clone N418). FITC-conjugated anti-Gr1 (Biolegend, clone RB6-8C5). Anti-Siglec H-PE (Miltenyi-Biotec, clone 551.3D3). Unconjugated anti-CD11b (BD Pharmingen, clone M1/70).

Bone marrow-derived dendritic cell (BMDC) experiments

Bone marrow was isolated from mouse femurs and tibias. Bone marrow cell suspension was plated on non-tissue culture-treated petri dishes in BMDC media at 37°C (RPMI with 10% FBS, 1% penicillin-streptamycin, 2% L-glutamine, 2% GM-CSF supernatant, 1mM sodium pyruvate, 0.1mM nonessential amino acids, 50uM beta-mercaptoethanol). After 4 days, cells were replated, and on day 6, media was changed. Cells were treated with polyI:C on day 7 after initial plating and cells harvested for RNA on day 8. Cell lysates and cell supernatants for Type I IFN bioassay were also isolated on day 8.

Intestinal epithelial spheroids

Colonic and small intestinal crypts were isolated from mice and cultured in a 3D-Matrigel as previously described (Miyoshi et al., 2012; Miyoshi and Stappenbeck, 2013). Briefly, 1-2cm of tissue was harvested, minced into a fine homogenate with scissors, and Type I collagenase-treated (Invitrogen) in 37°C with vigorous pipetting until epithelial crypts were dissociated from tissue. Crypts were suspended in Matrigel basement membrane matrix (BD Biosciences) and incubated with 50% conditioned media from L-cells containing Rspo3, Wnt3a and Noggin (L-WRN). Crypt cells grew into spheroids, which were passaged every 2-4 days.

Ifnar surface expression measurements

Whole bone marrow was isolated from WT, *Irgm1*$^{-/-}$ and *Irgm1*$^{-/-}$ *Ifnar*$^{-/-}$ mice. After red blood cell lysis and washing, cells were either left unstained, or stained with anti-Ifnar-APC antibody (Biolegend, clone MAR1-5A3) or isotype control (mouse IgG1). Cells were run through a FACSCalibur flow cytometer and data analyzed using FloJo software.

Clodronate liposome macrophage depletion

250µL of clodronate or control liposomes (Encapsula) were delivered intravenously (i.v.) to WT and *Irgm1*$^{-/-}$ mice on d0 and d3. Mice were sacrificed on d6. Blood was obtained using cardiac puncture and kept at 4°C overnight. Blood was then spun down and serum was extracted and stored at -20°C.

Antibiotic treatment

Mice were given antibiotics dissolved in Kool-Aid or Kool-Aid alone (control) instead of drinking water for two weeks. Antibiotics: 500mg ampicillin, 250mg vancomycin, 500mg neomycin-sulfate, 500mg metronidazole, 10g grape Kool-Aid in 500mL water, sterile filtered through a 0.22um filter. Mice were sacrificed on day 15 and serum and tissue was harvested.

Statistics

GraphPad Prism software (version 6) was used to perform all statistical analyses unless otherwise specified.

RESULTS

Irgm1$^{-/-}$ *mice were resistant to flu infection due to heightened baseline Type I IFNs*

We first re-derived *Irgm1*$^{-/-}$ mice into our enhanced barrier facility (Cadwell et al., 2010), and fully backcrossed them to a C57BL/6 (B6) background. We implemented a heterozygote breeding scheme to obtain littermate controls. *Irgm1*$^{-/-}$ mice bred at near Mendelian ratios (**Figure 2.1A**) and displayed no overt signs of ill health (observed up to the age of 13 months). However, we noticed that *Irgm1*$^{-/-}$ mice had consistently smaller mass than their wild-type (WT) littermates at multiple ages (**Figure 2.1B**). However, bone volume fractions and multiple other bone parameters were comparable between *Irgm1*$^{-/-}$ and WT mice, indicating the smaller size of *Irgm1*$^{-/-}$ mice was not due to a bone-intrinsic defect (**Figure 2.1C, Table 2.1**).

Irgm1$^{-/-}$ mice bred outside our institutional facility have previously been shown to be susceptible to multiple intracellular pathogens, including *Mycobacterium tuberculosis*, *Toxoplasma gondii*, and *Listeria monocytogenes* (Coers et al., 2008; Collazo et al., 2001; Feng et al., 2004; Henry et al., 2007; MacMicking et al., 2003; Santiago et al., 2005). We found that our re-derived *Irgm1*$^{-/-}$ mice were still highly susceptible to *T. gondii* infection (**Figure 2.1D**).

To determine the function of Irgm1 at mucosal surfaces, we performed whole genome microarray analysis of RNA from the intestinal epithelium of wild-type (WT) and *Irgm1*$^{-/-}$ mice. This was accomplished using laser capture microdissection, a technique that allows for RNA isolation from specific areas of tissue on a slide under microscopic guidance (Emmert-Buck et al., 1996). Functional gene annotation analysis of 461 genes that were enriched greater than 2-fold in *Irgm1*$^{-/-}$ epithelium identified significant elevations in "Interferon-mediated immunity" genes (Bonferonni value = 2.47 E-13) (**Figure 2.2**). These genes include those stimulated by Type I Interferon (IFN) (IFNαs, β, and other subtypes) as well as those induced by Type II IFN

(IFNγ). Previous studies have found that *Irgm1*$^{-/-}$ mice have elevated serum IFNγ ((King et al., 2011). However, *Irgm1*$^{-/-}$ mice bred in our enhanced barrier facility did not have detectable serum IFNγ, and organ levels of IFNγ were not different in wild-type (WT) C57BL/6 and *Irgm1*$^{-/-}$ mice (**Figure 2.3**). Instead, manual inspection of highly-enriched genes in our microarray data set revealed elevations in IFN-stimulated genes (ISGs), a group of transcripts that are expressed downstream of Type I IFN signaling (**Table 2.2**). In addition, we found that Type I IFNs were elevated in the serum and lung homogenate of uninfected *Irgm1*$^{-/-}$ mice (**Figure 2.4A**). The systemic elevation of Type I IFNs in *Irgm1*$^{-/-}$ mice has not been previously reported and was unusual, as these cytokines are typically only transiently elevated upon infection, with constitutive levels in the serum and tissues barely detectable by current assays (Gough et al., 2012). To measure Type I IFN, we used a bioassay system in which we incubated serum of *Irgm1*$^{-/-}$ and WT mice with L929 cells, then subsequently infected the cells with a GFP-tagged vesicular stomatitis virus (VSV; **Figure 2.5A** and (Newby et al., 2007)). We then used flow cytometry to measure the levels of VSV-GFP per cell, which negatively correlated with the amount of anti-viral activity in the mouse sample (**Figure 2.5A**). All Type I IFNs signal through the Type I IFN receptor (Ifnar), which is a heterodimer composed of two subunits, Ifnar1 and Ifnar2 (de Weerd et al., 2007). The addition of an antibody against Ifnar1 neutralized the anti-viral activity found in *Irgm1*$^{-/-}$ serum. A pan-anti-IFNα antibody, but not an anti-IFNβ1 antibody, was also able to neutralize the anti-viral activity present in the serum of *Irgm1*$^{-/-}$ mice, showing that these mice have elevated systemic levels of IFNα (**Figure 2.4B** and **Figure 2.5B**). Type I IFNs were not present at elevated levels in *Irgm1*$^{+/-}$ mice, suggesting that a complete loss of Irgm1 function was required to induce these cytokines (**Figure 2.4C**). Increased Type I IFNs in *Irgm1*$^{-/-}$ mice could be found as early as day 7 and as late as12 months of age (**Figure 2.4D-E**).

We then investigated whether these elevated Type I IFN levels were functional, and therefore examined the response of *Irgm1*$^{-/-}$ mice to influenza A infection. *Irgm1*$^{-/-}$ mice were resistant to influenza A infection at doses that were lethal to 50% of WT mice (**Figure 2.6A**). Interestingly, viral titers were not different in the lung at day 3 between WT and *Irgm1*$^{-/-}$ mice (**Figure 2.6B**). As expected, systemic Type I IFNs induced the expression of interferon-stimulated genes (ISGs) such as *Oas2* and *Mx2* in numerous tissues, including the lung (**Figure 2.6C-D**). These results indicated that high Type I IFN levels in *Irgm1*$^{-/-}$ mice chronically stimulated gene expression with consequent changes in susceptibility to infection.

Irgm1$^{-/-}$ *mice had lymphoid aggregates in the lung parenchyma dependent on Type I IFN signaling*

To investigate possible mechanisms of anti-viral defense, we examined the histology of the lungs of WT, *Irgm1*$^{-/-}$ and *Irgm1*$^{-/-}$ *Ifnar*$^{-/-}$ mice. We found the presence of aggregates of lymphoid-appearing cells in *Irgm1*$^{-/-}$ mice but not WT mice, even without flu infection (**Figure 2.7A-B**). Aggregates were present in 100% of *Irgm1*$^{-/-}$ mice, but only in about one-third of *Irgm1*$^{-/-}$ *Ifnar*$^{-/-}$ mice (**Figure 2.7B**). The area of these aggregates was also decreased in *Irgm1*$^{-/-}$ *Ifnar*$^{-/-}$ mice (**Figure 2.7C**). Immunofluorescence staining revealed that the aggregates were composed of CD45+ leukocytes (**Figure 2.8A**). Specifically, there was a core of B220+ cells, most of which were CD19+, suggesting that these were B cells, surrounded by CD3+ T cells (**Figure 2.8B-C**). There were also CD11c+ and Gr1+ cells scattered throughout the aggregate (**Figure 2.8D-E**). The plasmacytoid dendritic cell marker Siglec-H was present on some but not all B220+ cells (**Figure 2.10F**). There were very few CD11b+ cells in the aggregates of *Irgm1*$^{-/-}$ mice (**Figure 2.8G**). These staining results suggested that the lymphoid aggregates in *Irgm1*$^{-/-}$

lungs were composed of mostly B cells with some T cells and dendritic cells, and possibly macrophages. These immune cell populations may have played a role in anti-viral defense against flu infection.

Type I IFNs were elevated in lung, serum, and bone marrow of Irgm1$^{-/-}$ mice, but mRNA levels of IFNα and IFNβ were unchanged between multiple tissue types

We next sought to determine the source of the Type I IFNs in *Irgm1*$^{-/-}$ mice. Using the bioassay system, we assayed various tissue and blood cell types for elevations in these cytokines. Anti-viral activity was not detected in the spleen, colon, or bone marrow of *Irgm1*$^{-/-}$ mice (**Figure 2.9A-B**). However, anti-viral activity was found in the lung homogenate of *Irgm1*$^{-/-}$ mice in addition to the serum (**Figure 2.9C-D**). The plasma fraction of blood, not red or white blood cell lysates, contained the anti-viral activity, implying that it is not cells circulating within the bloodstream that are releasing the interferons (**Figure 2.9E**). Cells within the lung may be responsible for elevated levels of Type I IFNs in *Irgm1*$^{-/-}$ mice.

However, when we examined mRNA expression using primers against IFNβ1, and a pan-IFN-α primer set, we did not observe any significant differences in lung, small intestine, colon, spleen, or bone marrow (**Figure 2.10A-B**). This suggests either that 1) Irgm1 negatively regulates Type I IFNs at the post-transcriptional level, or 2) the interferon that was elevated is of a type that was not detected using our primer set.

Irgm1-deficient dendritic cells and epithelial cells did not have enhanced sensitivity to polyIC.

We wondered whether cells lacking Irgm1 had enhanced sensitivity to Type I IFN-inducing stimuli. We tested WT and Irgm1-deficient bone marrow-derived dendritic cells

(BMDCs) for production of Type I IFNs upon polyinosinic:polycytidylic acid (polyI:C) treatment. We chose to examine these cell types because DCs are important producers of Type I IFNs during anti-viral responses (Asselin-Paturel and Trinchieri, 2005). We found no difference between *Irgm1*$^{-/-}$ and WT BMDC expression of pan-IFN-α, IFN-β1, or IFN-α4 in response to increasing doses of polyI:C (**Figure 2.11A-C**). ISG expression was also comparable in both WT and Irgm1-deficient BMDCs (**Figure 2.11E-F**). In addition, Type I IFN activity in BMDC culture supernatant and cell lysate was similar as measured by bioassay (**Figure 2.12A-B**).

We also assessed the sensitivity of non-hematopoietic cells, intestinal epithelial spheroids, to polyI:C treatment. Again, we did not discern any differences in IFNβ1 or pan-IFNα expression in response to polyI:C (**Figure 2.13A-B**). Together, these results suggest that neither bone marrow dendritic cells nor intestinal epithelial cells deficient in Irgm1 had enhanced sensitivity to dsRNA stimuli.

Cells deficient in Irgm1 did not have altered cell surface expression of Ifnar

One possible reason for increased levels of circulating Type I IFNs is diminished cell surface expression of the Type I IFN receptor, Ifnar. Lower expression of Ifnar would result in less Type I IFN being bound to the cell and/or internalized, resulting in higher measurable levels of Type I IFNs. We measured Ifnar cell surface expression on whole bone marrow cells and found that there was no difference in levels of expression between WT and Irgm1-deficient bone marrow (**Figure 2.14**). In contrast, bone marrow from *Irgm1*$^{-/-}$ x *Ifnar*$^{-/-}$ mice had low Ifnar expression, as expected (**Figure 2.14C-D**).

T and B lymphocytes were not involved in the production of Type I IFNs in Irgm1$^{-/-}$ mice.

Since Irgm1 is highly expressed in naïve T lymphocytes (Immgen.org, **Figure 2.15**), and both T and B cells were present in lymphoid aggregates in *Irgm1*$^{-/-}$ mice, we investigated whether these lymphocytes were involved in Type I IFN overproduction in Irgm1-deficient mice. We crossed *Irgm1*$^{-/-}$ mice to *Rag1*$^{-/-}$ mice, which lack both mature T and B cells. *Irgm1*$^{-/-}$ *Rag1*$^{-/-}$ mice still maintained elevated serum levels of Type I IFNs, suggesting that T and B lymphocytes, and the adaptive immune response, were not involved in overproduction of Type I IFNs in Irgm1-deficient animals (**Figure 2.16**). As expected, *Irgm1*$^{+/-}$*Rag1*$^{-/-}$ mice had levels of Type I IFNs similar to WT (**Figure 2.16**).

Clodronate liposome-mediated depletion of macrophages decreased Type I IFN serum levels in Irgm1$^{-/-}$ *mice*.

Macrophages are an additional candidate cell type for Type I IFN production (Kim et al., 2012; Kumagai et al., 2007). We depleted tissue macrophages using intravenous (i.v.) injection of clodronate liposomes (Van Rooijen and Sanders, 1994). After 2 injections once every 3 days, *Irgm1*$^{-/-}$ mice injected with clodronate liposomes had decreased levels of Type I IFNs compared to *Irgm1*$^{-/-}$ injected with control liposomes (**Figure 2.17A-C**). At this time, macrophages were depleted in the liver but not in the kidney (**Figure 2.17D and data not shown**). Clodronate liposome-mediated depletion of macrophages in WT mice did not have a significant effect on serum Type I IFN levels (**Figure 2.17A-B**). These findings demonstrate that liver macrophages played an important role in Type I IFN production in *Irgm1*$^{-/-}$ mice.

Antibiotic treatment did not affect Type I IFN production in Irgm1$^{-/-}$ mice

A further question was whether the Type I IFNs were being produced in response to gut microbial stimuli in *Irgm1*$^{-/-}$ mice. To address this possibility, we treated mice with a broad-spectrum antibiotic regimen of vancomycin, neomycin, ampicillin, and metronidazole for 2 weeks. We found that antibiotic treatment did not diminish Type I IFN levels in Irgm1-deficient mice, and in fact may have increased Type I IFNs (**Figure 2.18**). This suggests that the microbial stimuli for Type I IFNs in *Irgm1*$^{-/-}$ mice were not susceptible to this antibiotic regimen.

DISCUSSION

Irgm1 has previously been reported to have a variety of roles in the immune system, but its exact function within the cell is controversial. We found that *Irgm1*$^{-/-}$ mice in our enhanced barrier facility had elevated circulating Type I IFNs even in the absence of pathogenic viral infection.

Notably, the previous observations regarding the susceptibility of *Irgm1*$^{-/-}$ mice to intracellular pathogens are compatible with the known effects of Type I IFNs. First, Type I IFNs have been shown to be detrimental to the host during infection with *L. monocytogenes*, *M. tuberculosis,* and *C. muridarum* (Auerbuch et al., 2004; Carrero et al., 2004; O'Connell et al., 2004; Qiu et al., 2008; Stanley et al., 2007). The mechanisms for this process have not yet been well elucidated, but previous studies have implicated loss of Ifnar signaling with changes in macrophage cytokine production and IFNγ responsiveness in these infectious systems (Auerbuch et al., 2004; Rayamajhi et al., 2010a; Rayamajhi et al., 2010b). In addition, reports on *L. monocytogenes* showed that Type I IFNs increased sensitization of lymphocytes to cell death (Carrero et al., 2004, 2006), similar to what was observed in *Irgm1*$^{-/-}$ mice upon infection (Feng et al., 2004; Feng et al., 2008b). This finding was supported by further studies using vesicular stomatitis virus (VSV), polyinosinic:polycytidylic acid (polyI:C), a synthetic double-stranded RNA TLR3 agonist and R848, an imidazoquinoline TLR7/8 agonist, all of which stimulate Type I IFN production *in vivo* (Kamphuis et al., 2006). Subsequently, two reports published in 2009 demonstrated that Type I IFNs promoted exit of hematopoietic stem cells (HSCs) from the quiescent state, resulting in subsequent proliferation and finally functional exhaustion of the HSCs and decreased production of mature blood cells (Essers et al., 2009; Sato et al., 2009). HSC function was compromised after 2-3 weeks of chronic Type I IFN production (Essers et al.,

2009; Sato et al., 2009). These results are comparable timeline-wise to the lymphopenia that was observed in *Irgm1*$^{-/-}$ mice after *M. avium* infection (measured 4 weeks after infection) (Feng et al., 2004). Although the authors did not examine Type I IFN levels, *M. avium* infection may have stimulated production of those cytokines above even baseline amounts in *Irgm1*$^{-/-}$ mice, resulting in HSC exhaustion and lymphopenia. The report by King *et al* in 2011 demonstrated that even in the absence of overt infection, aged 12 month-old *Irgm1*$^{-/-}$ mice had reduced numbers of HSCs (King et al., 2011). While they focused on the importance of IFNγ in this effect, their results suggested a significant and unexamined role for Type I IFNs in mediating HSC dysfunction. For example, their results showed elevated levels of IFN-stimulated genes in HSCs from *Irgm1*$^{-/-}$ mice compared to WT mice. However, out of 19 genes listed, only 15 were classified as interferon-stimulated genes by the Interferome database and out of those genes, 3 were classified as only being induced by Type I IFNs, not Type II. In addition, they only saw partial rescue of HSC defects in *Irgm1*$^{-/-}$ mice with deficiency in IFNγ receptor, but a full rescue in *Irgm1*$^{-/-}$ x *Stat1*$^{-/-}$ mice (King et al., 2011). Thus, it is possible that the previous findings regarding the role of Irgm1 in host defense are attributable to elevated Type I IFNs that we observed in *Irgm1*$^{-/-}$ mice. This would suggest that Irgm1 does not act in a cell-autonomous manner to mediate protection, but by modulating the innate immune system.

Our data suggests that not all cell types are required for the production of Type I IFNs in *Irgm1*$^{-/-}$ mice. In particular, loss of T and B cells did not affect Type I IFN levels, but loss of liver macrophages in *Irgm1*$^{-/-}$ mice resulted in reduced Type I IFN levels in the serum. These tissue-resident macrophages, also called Kupffer cells, are important for clearance of erythroid nuclei, senescent erythrocytes, and apoptotic cells and other debris (Davies et al., 2013). In addition, their localization within the hepatic sinusoid allows them to phagocytose pathogens

entering from the portal or arterial circulation (Dixon et al., 2013). Recent studies have also identified a contributing role for Kupffer cells in liver injury, such as during alcoholic liver disease and metabolic syndrome (Dixon et al., 2013). Due to their sentinel location within the circulatory system, these cells may encounter self or foreign triggers of Type I IFN signaling. Loss of Irgm1 in Kupffer cells could thus result in aberrant function and enhanced Type I IFN production.

The molecular mechanism by which Irgm1 negatively regulates Type I IFN production is unclear. Based on its localization pattern at the ER, Golgi and mitochondrial membranes, Irgm1 could interact with MAVS or STING, adaptors downstream of pattern recognition receptors (PRRs) that induce Type I IFN production (Martens et al., 2004; Zhao et al., 2010). STING is thought to be located on the endoplasmic reticulum (ER), possibly at the interface between the mitochondria and the ER (Ishikawa and Barber, 2008). MAVS, on the other hand, is localized to the mitochondrial membrane (Seth et al., 2005). STING is downstream of a DNA-sensing pathway, and MAVs is an adaptor for RIG-I-like receptor (RLR) signaling, both of which stimulate Type I IFN expression (Belgnaoui et al., 2011; Tanaka and Chen, 2012).

Studies of human IRGM provide further evidence that Irgm1 and IRGM could play a role in the negative regulation of Type I IFN production. For example, IRGM has been associated with ATG5, which in turn has been shown to inhibit Type I IFN production by associating with mitochondria and binding MAVS. Association of an ATG5-ATG12 complex with MAVs inhibited Type I IFN production upon viral infection or double-stranded RNA stimulation of mouse embryonic fibroblasts (MEFs) (Jounai et al., 2007). Whether the process of autophagy was involved in this process was not definitively examined. IRGM could thus limit Type I IFN production by promoting the association of ATG5 with MAVs. Similar functions have been

shown for mitofusin 2 and Tu translation elongation factor, mitochondrial proteins that both induce autophagy and inhibit Type I IFN production (Lei et al., 2012; Yasukawa et al., 2009).

The importance of IRGM in regulating antiviral defense is underscored by a study that showed that IRGM is a common target of RNA viruses (Gregoire et al., 2011). Using yeast-2-hybrid arrays and bioinformatics analysis, Gregoire *et al* found that IRGM could interact with proteins from 5 different families of RNA viruses. They proposed that RNA viruses target IRGM to manipulate the autophagy pathway and enhance viral replication *in vitro*. However, it was unclear whether this mechanism was of importance *in vivo.* An alternative hypothesis would be that viruses target IRGM (or Irgm1) as a viral evasion mechanism because of its role in regulating the Type I IFN response. Interaction with IRGM could promote negative regulation of Type I IFN signaling and thus inhibit the antiviral response. While it is not known if Irgm1 and IRGM have similar functions, it would still be informative to investigate whether phenomena observed in humans are also found in mice, and vice versa.

Finally, a single study in a Chinese population also linked IRGM variants to SLE (Zhou et al., 2011). While this was a small study in a limited population, it would be revealing to see if the results hold up in a larger cohort. Since an elevation in Type I IFN signatures is associated with some forms of SLE, it would be wise to separate out the study population into Type I IFN-associated and unassociated. It is tempting to speculate that IRGM variants could also result in increased Type I IFN production in humans.

Finally, we observed that antibiotic treatment of *Irgm1*$^{-/-}$ mice did not normalize the Type I IFN levels. However, even a broad-spectrum antibiotic regimen does not completely eliminate all bacteria, and of course there could still be commensal viruses that could drive Type I IFN

production. It would be of interest to re-derive the *Irgm1*$^{-/-}$ mice into a germ-free facility, and determine whether Type I IFNs levels are still increased in the absence of any microbiota.

Based on the published literature and our current results, I propose that Irgm1 is important for the regulation of proteins at intracellular membranes. I speculate that Irgm1 regulates the ability of STING, MAVs, or downstream signaling components, to effectively localize to or function at the endoplasmic reticulum and the mitochondrial membrane, respectively. Thus, in the absence of Irgm1, these signaling pathways are increased and Type I IFN production augmented. It is possible that the variants observed in human IRGM could also influence Type I IFN levels and affect disease pathogenesis and/or progression in Crohn's disease and tuberculosis.

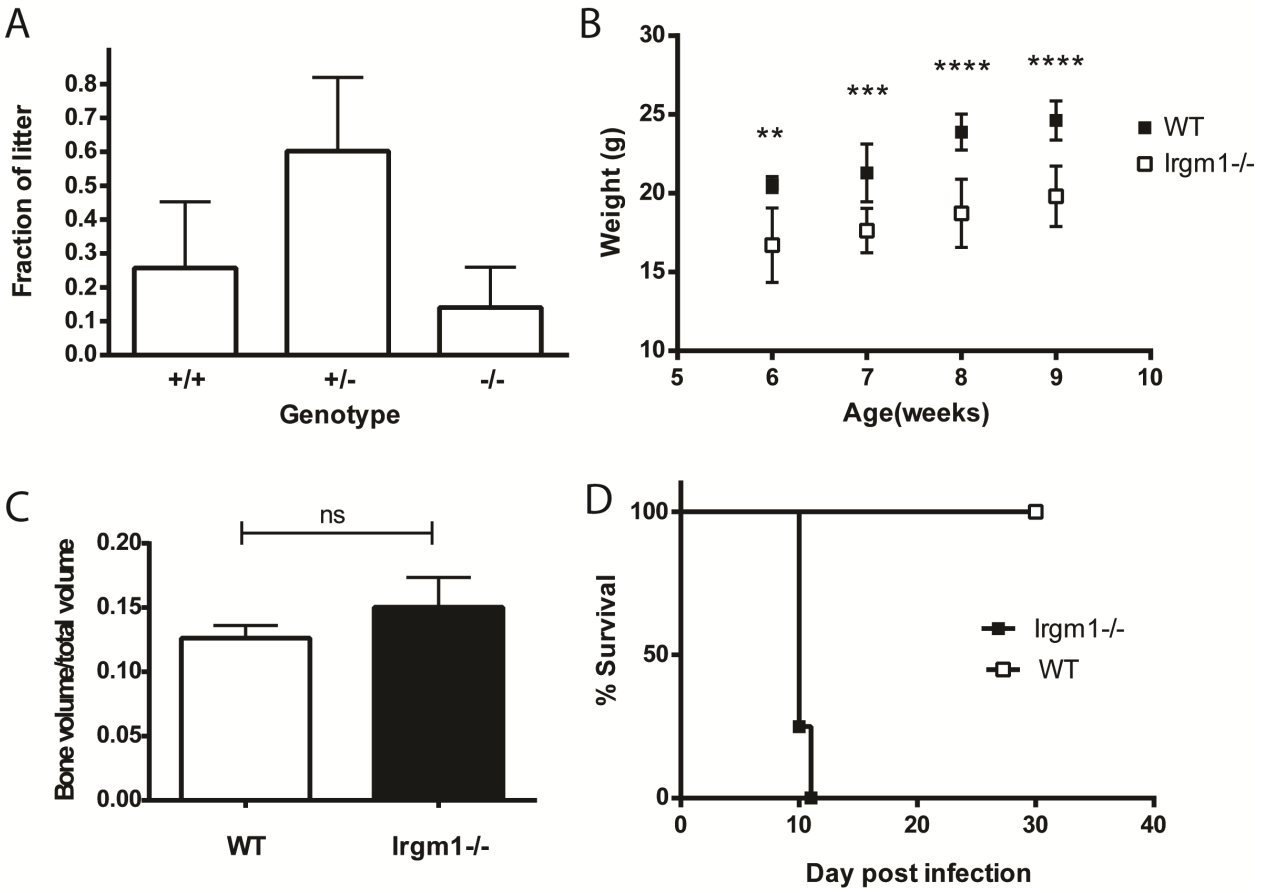

Figure 2.1. *Irgm1*$^{-/-}$ mice bred at near-Mendelian ratios, were slightly smaller than WT littermates, and were susceptible to *Toxoplasma gondii* infection. A) Graph of the average fraction ± standard deviation (SD) of *Irgm1*$^{+/+,}$ *Irgm1*$^{+/-}$ and *Irgm1*$^{-/-}$ mice for 36 litters (193 mice total). B) Graph of the average weights ± SD of differently-aged male Irgm1-/- mice compared to WT male littermates. N=4-15 per group per age. P<0.0001 by 2 way ANOVA. **p<0.01, ***p<0.001, ***p<0.0001 by Sidak's multiple comparisons test. C) Graph of the mean bone volume fraction of femurs of *Irgm1*$^{-/-}$ mice (n=2) and WT mice (n=3) at 12 weeks of age, as measured by microCT scanning of the long bones. D) Kaplan-Meier survival curve of *Irgm1*$^{-/-}$ mice (n=4) and age-matched WT mice (n=4) after oral infection with 7 cysts of *T. gondii* (Prugniaud strain). p<0.01 by log rank test.

Genotype	WT		Irgm1-/-		
	Avg.	St. Dev.	Avg.	St. Dev.	p value
TV (mm3)	0.8033	0.0789	0.9663	0.0583	0.0731
BV (mm3)	0.1221	0.0383	0.1214	0.0101	0.9778
BV/TV	0.1503	0.0328	0.1263	0.0171	0.3449
Conn.Dens (1/mm3)	95.7810	33.2861	57.5518	16.2248	0.1707
SMI	3.3401	0.4043	3.5395	0.2684	0.5441
Tb.N (1/mm)	5.8145	0.2448	5.0604	0.3097	0.065
Tb.Th (mm)	0.0505	0.0045	0.0551	0.0023	0.2197
Tb.Sp. (mm)	0.1758	0.0095	0.2040	0.0109	0.0603

Table 2.1. *Irgm1*$^{-/-}$ mice did not differ in multiple microCT femur measurements compared to WT mice. Table of multiple parameters measured by microCT of the femur in WT and *Irgm1*$^{-/-}$ mice. TV - total volume, BV - bone volume, Conn.Dens - connective density, SMI - structure model index, Tb. N- trabecular number, Tb.Th - trabecular thickness, Tb.Sp. - trabecular separation. WT n=3 mice, *Irgm1*$^{-/-}$ n=2 mice. P value shown is by Student's *t* test.

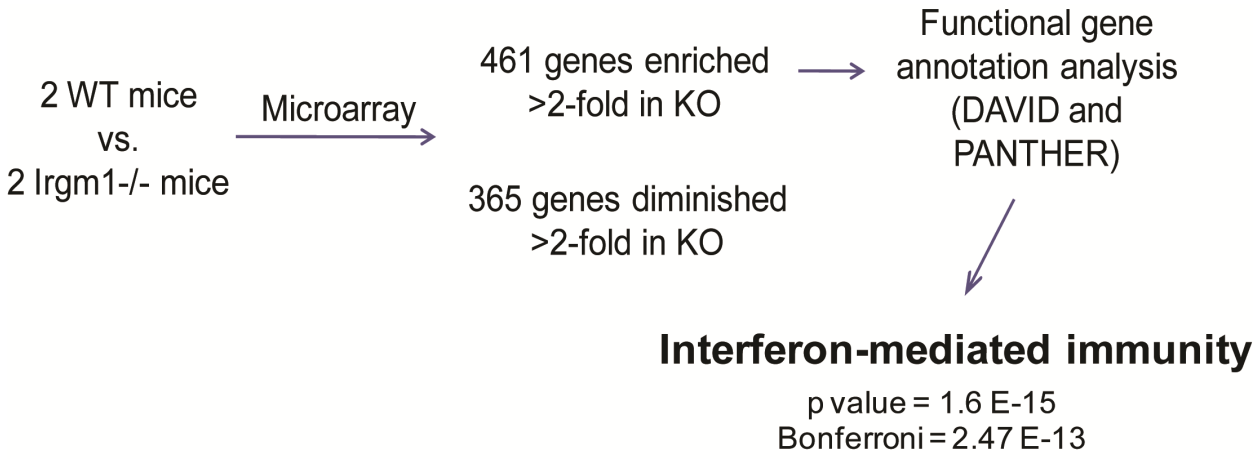

Figure 2.2. Microarray analysis of intestinal epithelium in *Irgm1*$^{-/-}$ and WT mice.

Microarray analysis was performed on RNA isolated from small intestinal epithelium of *Irgm1*$^{-/-}$ and WT mice by laser capture microdissection (n=2 mice each genotype). Functional gene annotation analysis of these genes identified significant elevations in "Interferon-mediated immunity" genes (Bonferroni value = 2.47 E-13).

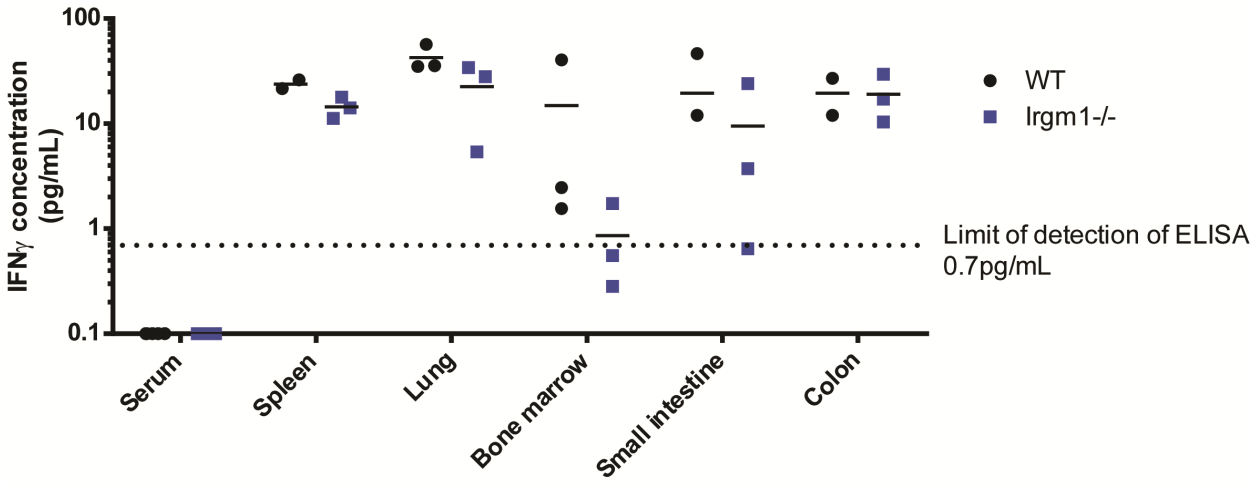

Figure 2.3. *Irgm1*$^{-/-}$ mice did not have elevated IFNγ in the serum or tissues. Graph of IFNγ levels as measured by ELISA in 6-9 week-old *Irgm1*$^{-/-}$ and WT serum, spleen, lung, bone marrow, small intestine and colon. The limit of detection by ELISA (0.7pg/mL) is indicated by the dotted line. N=2-4 mice per genotype for tissue homogenates; n=6 mice per genotype for serum samples. No significant differences were observed between WT and *Irgm1*$^{-/-}$ values in serum and all organs by Sidak's multiple comparisons test or by individual uncorrected Student's *t* test.

Annotation	Gene Symbol	Fold change (*Irgm1*$^{-/-}$/WT)
2'-5' oligoadenylate synthetase 2 (Oas2)	Oas2	11.8
immunoglobulin kappa chain complex (Igk) on chromosome 6	Rprl1	10.3
interferon-induced protein 44 (Ifi44)	Ifi44	5.0
similar to Interferon-activatable protein 203 (Ifi-203)	LOC623121	4.6
2'-5' oligoadenylate synthetase 1C (Oas1c)	Oas1c	4.5
interferon, alpha-inducible protein 27 like 2A	Ifi27l2a	4.1
ubiquitin specific peptidase 18 (Usp18)	Usp18	3.8
interferon-induced protein with tetratricopeptide repeats 2 (Ifit2)	Ifit2	3.4
myxovirus (influenza virus) resistance 2 (Mx2)	Mx2	3.4
interferon-induced protein with tetratricopeptide repeats 3 (Ifit3)	Ifit3	3.2
interferon-induced protein with tetratricopeptide repeats 1	Ifit1	3.1
2'-5' oligoadenylate synthetase 3 (Oas3)	Oas3	3.1
receptor transporter protein 4 (Rtp4)	Rtp4	3.0
immunoresponsive gene 1	Irg1	2.9

Table 2.2. Interferon-stimulated genes are enriched in *Irgm1*$^{-/-}$ intestinal epithelium compared to WT. Microarray data (see Figure 2) was manually inspected for genes expressed downstream of Type I IFN signaling (ISGs). The top 14 ISGs enriched in *Irgm1*$^{-/-}$ intestinal epithelium compared to WT intestinal epithelium are shown.

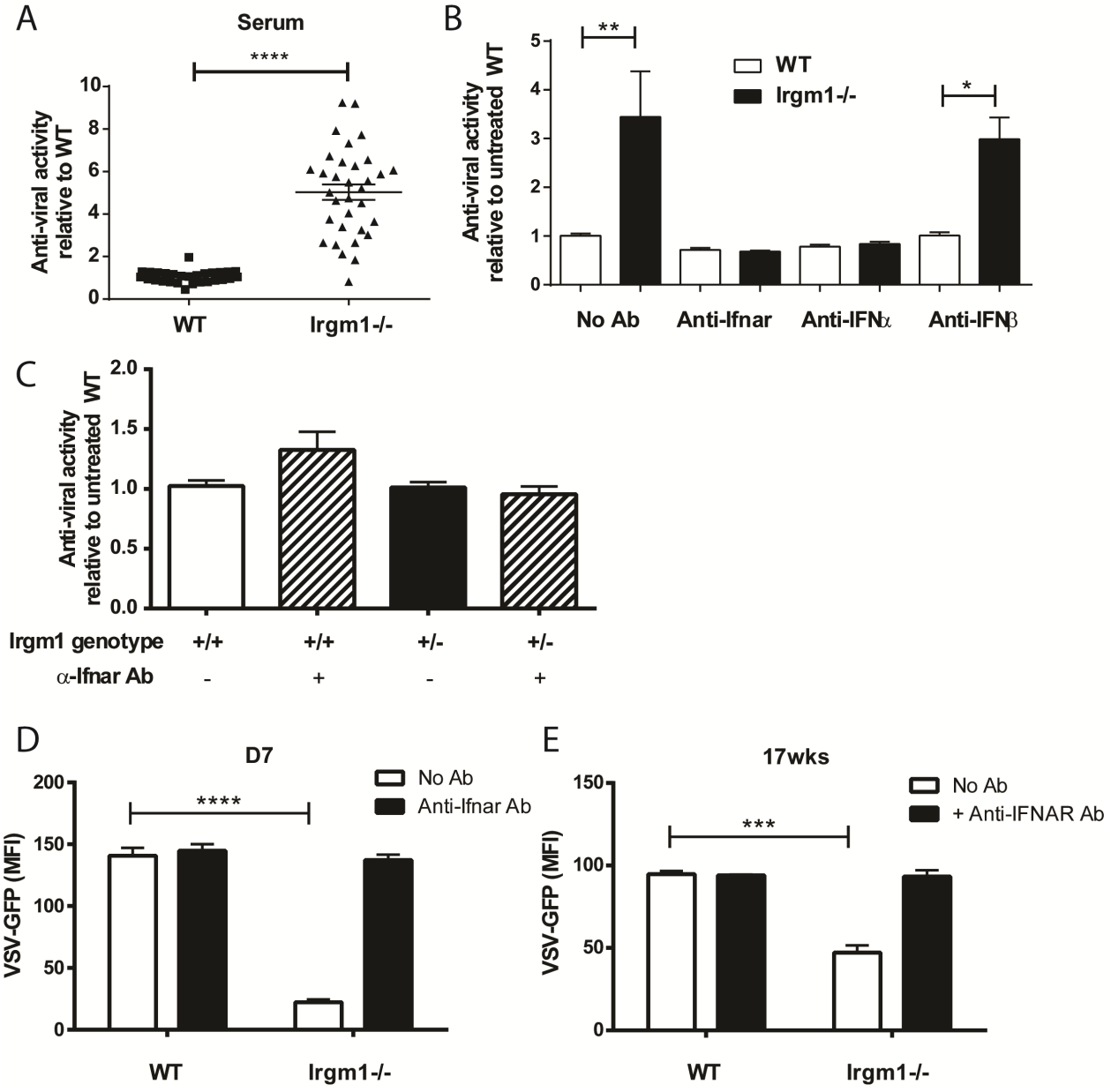

Figure 2.4. *Irgm1*$^{-/-}$ mice had persistent, elevated circulating Type I IFNs.

Figure 2.4. *Irgm1*$^{-/-}$ mice had persistent, elevated circulating Type I IFNs. A) Graph of antiviral activity measured in serum using a bioassay system (described in Fig. 5). Mean values ± SEM are plotted relative to WT. WT n=28 mice, *Irgm1*$^{-/-}$ n=33 mice from 9 independent experiments. B) Bars show anti-viral activity of WT and *Irgm1*$^{-/-}$ serum after administration of anti-Ifnar1 anti-pan-IFNα, and anti-IFNβ1 antibodies during the serum bioassay. WT n=4 mice, *Irgm1*$^{-/-}$ n=6 mice. C) Graph of average ± SEM of antiviral activity relative to untreated WT serum samples in the Type I IFN VSV-GFP bioassay. WT n=19 mice, *Irgm1*$^{+/-}$ n=7 mice. Means are not significantly different by one-way ANOVA. D) Graph of the average MFI ± SEM of VSV-GFP-infected L929 cells incubated with lung homogenate from WT and *Irgm1*$^{-/-}$ mice at 7 days of age. WT n=4 mice, *Irgm1*$^{-/-}$ n=3 mice. E) Graph of the average MFI ± SEM of VSV-GFP-infected L929 cells incubated with serum from WT and *Irgm1*$^{-/-}$ mice at 17 weeks of age. WT n=2 mice, *Irgm1*$^{-/-}$ n=4 mice. For B) to C), ***p<0.001; ****p<0.0001 by Sidak's multiple comparisons test.

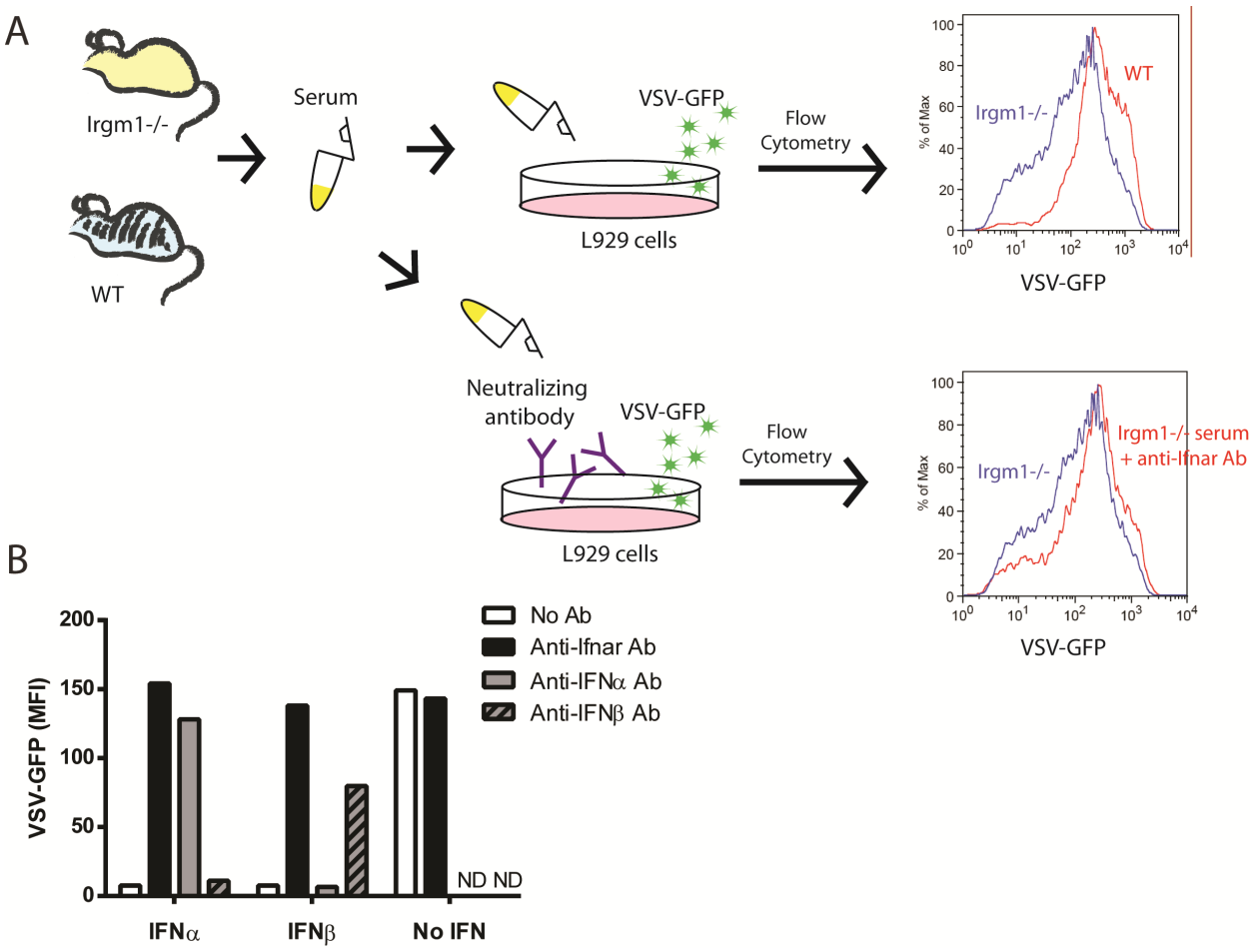

Figure 2.5. Description of Type I IFN bioassay and validation of antibody specificity.

Figure 2.5. Description of Type I IFN bioassay and validation of antibody specificity. A) Schematic of Type I IFN bioassay (Newby et al., 2007). L929 cells were incubated with serum or lung homogenate samples overnight, then infected with VSV-GFP for 10h. Levels of viral infection were measured as median fluorescence intensity (MFI) of L929 cells via flow cytometry. Antiviral activity relative to WT was calculated based on standard curves generated using recombinant IFNαA for each experiment. The addition of neutralizing antibodies during the incubation step allowed for determination of the source of antiviral activity. B) Graph showing the specificity of neutralizing antibodies. Plot shows the MFI of VSV-GFP-infected L929 cells incubated with 5 units/mL of recombinant murine IFNαA, 0.1 units/mL of recombinant murine IFNβ, or no type I IFNs added. Anti-Ifnar (black bar), anti-pan-IFNα (gray bar), and anti-IFNβ1 (gray striped bar) antibodies were administered. After VSV-GFP infection, levels of viral infection (MFI) were measured by flow cytometry. ND: not done.

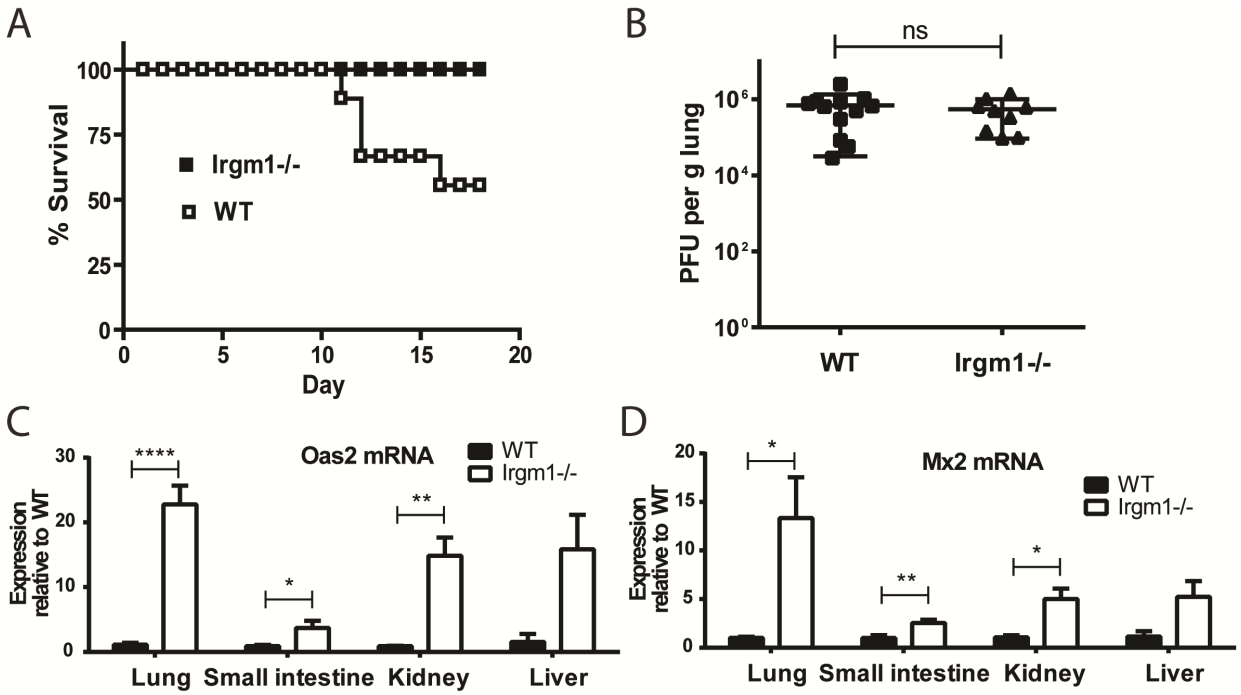

Figure 2.6. Elevated Type I IFNs in *Irgm1*$^{-/-}$ mice were functional and protected against influenza infection. A) Survival curve of 8-10 week-old male *Irgm1*$^{-/-}$ and WT mice upon infection with 5000 pfu of influenza A/33/WSN. n=9 mice per genotype compiled from 3 experiments. $p < 0.05$ by Kaplan-Meier analysis (log-rank test). Type I IFNs and Ifnar have been shown to be essential for host defense against influenza infection (Arimori et al., 2013; Koerner et al., 2007). *Ifnar*$^{-/-}$ mice succumb to flu infection within days, and we would expect that *Irgm1*$^{-/-}$*Ifnar*$^{-/-}$ mice would have similar susceptibility. B) Graph of influenza viral titers from whole lung homogenate of WT (n=12 mice) and *Irgm1*$^{-/-}$ (n=9 mice) mice 6 days after infection with 5000pfu influenza A/WSN/33 virus. Viral titers were measured by plaque assay. C) to D) Graphs of mean fold change ± SEM in B) Oas2 and C) Mx2 mRNA in *Irgm1*$^{-/-}$ tissues compared to WT tissues. N=2-9 mice per genotype per organ. *p<0.05; ** p < 0.01, ****p<0.0001 by Student's *t* test.

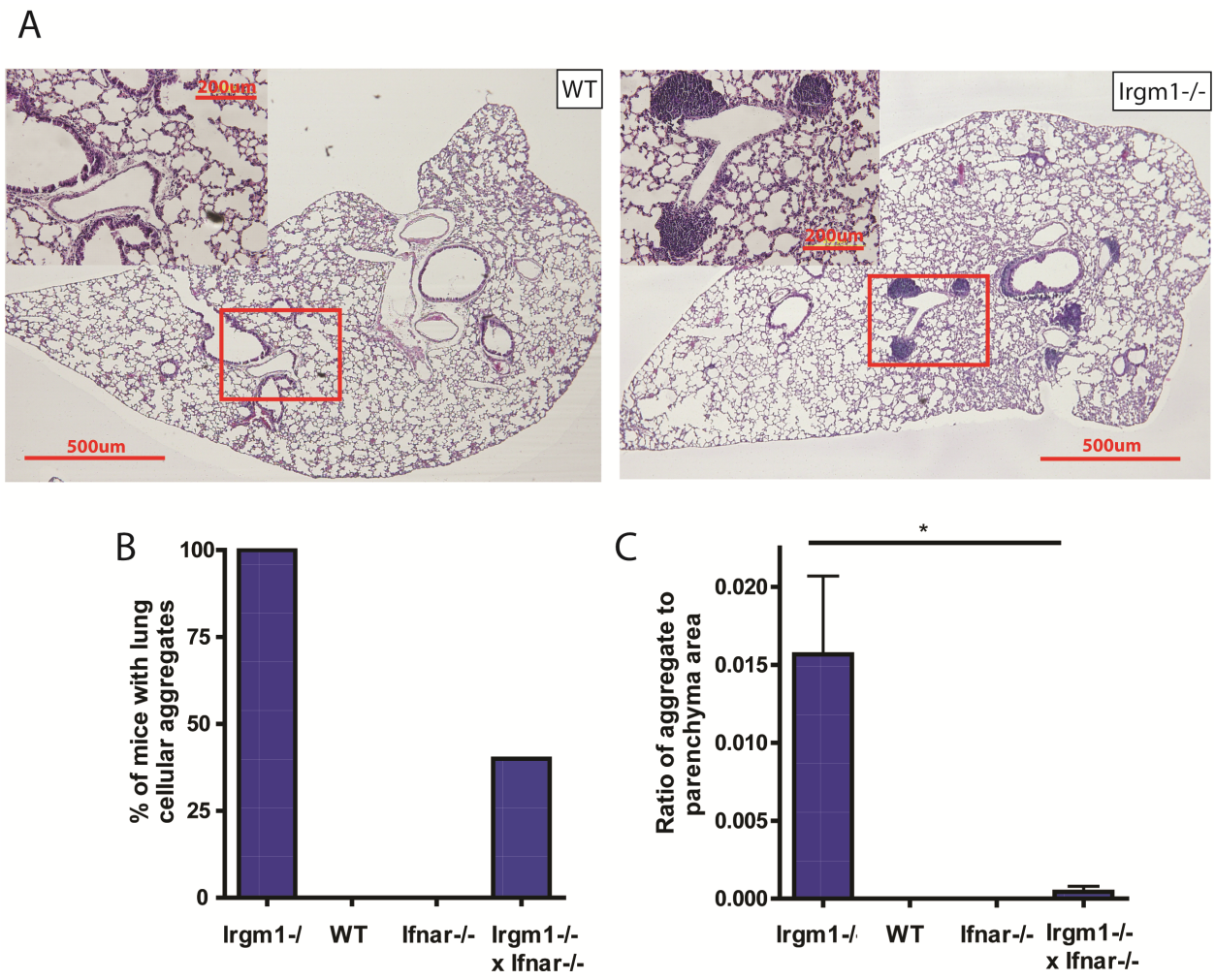

Figure 2.7. *Irgm1*$^{-/-}$ mice had Type I IFN-dependent cellular aggregates in the lung. A) Representative images of lung cross sections in WT and *Irgm1*$^{-/-}$ mice. Length of red bar in larger picture is 500µm; inset (red box) bar is 200µm. Graphs of B) the presence of lymphoid tissue aggregates and C) the average ratio ± SD of lymphoid tissue aggregate to lung parenchyma area was measured in *Irgm1*$^{-/-}$ (n=4), WT (n=4), *Ifnar*$^{-/-}$ (n=4), and *Irgm1*$^{-/-}$*Ifnar*$^{-/-}$ (n=5) mice using ImageJ software. *p<0.05 by Student's *t* test.

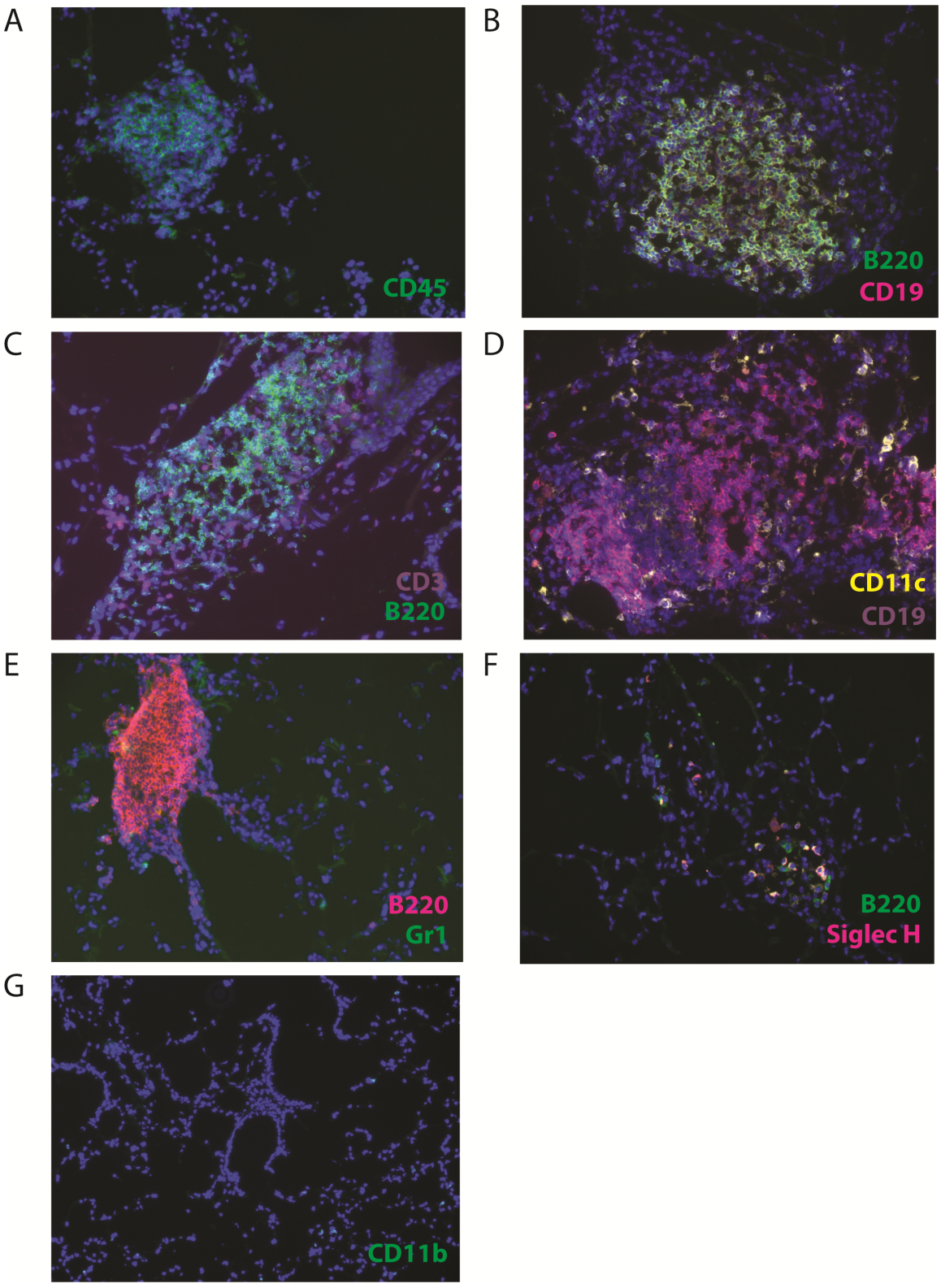
A
CD45
B
B220
CD19
C
CD3
B220
D
CD11c
CD19
E
B220
Gr1
F
B220
Siglec H
G
CD11b

Figure 2.8. Lung aggregates in *Irgm1*$^{-/-}$ mice were composed of a mixed lymphocyte and myeloid population.

Figure 2.8. Lung aggregates in *Irgm1*$^{-/-}$ mice were composed of a mixed lymphocyte and myeloid population. Representative immunofluorescence images of lung aggregates in *Irgm1*$^{-/-}$ mice. A) CD45 – green. B) B220 – green, CD19 – pink. C) CD3 – purple, B220- green. D) CD11c – yellow, CD19 – purple. E) B220 – pink, Gr1 – green. F) B220 – green, Siglec H – pink. G) CD11b – green. All images at 200X.

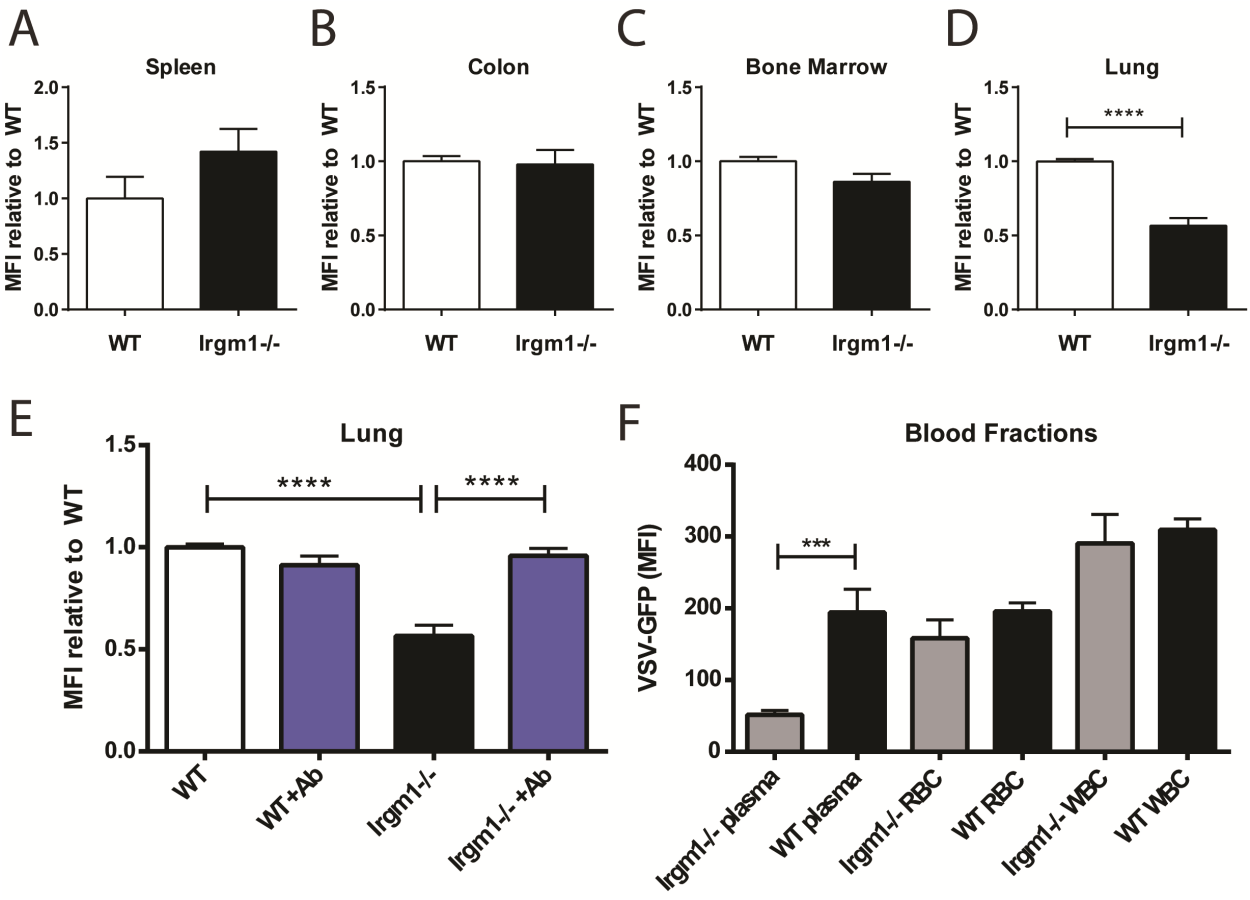

Figure 2.9. Antiviral activity was present in the lung and plasma fraction of the blood of *Irgm1*$^{-/-}$ mice. Graphs of the average median fluorescent intensity (MFI) relative to WT MFI ± SEM of VSV-GFP-infected L929 cells incubated with A) spleen, B) colon, C) bone marrow or D-E) lung homogenate, or E) blood fractions. A) WT n=4 mice, *Irgm1*$^{-/-}$ n=8 mice. B) WT n=6 mice, *Irgm1*$^{-/-}$ n=10 mice. C) WT n=12 mice, *Irgm1*$^{-/-}$ n=18 mice. D-E) WT n=23 mice, *Irgm1*$^{-/-}$ n=27 mice. F) WT n=2 mice, *Irgm1*$^{-/-}$ n=5 mice. *** p<0.001, ****p<0.0001 by Student's *t* test, or by Tukey's multiple comparisons test (E only).

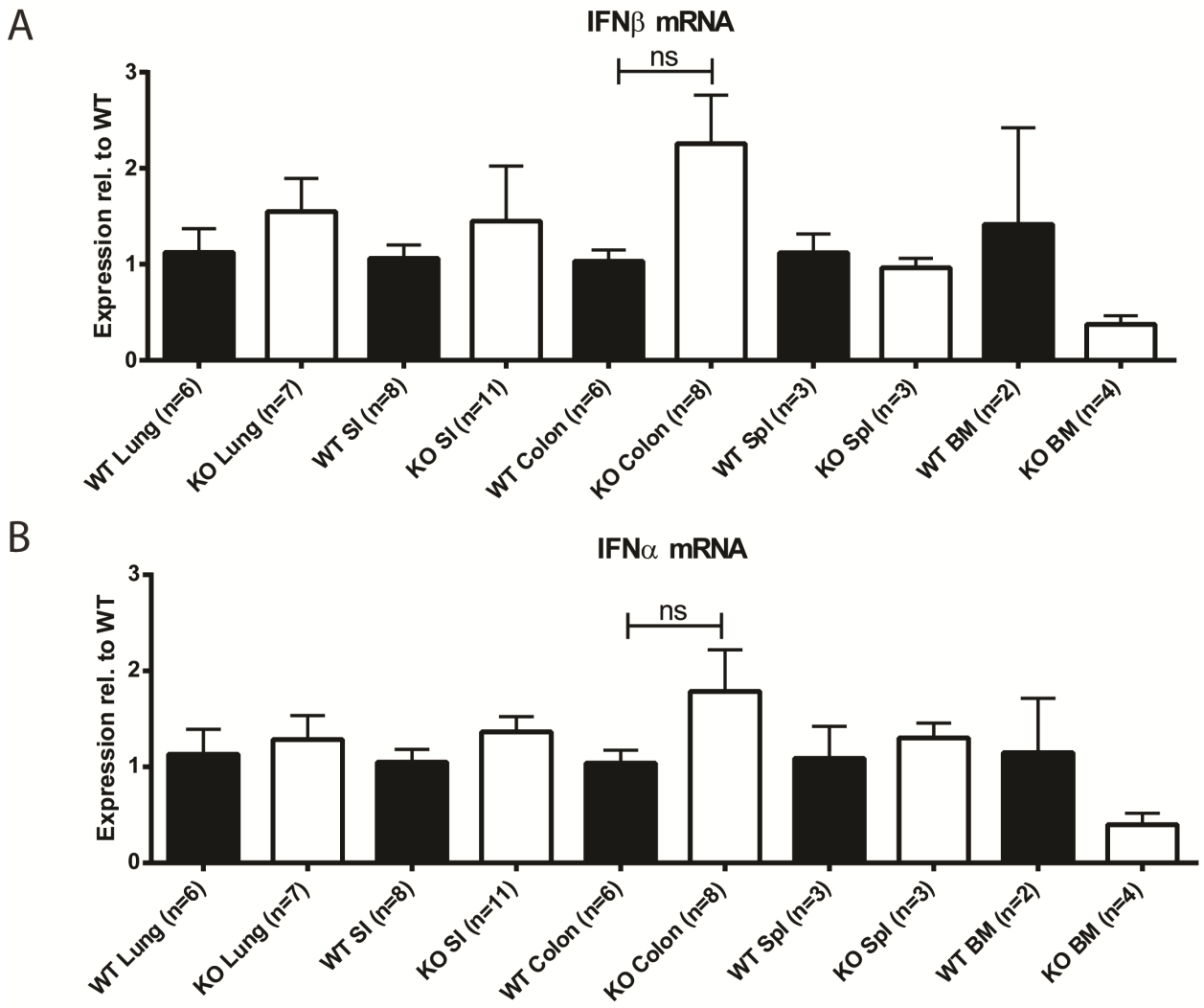

Figure 2.10. No significant differences were observed in IFNα and IFNβ1 mRNA between *Irgm1*$^{-/-}$ and WT organs. Graphs of A) IFNβ1 and B) pan-IFNα average mRNA expression relative to WT in lung, small intestine (SI), colon, spleen (Spl), and bone marrow (BM) homogenates in WT and *Irgm1*$^{-/-}$ (KO) mice. Ns as listed.

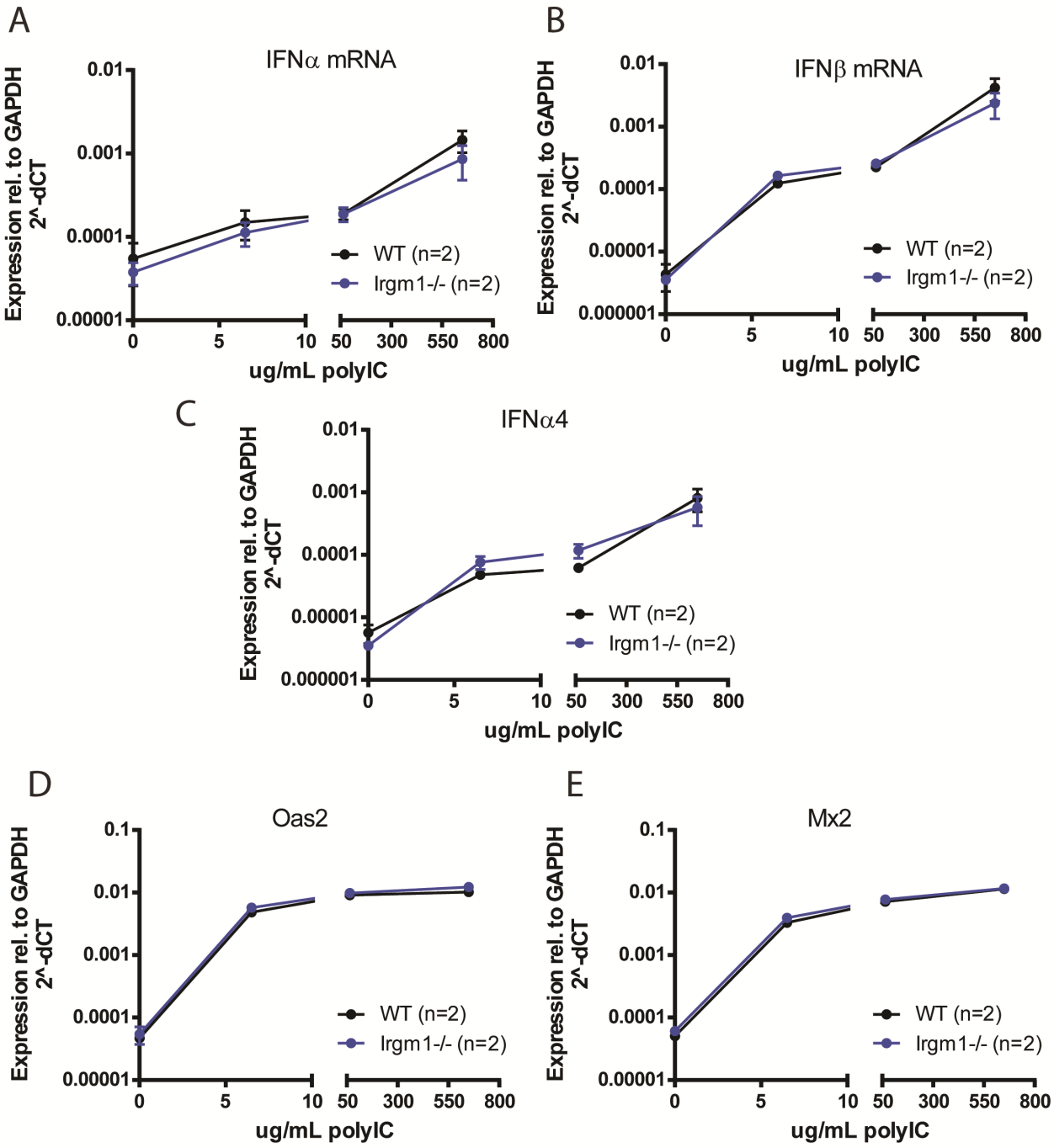

Figure 2.11. *Irgm1*$^{-/-}$ and WT bone marrow-derived dendritic cells (BMDCs) had similar sensitivity to polyI:C stimuli. Graph of A) pan-IFNα, B) IFNβ and C) IFNα4 average mRNA expression ± SEM in BMDCs after 24hr stimulation with increasing amounts of polyI:C. WT n=2 mice, *Irgm1*$^{-/-}$ n=2 mice with 2 technical replicates per sample.

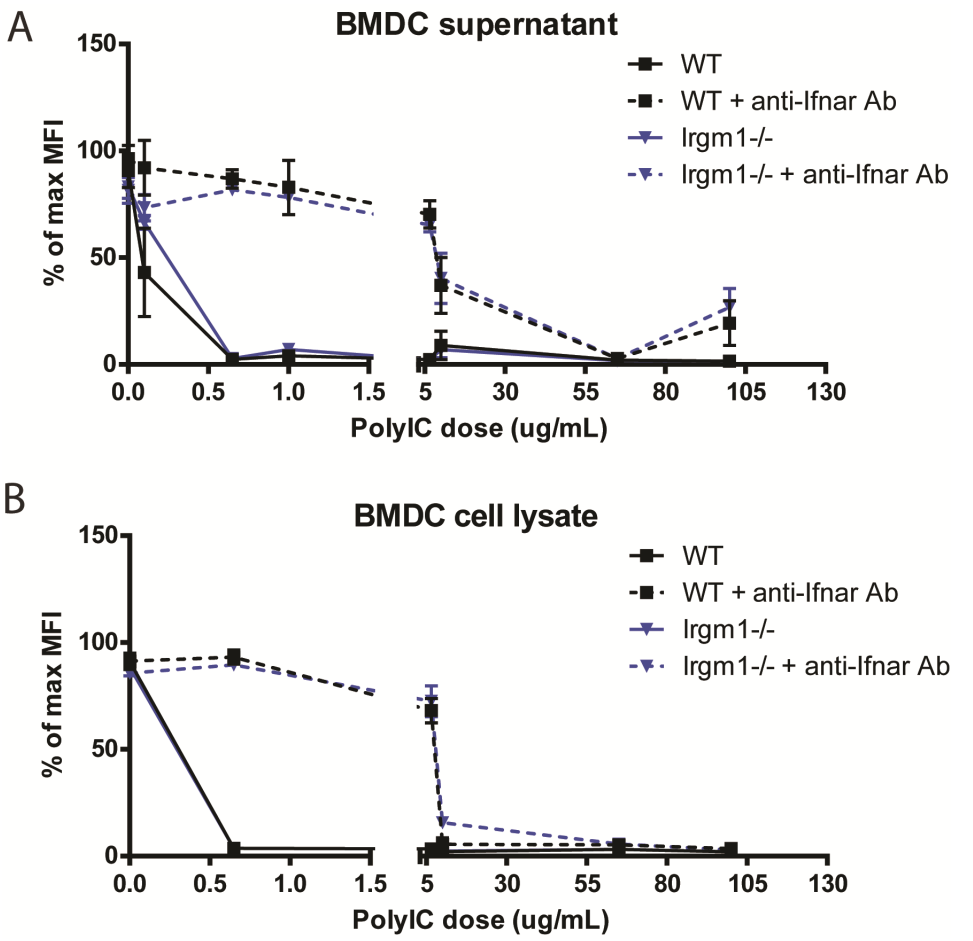

Figure 2.12. *Irgm1*$^{-/-}$ and WT bone marrow-derived dendritic cells had similar production of Type I IFNs in response to polyI:C. Graphs of the average Type I IFN activity ± SEM of A) BMDC supernatant and B) cell lysate 24hrs after administration of increasing polyI:C doses. Type I IFN activity is shown as percentage of maximum MFI as measured by bioassay. N=2-8 mice per genotype per dose. Data is compiled from 3 independent experiments.

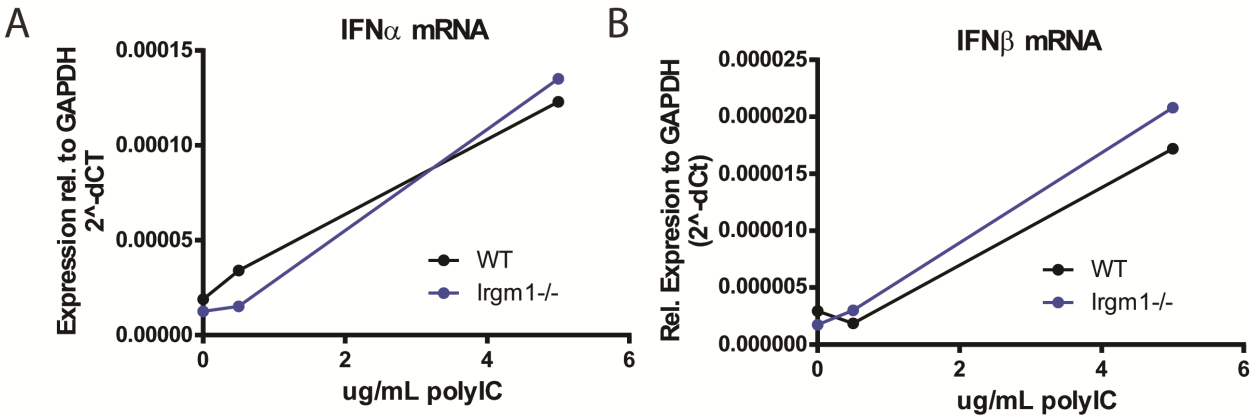

Figure 2.13. WT and Irgm1-deficient intestinal epithelial cells had similar Type I IFN production upon polyI:C treatment. Graphs of mRNA expression of A) pan IFNα, and B) IFNβ1 after increasing doses of polyIC were added to primary intestinal epithelial cells from WT and *Irgm1*$^{-/-}$ mice for 6 hours.

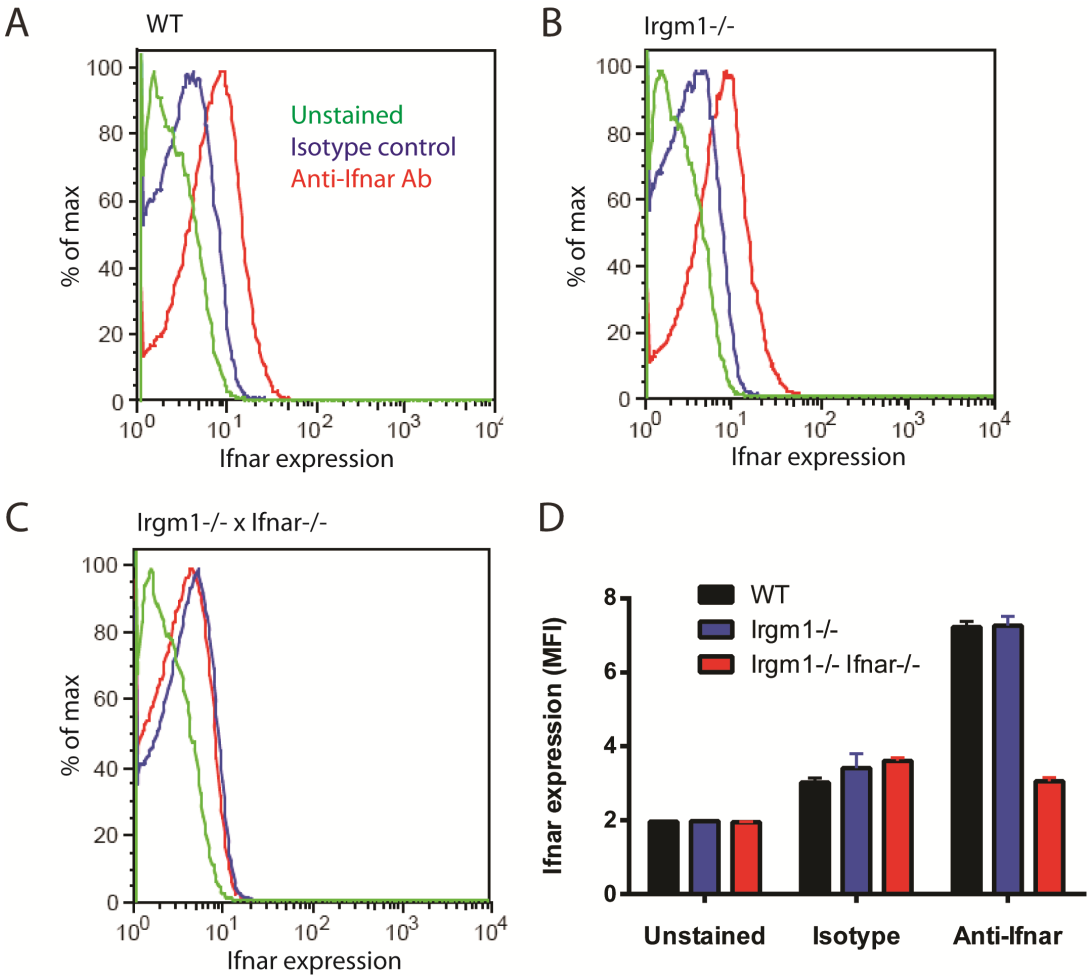

Figure 2.14. WT and Irgm-deficient bone marrow cells had similar levels of Ifnar cell surface expression. Representative flow cytometry histograms of A) WT, B) *Irgm1*$^{-/-}$, and C) *Irgm1*$^{-/-}$ *Ifnar*$^{-/-}$ whole bone marrow. D) Graph of the average MFI ± SEM of Ifnar expression in WT, *Irgm1*$^{-/-}$, and *Irgm1*$^{-/-}$ *Ifnar*$^{-/-}$ bone marrow using unstained cells, cells stained with isotype control, and cells stained with an anti-Ifnar antibody. N = 2 mice per genotype.

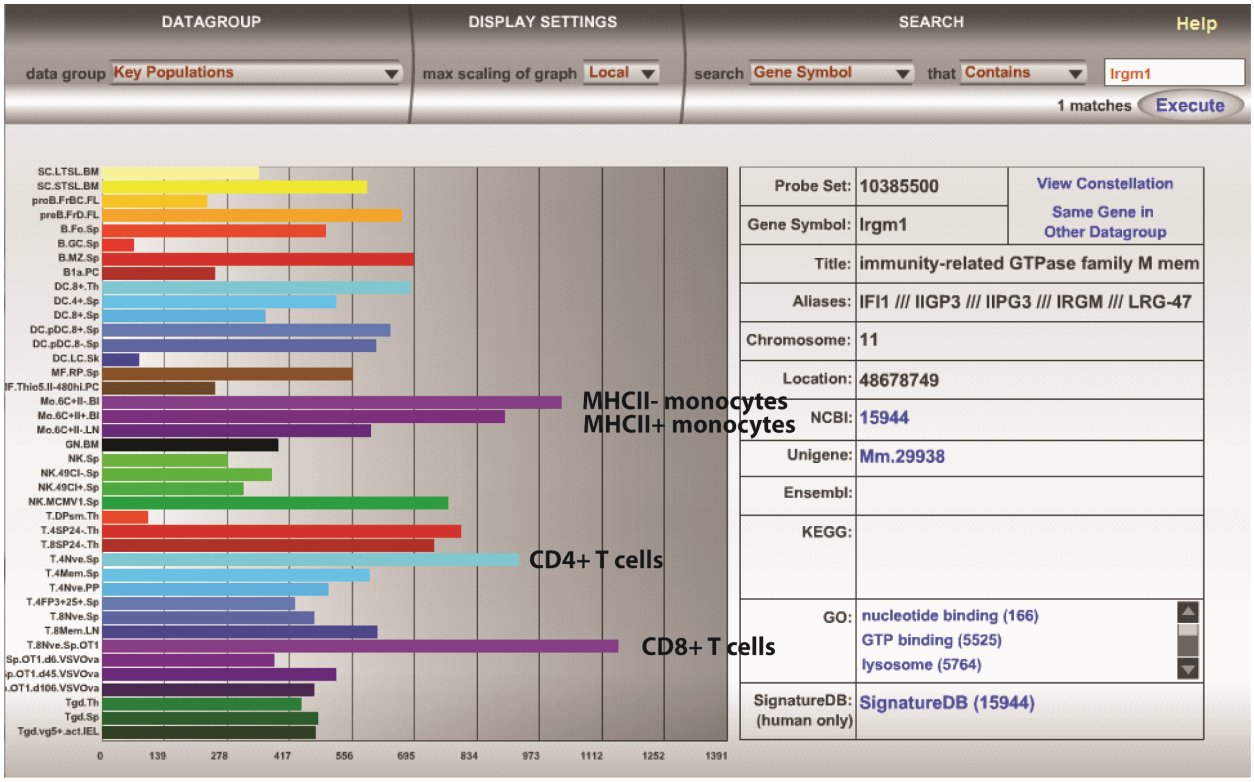

Figure 2.15. Irgm1 is expressed in T cells and monocytes. Immgen.org Gene Skyline display for murine gene Irgm1.

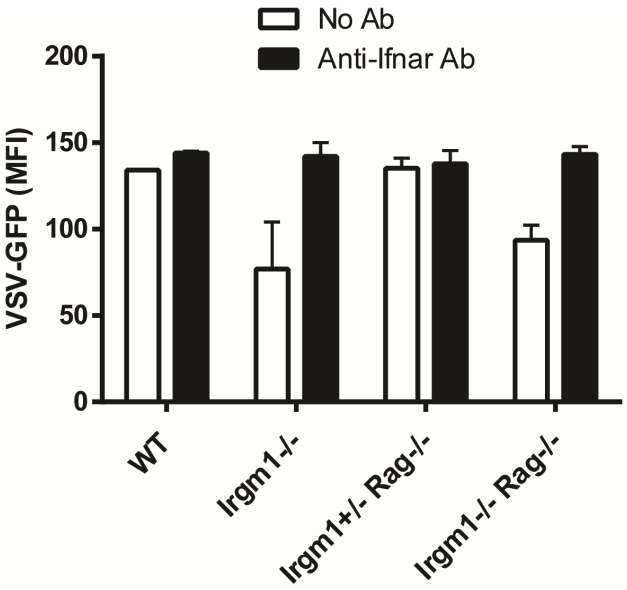

Figure 2.16. T and B cells were not required for elevated Type I IFN production in *Irgm1*$^{-/-}$ mice. A graph of average antiviral activity in serum is shown as diminished average median VSV-GFP expression ± SEM. Specificity for Type I IFN is shown in black bars by the addition of anti-Ifnar antibody (Ab). WT n=2 mice, *Irgm1*$^{-/-}$ n=2 mice, *Irgm1*$^{+/-}$*Rag1*$^{-/-}$ n=3 mice, *Irgm1*$^{-/-}$ *Rag1*$^{-/-}$ n=3 mice.

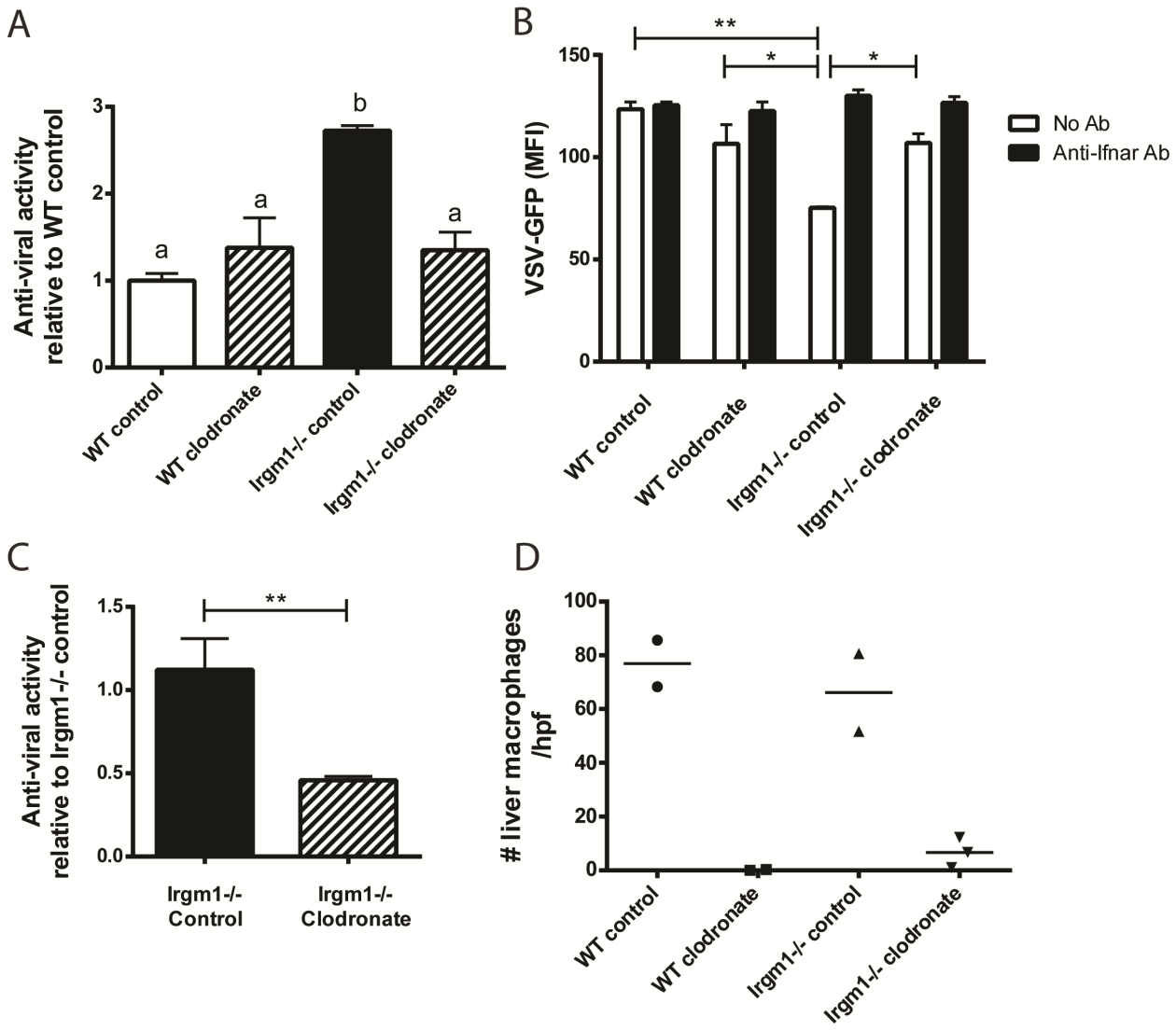

Figure 2.17. Liver macrophages played an important role in Type I IFN production in *Irgm1*$^{-/-}$ mice.

Figure 2.17. Liver macrophages played an important role in Type I IFN production in *Irgm1*$^{-/-}$ mice. For A-B), mice were injected i.v. with 250μL of liposomes on d0, d3, and sacrificed on d6. WT control n=2 mouse, WT clodronate n=2 mice, *Irgm1-/-* control n=2 mice, *Irgm1-/-* clodronate n=3 mice. A) Graph of antiviral activity relative to WT control ± SEM of serum from WT and *Irgm1-/-* mice injected with control and clodronate liposomes. Different letters indicate significantly different means by Tukey's multiple comparisons test. B) Graph of average MFI ± SEM of VSV-GFP-infected cells incubated with serum showing specificity for Type I IFN by the addition of anti-Ifnar antibody (Ab) (black bars). *$p<0.05$; ** $p<0.01$ by Tukey's multiple comparisons test. C) Graph of the average anti-viral activity ± SEM of serum from *Irgm1-/-* mice injected with control (n=7 mice) and clodronate (n=8 mice) liposomes. Data compiled from 2 independent experiments. **$p<0.01$ by Student's *t* test. D) Graph of the average number of liver macrophages counted per 200X high power field (hpf) after staining frozen liver sections with F4/80. 3 hpf were counted/mouse.

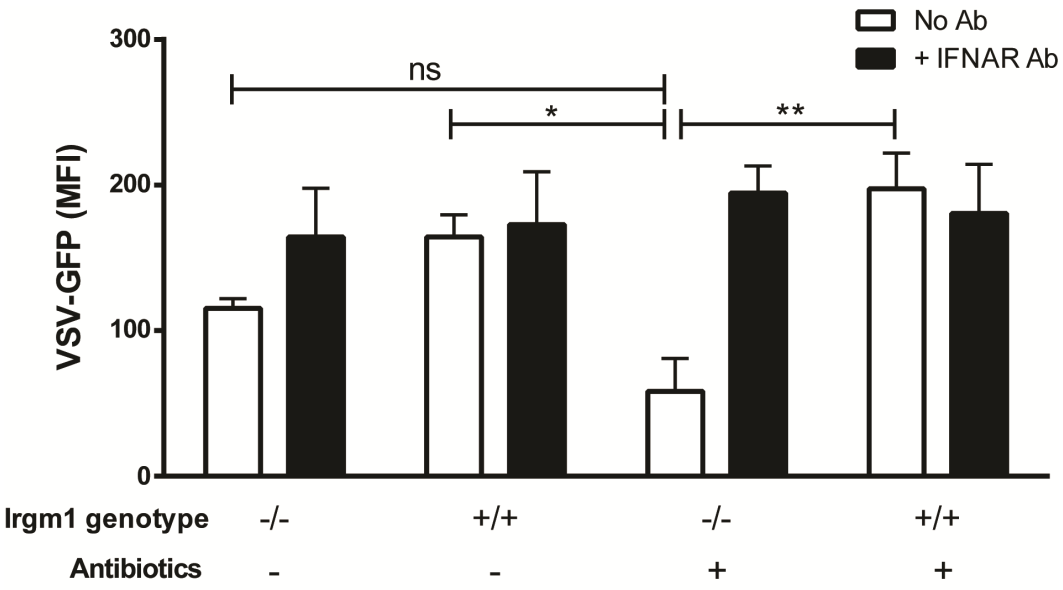

Figure 2.18. Antibiotic treatment did not decrease Type I IFNs in Irgm1-deficient mice.

Graph of the average Type I IFN activity ± SD (shown as levels of VSV-GFP MFI) in serum as measured by bioassay in mice after 2 weeks of antibiotic treatment (ampicillin, vancomycin, neomycin, metronidazole) or mock treatment (Kool-Aid). Antibiotic treated mice n=4 each genotype, vehicle-treated mice n=3 each genotype. * $p<0.05$, ** $p<0.01$, ns = not significant by Tukey's multiple comparisons test.

CHAPTER 3:

Type I Interferons link viral infection to enhanced epithelial turnover and repair

INTRODUCTION

Epithelial cells create lining and duct structures that are associated with many organs in the body (Blanpain et al., 2007). One major function of these structures is to provide a first-line barrier of protection against the environment (Ashida et al., 2012; Diamond et al., 2000). A central component of this protection is cellular turnover. This is a highly regulated process of shedding and regeneration of differentiated cells while at the same time maintaining barrier integrity. Loss of balance in this process (i.e. complete loss of regenerative capacity) results in the eventual loss of barrier function. This concept is most obvious in the intestine, which normally has a high epithelial turnover rate (Kuhnert et al., 2004; Lee et al., 2009). At homeostasis, each distinct epithelial structure has a different rate of turnover, but the determinants of these unique rates are poorly understood (Blanpain et al., 2007; Pellettieri and Sanchez Alvarado, 2007).

Regardless of the intrinsic rate within a specific organ, turnover rates must be capable of modulation in response to injury so that wound repair can efficiently occur. Damaged epithelial cells must be shed and rapidly replaced with new cells generated by self-renewing stem cells (Blanpain et al., 2007). In more severe injuries, stem cells themselves must also be replaced and reorganized (Ito et al., 2007; Miyoshi et al., 2012). Examples of damage that can alter turnover rates of the remaining stem cells include irradiation, malnutrition, and bacterial and parasitic infection (Cliffe et al., 2005; Creamer, 1967; Luperchio and Schauer, 2001; Rijke et al., 1975).

The microbiome of the host is a key component of the environment that is involved in homeostasis and injury response (Lai et al., 2009; Packey and Ciorba, 2010; Pfefferle and Renz, 2014; Scales and Huffnagle, 2013). The virome is a relatively unexplored component of the microbiome and is the complex collection of chronic viruses within a given host (Virgin, 2014;

Virgin et al., 2009). The role of these chronic viral infections in epithelial cellular turnover has not been previously addressed.

Type I interferons (IFNs) are a candidate for mediating systemic alterations in response to viruses. Type I IFNs are a family of innate immune cytokines that are produced as a result of viral and other types of infection (Durbin et al., 2000; Muller et al., 1994) . They include multiple IFNαs, IFNβ, and other subtypes (Hardy et al., 2004; Pestka et al., 2004). Once expressed and secreted from the cell, Type I IFNs all bind to a common Type I IFN receptor, IFNAR, which is expressed on most cell types (de Weerd et al., 2007). Despite sharing a single receptor, Type I IFNs can have different cellular effects depending on the IFN subtype (α1 vs β, etc.), the cell type, and the context (i.e. additional cytokine signals) (de Weerd and Nguyen, 2012; Ivashkiv and Donlin, 2014; Thomas et al., 2011). IFNAR lacks intrinsic kinase activity, and is constitutively associated with the Janus kinases (JAKs) (Platanias, 2005). Upon ligand binding, the JAKs phosphorylate the receptor and the signaling transducers and activators of transcription (STATs) molecules (de Weerd et al., 2007). Upon phosphorylation, STATs form complexes that translocate to the nucleus to induce the expression of hundreds of interferon stimulated genes (ISGs).

It has been challenging to decipher the effects of Type I IFNs and downstream ISGs on certain host physiologic processes such as epithelial turnover due to their critical and direct role in anti-viral defense. However, ISGs can be involved in a plethora of additional cellular processes. These include apoptosis, transcriptional activation and repression, modulation of immune cells and cytokine expression, protein degradation, and post-transcriptional regulation of gene expression (de Veer et al., 2001). The diversity of ISGs allows for pleiotropic responses and the fine-tuning of host reactions to infection. Nevertheless, the functions of many ISGs are yet to

be discovered, as it is difficult to use viral infection models to clarify the consequences of Type I IFNs and ISGs on host physiology. To definitively show that Type I IFNs mediate an effect, loss of function studies are required, but deficiency of Type I IFNs during a viral infection typically results in unhindered viral replication, alterations in the immune response, and significant morbidity and mortality. For example, loss of Type I IFN signaling during infection with murine homologues of ubiquitous chronic viruses such as herpesvirus and cytomegalovirus results in increased viral titers and mortality (Barton et al., 2005; Chong et al., 1983; Dutia et al., 1999; Grundy et al., 1982). Here, we use an *in vivo* model, the *Irgm1*$^{-/-}$ mouse, that we found has persistently elevated Type I IFNs in the absence of pathogenic viral infection and thus allowed us to study the impact of Type I IFNs on host physiology. We showed that chronic viral infection promoted epithelial turnover in multiple organs and was associated with enhanced injury repair. We then demonstrated that Type I IFNs signaling through macrophages promoted epithelial proliferation via novel functions of the ISGs, *Apolipoprotein L9a* and *b*.

MATERIALS AND METHODS

Mice

All experimental procedures were performed under approval by Washington University's Animal Studies Committee. *Irgm1*$^{-/-}$ mice were provided by Dr. Gregory A. Taylor (Duke University, Durham, NC; (Collazo et al., 2001)). *Ifnar*$^{-/-}$ mice are deficient in *Ifnar1* (Muller et al., 1994) and *Ifnar*$^{f/f}$ mice have a floxed allele of *Ifnar1 (Kamphuis et al., 2006)*. These mice were provided by Dr. Robert D. Schreiber and Dr. Herbert W. Virgin (Washington University in St. Louis, St. Louis, MO; (Thackray et al., 2012)). *Villin-Cre* (Madison et al., 2002) and *LysM-Cre* (Clausen et al., 1999) mice were obtained from Jackson labs. All mice were re-derived into our enhanced barrier facility and were fully backcrossed to a C57BL/6 background. For experiments with knockout mouse lines, heterozygote breeding pairs were used to obtain WT controls. For experiments using lineage specific knockouts, heterozygous crosses were used to generate Cre-negative controls. *Cdc25A-CBRLuc* reporter mice were generated on a B6(Cg)-Tyr^{c-2J}/J (B6-albino) background. Briefly, a targeting construct containing DNA encoding a fusion protein of Cdc25A and click beetle red luciferase (CBRLuc) was knocked-in to the Cdc25A locus by homologous recombination. Mice were backcrossed using speed congenics to create the *Cdc25A-CBRLuc* congenic mouse line.

In vivo treatment of mice

For murine cytomegalovirus (MCMV) infection, 6-8 week-old male and female mice were injected intraperitoneally (i.p.) with $5x10^4$ plaque-forming units (pfu) MCMV Smith strain (salivary gland-derived). Mice were sacrificed 7 days post-infection. For gammaherpesvirus 68 (MHV68) infection, 6-8 week-old male and female mice were injected i.p. with $1x10^6$ pfu virus.

Mice were sacrificed 7 days post-infection. Titer determinations for both MCMV and MHV68 were performed on NIH 3T12 fibroblasts with methylcellulose overlay as previously described (Canny et al., 2014). The limit of detection of the MCMV plaque assays was 40PFU/organ, while the limit of detection of the MHV68 assay was 100PFU/organ. For polyinosinic:polycytidylic acid (polyI:C) experiments, 5mg/kg polyI:C (GE Healthcare Life Sciences) diluted in sterile saline or saline alone was injected intraperitoneally (i.p.) once every 24h for 4 days. Mice were sacrificed on day 5. For neutrophil-depletion experiments, 500μg/mouse of monoclonal anti-Ly6G antibody (BioXCell) or rat IgG2a isotype control (BioXCell) diluted in 250μL sterile saline was injected i.p. one day prior and 2 days following the onset of polyI:C injections.

Enzyme-linked immunosorbent assay

The mouse angiogenesis ELISA strip for profiling 8 cytokines (Signosis) was used to measure levels of pro-proliferative cytokines in serum diluted at either 1:10 or 1:5 in assay diluent.

Type I IFN bioassay

Type I IFN bioassay was performed as previously described in Chapter 2 Materials and Methods (Newby et al., 2007).

RNA isolation and Quantitative real-time PCR

RNA isolation and qPCR was performed as described in Chapter 2 Materials and Methods.

Tissue histology

Tissue sections were harvested and fixed in Bouin's fixative, methacarn, or 10% neutral-buffered formalin for 3h at room temperature (RT), 1-2h at RT, or overnight at 4°C, respectively. Sections were then washed in 70% ethanol and stored at 4°C until blocking. Organs were blocked in 2% agar, paraffin-embedded, and 5µm sections were cut. Epithelial mitotic figures were quantified from H+E-stained sections of Bouin's fixed small intestines. Crypt depth was measured from the same sections by ImageJ software. All slides were blinded prior to quantification.

Ki67and β-catenin staining

Ki-67 immunohistochemistry staining was performed on formalin-fixed sections by first performing antigen-retrieval with heated 10mM citrate buffer (pH 6.0). Antibody staining was completed with rat monoclonal anti-Ki-67 primary antibody (clone TEC-3: DAKO) at a 1:100 dilution followed by a mouse-adsorbed rabbit anti-rat biotinylated secondary antibody (Vector Laboratories) at a 1:200 dilution. Staining was visualized by Vectastain ELITE ABC kit (Vector Laboratories) and DAB (3,3'-diaminobenzidine) peroxidase substrate (Vector Laboratories). The number of Ki67 positive cells per high power field (hpf) at 400X was quantified. β-catenin staining was performed on formalin-fixed sections without antigen retrieval. The primary antibody used was a mouse monoclonal antibody (BD Transduction Laboratories C19220) at a 1:1000 dilution, and the secondary antibody was a biotinylated goat anti-mouse IgG diluted 1:200. DAB staining was visualized as described above for Ki67.

Terminal deoxynucleotidyl transferase dUTP nick end labeling (TUNEL)

TUNEL staining was carried out on formalin-fixed, paraffin-embedded sections. Labeling was done with terminal transferase (New England Biolabs M0315S) and DIG-dUTP (Roche 11093088910) for 2h at 37°C. Anti-DIG-AP FAb fragments were applied for 1h at RT. Alkaline-phosphatase staining was then visualized with nitro blue tetrazolium chloride (NBT) (Roche 11383213001) and 5-bromo-4-chloro-3-indolyl phosphate (BCIP) (Roche 11383221001).

Thymidine analog experiments

BrDU/FrDU (5-Bromo-2'-deoxyuridine/5-Fluoro-2'-deoxyuridine; Sigma) was injected intraperitoneally 1h before sacrifice. Goat anti-BrDU was used to label S phase cells. The number of BrDU positive cells per 50 crypts was counted. IdU (Sigma I7125) and CldU (Sigma C6891) were prepared in sterile saline at a concentration of 4mg/mL and 17mg/mL, respectively. CldU was injected i.p. at 42.5mg/kg 36 h before sacrifice and IdU at 42.5mg/kg 24h before sacrifice. Detection of CldU was performed with rat anti-BrdU (clone BU1/75: Accurate Chemical and Scientific Corporation, #OBT0030) and Alexa 594-conjugated donkey anti-rat antibody (Life Technologies). IdU was detected using mouse anti-BrdU (clone B44: BD #347580) and Alexa 488-conjugated donkey anti-mouse antibody (Life Technologies). The distance migrated in a 12h period was calculated by measuring the distance between the highest positioned CldU-stained cell and the first IdU-stained cell (along the crypt-villus axis) using ImageJ software.

Intestinal spheroid epithelial culture

Colonic and small intestinal crypts were isolated from mice and cultured in a 3D-Matrigel as described in Chapter 2 Materials and Methods.

EdU Click-iT cell cycle flow cytometry assay

For serum and recombinant interferon experiments, cells were incubated with 5% L-WRN conditioned media at 37°C for 24h after passage, washed, and then treatment was added for an additional 24h. 10μM EdU was administered at 22h post-treatment. 2h later, spheroids were isolated out of 3D culture in PBS-EDTA. A single cell suspension was obtained by trypsinization. The EdU Click-iT Flow Cytometry Assay kit (Invitrogen) was then used to determine the percentage of S-phase cells according to the manufacturer's instructions. Flow cytometry data was analyzed using FloJo software.

Microarray

RNA was extracted using an RNeasy kit (Qiagen) from small intestine tissue, submandibular salivary gland tissue, and colonic macrophages. Colonic macrophages were isolated as previously described (Malvin et al., 2012). RNA from colonic macrophages was amplified using a complete whole transcriptome amplification kit (Sigma WTA2 kit). Microarray analysis was performed on 4x44K mouse whole genome microarrays (Agilent) as previously described (Cadwell et al., 2010). Hierarchical clustering and statistical analysis were performed using Partek software.

In situ hybridization

Probe synthesis and *in situ* hybridization was performed as previously described (Miyoshi et al., 2012) with the exception that tissue was fixed in methacarn solution (60% MeOH, 30% chloroform stabilized with ethanol, 10% acetic acid) followed by paraffin embedment. Anti-sense RNA probe was synthesized from an Apol9a cDNA clone (clone ID: 2649139, GE Healthcare).

293FT supernatant harvest and transfer

293FT cells were plated in a 90mm dish with antibiotic-free media for 24h. Media was changed and 10ug of Apol9a-Myc-DDK (Origene, Accession No. NM_001162883) plasmid transfected with lipofectamine. The next day, cells were washed and media was changed to serum-free primary epithelial cell culture media. Supernatant was harvested 24h later and spun down to remove cells. Flag-tagged protein was then detected by immunoblotting (see below). For supernatant transfer experiments, 293FT cells were plated as above and transfected with untagged Apol9a (clone ID: 2649139, GE Healthcare). Cells were washed the next day and media was changed to serum-free primary epithelial cell culture media. Supernatant was harvested 24h later and concentrated 5X with Centriprep Centrifugal filter units (Millipore) that enables concentration of proteins >10kDa. Supernatant was then diluted 1:1 with 50% L-WRN conditioned media and incubated with primary intestinal epithelial cells for 24h before cells were harvested for RNA and qRT-PCR analysis.

Lentivirus expression in intestinal epithelial spheroid cultures

Apol9a (clone ID: 2649139, GE Healthcare), Rspo3 (Miyoshi et al., 2012), and puromycin (negative control) cDNAs were individually cloned into C274-IRES-GFP lentivirus constructs. Virus was generated in 293FT cells, and concentrated with PEG-it virus precipitation solution (Miyoshi and Stappenbeck, 2013). Spheroid cells were trypsinized into single cell and multi-cell clusters, suspended in media, and incubated with virus constructs for 6h at 37°C in the presence of ROCK inhibitor (Y27632, R&D Systems). Cells were then plated in Matrigel and expanded as described above.

Characterization of the proliferation reporter Cdc25A-CBRLuc

Mice were injected intraperitoneally with D-luciferin (Biosynth, 150 mg/kg body weight). Within 30min of injection, mice were sacrificed and organs were rapidly isolated. Imaging was performed using an IVIS Lumina at 37°C (Caliper) using the following acquisition parameters: Exposure time-5min, Binning-8, no filter; f/stop, FOV-12.5cm. Grayscale photographs and color luciferase images were superimposed and analyzed with Living Image software 3.2 (Caliper) and Igor (Wavemetrics) image analysis software (Gross and Piwnica-Worms, 2005).

Bioluminescence imaging of whole organs and intestinal epithelial spheroids

Colonic crypts were isolated from knock-in mice that were homozygous (*ALuc/ALuc*) for the Cdc25A-CBRLuc fusion protein and intestinal spheroids were cultured in conditioned media as described above. For initial luminescence imaging, spheroids were trypsinized and seeded onto 96-well plates. After overnight culture, fresh media with 300µg/ml D-luciferin (Biosynth) was added to each well, and 30 min later, cells were imaged at 37°C in an IVIS Lumina (Caliper)

using the following acquisition parameters: Exposure time-3min, Binning-8, no filter; f/stop, FOV-12.5cm. To measure photon flux, Regions of Interest (ROIs) of identical size were drawn over every well (red square grids) and analyzed as photons emitted per second. Identical instrument, field of view, f-stop, exposure and binning settings were used within an experiment. Color luciferase images and grayscale photographs were superimposed and analyzed with Living Image software 3.2 (Caliper) and Igor (Wavemetrics) image analysis software. For luminescence experiments with lentivirus construct-expressing cells, spheroids were trypsinized and seeded onto 96-well plates. Media containing 200µg/mL D-luciferin (Biosynth) was added to each well, and 20-30min later, cells were imaged at 37°C in an Envision Multilabel Plate reader (Perkin Elmer) with a 1 second exposure per well. Luminescence was reported as relative light units. Luminescence was measured every 4h for 24h and the fold change in luminescence relative to luminescence measured at 4h was plotted. In MEK inhibitor experiments, different concentrations of U0126 (Promega) in DMSO or DMSO alone was added once immediately after seeding cells.

MTS assay of intestinal spheroids

To measure the number of viable cells, intestinal epithelial spheroids were plated as described above and subjected to MTS assay (tetrazolium compound [3-(4,5-dimethylthiazol-2-yl)-5-(3-carboxymethoxyphenyl)-2-(4-sulfophenyl)-2H-tetrazolium, inner salt; MTS) and an electron coupling reagent (phenazine methosulfate; PMS) as described by CellTiter 96® AQueous Assay Kit (Promega). Metabolism of MTS to soluble formazan by living cells was measured by absorbance at 490 nM using a luminometer (Multiskan). All graphs were plotted using Kaleidagraph software (Synergy).

Phospho-kinase dot blot array

A phospho-kinase array kit (R&D) was used according to the manufacturer's instructions. Briefly, control, Rspo3- and Apol9a-expressing cells were plated in 50% conditioned media for 24h. Cells were harvested using Cell Recovery Solution (BD Biosciences) and lysed with phospho-kinase array kit lysis buffer to obtain protein. Lysates were incubated overnight with the phospho-kinase array membranes. Membranes were washed and incubated with a cocktail of biotinylated detection antibodies. Streptavidin-HRP was added and signal detected by chemiluminescence.

Immunoblotting

Intestinal spheroid cells were plated as described above for the phospho-kinase array. Cells were harvested using Cell Recovery Solution (BD Biosciences), pelleted, and lysed in RIPA buffer with protease inhibitors (Sigma) and phosphotase inhibitors (Nacalai USA). Samples were run on Any-KD Mini-Protean gels (Bio-Rad) and transferred onto nitrocellulose membrane (Bio-Rad). Membranes were blocked with Blocking One (Nacalai USA) and washed with TBS-T buffer. Membranes were incubated with primary antibodies (anti-Phospho p44/42 MAPK (Thr202/Tyr204) and anti-p44/42 MAPK; Cell Signaling) in 5% BSA in TBS-T buffer overnight at 4°C. Membranes were then incubated with horseradish peroxidase (HRP) conjugated secondary antibodies (Bio-Rad) for 1h at room temperature. Signal was detected using the SuperSignal West Dura chemiluminescence kit (Thermo Fisher Scientific).

Statistics

GraphPad Prism software (version 6) was used to perform all statistical analyses unless otherwise specified.

RESULTS

Chronic viral infection promoted turnover of multiple epithelial organs

We first investigated whether chronic viral infection can modulate epithelial turnover. We infected C56BL/6 wild-type (WT) mice with murine cytomegalovirus (MCMV), a DNA herpesvirus that provides an animal model for infection with human CMV, a highly prevalent chronic virus (Brune et al., 2001; Virgin et al., 2009). Seven days after infection, we observed increased epithelial cell proliferation (by Ki67 staining) and cell death (by TUNEL staining) within organs that normally show low levels of epithelial turnover (i.e. kidney, liver, salivary gland, and pancreas; **Figure 3.1A-C**) (Pellettieri and Sanchez Alvarado, 2007). The continued local presence of infectious virus was not required for increased turnover, as only the salivary gland had detectable titers at this time (**Figure 3.2A**). A homologue of chronic human herpesvirus, murine gammaherpesvirus 68 (MHV68; (Virgin et al., 2009)), also promoted epithelial proliferation 16 days post-infection in the absence of detectable titers in target tissues (**Figure 3.3A**). At this time point, MHV68 is entering its chronic latent phase (Tibbetts et al., 2003). However, in the small intestine, an organ with high constitutive epithelial turnover, we found that while MCMV stimulated an increase in proliferation (**Figure 3.1D-E**), infection with MHV68 or a persistent strain of enteric murine norovirus (Nice et al., 2013) did not (**Figure 3.3B-E**). These results suggested that certain chronic viral infections can promote epithelial turnover in multiple organs.

Mice deficient in Irgm1 provided a useful model to study the effects of chronic elevated Type I IFNs

We hypothesized that Type I IFNs induced by viral infection stimulated epithelial turnover. However, we could not test this hypothesis in mice completely lacking Type I interferon responses because these cytokines are required for survival after infection with MCMV and MHV68 (Barton et al., 2005; Chong et al., 1983; Dutia et al., 1999; Grundy et al., 1982). Therefore, we used a mouse model that we discovered has chronic elevated Type I IFN levels in the absence of infection, the *Irgm1*$^{-/-}$ mouse. Irgm1 is a p47 GTPase initially studied for its role in host defense against intracellular protozoans and bacteria and in autophagy (Collazo et al., 2001; Feng et al., 2004; Liu et al., 2013; Santiago et al., 2005). The systemic elevation of Type I IFNs in *Irgm1*$^{-/-}$ mice is described in detail in Chapter 2 of this thesis, and provided us with a useful model to study the role of these cytokines on host physiology.

Type I IFNs promoted epithelial proliferation and turnover

To determine if Type I IFNs increased epithelial turnover, we compared WT, *Irgm1*$^{-/-}$, and *Irgm1*$^{-/-}$*Ifnar*$^{-/-}$ mice that lack responsiveness to Type I IFNs but still have elevated Type I IFN serum levels (**Figure 3.4**). We found increased epithelial proliferation and cell death in the kidney, pancreas, liver, and salivary gland of *Irgm1*$^{-/-}$ mice but not *Irgm1*$^{-/-}$*Ifnar*$^{-/-}$ mice compared to WT mice (**Figures 3.5A-B and 3.6A**). The effects of Type I IFNs were not global, as proliferation levels in skeletal muscle, lung alveolar cells, and thyroid gland epithelial cells in *Irgm1*$^{-/-}$ mice were similar to controls (**Figure 3.6B**).

We further examined the effect of Type I IFNs on proliferation in the intestine, where proliferation, cell death, and cell migration occur in defined areas (Creamer, 1967; Potten, 1998). *Irgm1*$^{-/-}$ but not *Irgm1*$^{-/-}$*Ifnar*$^{-/-}$ intestines showed increased epithelial proliferation compared to controls, as assessed by crypt height, number of mitotic figures per crypt, and incorporation of

the thymidine analog BrdU (**Figure 3.5C-F**). Increased proliferation was observed throughout *Irgm1*$^{-/-}$ small intestinal crypts, including regions enriched for stem cells (crypt base) and regions enriched for transit-amplifying cells (upper crypt) (**Figure 3.6D**). Turnover in the small intestine takes place, in part, via cell migration from the base of crypts that culminates with the eventual shedding of cells at the tips of villi (Creamer, 1967). Using a double thymidine analog method (Mahoney et al., 2008), we found that the distance migrated by epithelial cells was greater in *Irgm1*$^{-/-}$ mice than in either WT or *Irgm1*$^{-/-}$*Ifnar*$^{-/-}$ mice (**Figures 3.5E and 3.6G**). Notably, there was no excess cell death in crypts or villi of *Irgm1*$^{-/-}$ mice (**Figure 3.7A**). Furthermore, recombinant murine IFNαA did not induce cell death in epithelial spheroid cultures (Miyoshi et al., 2012; Miyoshi and Stappenbeck, 2013) derived from WT, *Ifnar*$^{-/-}$ and *Irgm1*$^{-/-}$ mice, despite the capacity of WT and *Irgm1*$^{-/-}$ cells to respond to type I IFNs by increasing ISG expression (**Figure 3.7B-C**). These findings suggest that enhanced proliferation, and not apoptosis, is the primary driver of Type I IFN stimulated epithelial turnover in *Irgm1*$^{-/-}$ mice.

Elevated Type I IFNs in Irgm1$^{-/-}$ *mice enhanced wound healing*

To determine whether Type I IFN-driven epithelial turnover had physiologic importance, we evaluated wound repair. We first administered diclofenac sodium salt, a non-steroidal anti-inflammatory drug (NSAID), which can induce small intestinal ulcerations within 24 hours after a single i.p. dose of 60mg/kg (Fujimori et al., 2010; Ramirez-Alcantara et al., 2009). While ulcers were formed in all mice after 18 hours, *Irgm1*$^{-/-}$ mice had fewer detectable intestinal ulcers compared to WT and *Irgm1*$^{-/-}$*Ifnar*$^{-/-}$ mice at day 2 and day 4 after injection (**Figures 3.8A-B and 3.9**). This result indicated that *Irgm1*$^{-/-}$ mice healed ulcerations more rapidly than controls. We confirmed this finding using a colonic biopsy injury model (Seno et al., 2009). In this model,

wound-associated epithelial (WAE) cells migrate over the wound bed surface to cover the injury, and decreased epithelial cell proliferation in wound-adjacent crypts is associated with slowed and incomplete wound healing (Seno et al., 2009). We observed a greater distance covered by WAE cells at day 4 post-injury in wounds of *Irgm1*$^{-/-}$ mice compared to wounds in WT and *Irgm1*$^{-/-}$ *Ifnar*$^{-/-}$ mice (**Figure 3.8C-D**). In addition, we examined wound healing responses in the context of MCMV infection. We injected diclofenac 4 days after systemic MCMV infection, and enumerated ulcers 18hours and 4 days afterward. Interestingly, MCMV-infected mice had fewer ulcers than mock-infected mice even at 18hours, suggesting that viral infection may have hindered ulcer formation (**Figure 3.8E-F**). In addition, many ulcers in MCMV-infected animals had an abnormal appearance, with what appeared to be slight villus ablation without the penetrating ulcers and wound debris seen in mock-infected and WT mice at this time point (**Figures 3.8F and 3.9**). Taken together, these findings suggest that elevated epithelial proliferation in response to Type I IFNs and enhanced healing after epithelial damage, and that the presence of viral infection altered NSAID-induced wound formation.

Type I IFNs signaled through macrophages to promote epithelial proliferation

We then tested whether Type I IFNs act directly on the epithelium to promote proliferation by crossing *Irgm1*$^{-/-}$ mice with mice lacking Ifnar solely in the intestinal epithelium (*Irgm1*$^{-/-}$*Ifnar*$^{f/f}$-Villin-Cre; *Irgm1*$^{-/-}$ *IfnarVC* mice (el Marjou et al., 2004)). Importantly, *Irgm1*$^{-/-}$ *IfnarVC* mice had elevated levels of serum Type I IFNs, and increased intestinal epithelial proliferation comparable to *Irgm1*$^{-/-}$ mice (**Figures 3.4 and 3.10A-B**). This finding suggested that non-epithelial cell type(s) must be responding to Type I IFNs to stimulate epithelial cell

proliferation. We verified this finding *in vitro*: addition of IFNα did not affect proliferation of primary intestinal epithelial cells in the absence of other cell types (**Figure 3.11**).

Next, to identify the cell type required for epithelial hyperproliferation to type I IFN, we assayed mice deficient in different cellular compartments after treatment with polyI:C, a synthetic dsRNA. Daily low dose polyI:C injection for 4 days induced elevated systemic Type I IFN and increased intestinal epithelial proliferation in WT but not *Ifnar*$^{-/-}$ mice (**Figures 3.10C and 3.12A-B**). PolyI:C treatment of *IfnarVC* mice also showed augmented intestinal epithelial turnover (**Figure 3.12D-E**). However, polyI:C treatment of mice lacking Ifnar on macrophages and granulocytes (*Ifnar*$^{f/f}$-LysM-Cre; *IfnarLysM* mice (Prinz et al., 2008)) did not induce epithelial cell proliferation to the same extent as in control mice (**Figure 3.10D**), even though Type I IFN levels were induced at similar levels in both *IfnarLysM* and control mice (**Figure 3.13A**). Endogenous lysozyme M is highly expressed on both neutrophils and macrophages (Cross et al., 1988; Faust et al., 2000). However, neutrophil depletion did not diminish epithelial hyperproliferation induced by polyI:C injection, indicating that macrophages mediate this effect (**Figures 3.10E and 3.13B-C**).

The ISG Apolipoprotein L9 was a candidate factor to mediate proliferation in Irgm1$^{-/-}$ *mice*

We next determined the factors downstream of IFN signaling that can mediate increased epithelial turnover. We assayed serum from *Irgm1*$^{-/-}$, WT, polyI:C-treated and saline-treated mice, but found no elevations in established pro-proliferative cytokines and growth factors TNFα, IL-6, IGF, leptin, EGF, VEGF, and FGFβ (**Figure 3.14A-B**). We therefore performed microarray expression analysis of whole genome RNA of salivary gland, small intestine and

isolated colonic macrophages from *Irgm1*$^{-/-}$ and WT mice (**Figure 3.15A**). Apol9a and Apol9b, highly homologous apolipoproteins (98% by nBLAST analysis), were two of the few factors with enhanced gene expression in *Irgm1*$^{-/-}$ mice that were also potentially secreted (**Figure 3.15B and Table 3.1**). These apolipoproteins are ISGs (Rusinova et al., 2013), however their function is unknown. We verified enriched gene expression of *Apol9a/b* using qRT-PCR in small intestine and salivary gland whole tissue, and isolated colonic macrophages of *Irgm1*$^{-/-}$ mice (**Figure 3.16A**). *Apol9a/b* gene expression was also elevated in MCMV-infected tissues with epithelial hyperproliferation compared to mock-infected animals (**Figure 3.16B**).

We further examined localization of *Apol9a* expression by *in situ* hybridization. Interestingly, *Apol9a* was expressed in discrete foci within the salivary gland and small intestine in *Irgm1*$^{-/-}$ mice (**Figure 3.16C-D**). *Apol9a* was not only expressed in the stroma, where macrophages reside, but also in epithelial cells themselves (**Figure 3.16C-D, insets**). Based on this pattern, we hypothesized that Apol9a/b may be secreted from macrophages in response to Type I IFN and stimulate its own expression in surrounding cells. Alternatively, other ISGs from macrophages could stimulate *Apol9a/b* expression in the epithelial cells. Indeed, we found that *Apol9a/b* expression was induced by IFNαA in WT but not *Ifnar*$^{-/-}$ macrophages (**Figure 3.17A**). We then transfected 293FT cells with Flag-tagged Apol9a. We could detect Flag-tagged Apol9a protein within the supernatant, suggesting that Apol9a can be secreted (**Figure 3.17B**). In addition, *Apol9a* expression could be found in the intestinal epithelium of *Irgm1*$^{-/-}$ *IfnarVC*- mice, which supported the idea that *Apol9a/b* expression in epithelium can be indirectly stimulated (**Figure 3.17C**).

Apolipoprotein L9 promoted epithelial proliferation through ERK activation

Notably, the pattern of *Apol9a* gene expression within the salivary gland was associated with areas of high epithelial proliferation (**Figure 3.18**). To determine whether Apol9a could promote proliferation, we quantified proliferation of Apol9a-expressing intestinal epithelial cells using a novel bioluminescence-based assay. This method utilized knock-in mice expressing a fusion protein between Cdc25A and click beetle red luciferase (CBRLuc) in the endogenous *Cdc25a* locus (**Figure 3.19A-B**). Cdc25A is a cell cycle phosphatase with peak protein levels during mitosis (Boutros et al., 2006) (Honaker and Piwnica-Worms, 2010). Luminescence from Cdc25A-CBRLuc-expressing cells upon addition of D-luciferin substrate thus provided a direct readout of mitotic activity and proliferation. Luminescence imaging of Cdc25A-CBRLuc colonic epithelial spheroid cultures revealed an increase in luminescence over a 48h culture period (**Figures 3.19C-D**) that correlated with the number of viable cells (**Figure 3.19E**).

We assessed luminescence levels of Cdc25A-CBRLuc intestinal epithelial cells expressing either Apol9a, a positive control R-spondin3 (Rspo3), or a negative control construct for 24 hours (**Figures 3.20A**). R-spondins enhance Wnt signaling to promote cell proliferation and survival of tissue stem cells, and exogenous R-spondin can increase intestinal crypt proliferation (Haegebarth and Clevers, 2009; Kim et al., 2005). Both R-spondin3 and Wnt3a are required in the normal growth media for primary intestinal epithelial spheroids (Miyoshi et al., 2012; Miyoshi and Stappenbeck, 2013). Under these conditions, small intestinal epithelial cells expressing Apol9a and the positive control Rspo3 showed greater proliferation compared to control cells (**Figure 3.19F**). To determine whether Apol9a could substitute for Rspo3 to enhance Wnt signaling, we grew cells in media with only Wnt3a present. In these conditions, only epithelial cells expressing Rspo3 were able to proliferate, suggesting that Apol9a functions through a different pathway (**Figure 3.19G**). Indeed, no significant enhancement of Wnt

signaling was observed *in vivo* in *Irgm1*$^{-/-}$ mice as assessed by two downstream indicators of Wnt activation, β-catenin nuclear localization or *Axin2* expression (**Figure 3.20B-C**). Similar results on proliferation were obtained in WT cells expressing Apol9a and Rspo3 using an EdU incorporation assay (**Figure 3.20D**). These results suggested that Apol9a expression within epithelial cells is able to stimulate epithelial proliferation.

Next, to discover potential pathways downstream of Apol9a expression, we analyzed cell lysates of control, Rspo3, and Apol9a-expressing intestinal epithelial cells using a phospho-kinase dot blot array. Out of 45 different phosphorylated kinase targets, Apol9a-expressing epithelial cells showed elevations in phospho-ERK1/2 compared to control cells (**Figure 3.21A**). We verified this finding by Western blot (**Figure 3.19H**). ERK kinases are the downstream signaling component of the mitogen-activated protein kinase (MAPK) pathway, and have been implicated in promoting cell cycle progression and proliferation (Rubinfeld and Seger, 2005; Shaul and Seger, 2007). Addition of the MEK inhibitor U0126 inhibited ERK1/2 phosphorylation and reduced proliferation of Apol9a-expressing intestinal epithelial cells, as well as control cells, in a dose-dependent manner (**Figures 3.19I and 3.20G-H**). These findings implicated activation of the ERK pathway, which is important for epithelial cell proliferation, downstream of Apol9a expression.

Macrophages expressing Apol9a were able to promote epithelial proliferation in trans

Finally, we investigated the role of Type I IFN signaling in macrophages on Apol9a-mediated epithelial proliferation. Based on the localization of Apol9a on macrophages by *in situ* hybridization (**Figures 3.16C-D**), we determined whether Type I IFN signaling could induce Apol9a/b in macrophages and stimulate proliferation *in trans*. We expressed Apol9a or a control

construct in WT bone marrow-derived macrophages and co-cultured these cells with Cdc25A-CBRLuc intestinal epithelial cells. Macrophages expressing Apol9a enhanced proliferation of epithelial cells greater than control macrophages or epithelial cultures alone (**Figure 3.22**). These results suggested that macrophages promoted epithelial proliferation in *trans* via Apol9a expression.

DISCUSSION

Taken together, these findings uncover a novel pathway linking viral infection with enhanced epithelial turnover via Type I IFNs. Specifically, we showed that elevated Type I IFNs can signal through macrophages to enhance epithelial proliferation and injury repair. We demonstrated that the highly related IFN-stimulated genes *Apol9a* and *b* promote epithelial proliferation. These results redefine the current view of Type I IFN effects on proliferation *in vivo* and enhance our understanding of conditions with elevations in these cytokines, such as viral infection and autoimmunity.

The indirect effect on epithelial proliferation driven by viral infection has not been previously described. The viruses used here that stimulated epithelial proliferation are murine homologues of highly prevalent human chronic viruses, CMV and herpesvirus, both well-known systemic DNA viruses (Virgin et al., 2009). In contrast, murine norovirus, an RNA virus, did not stimulate proliferation in the intestine, where it is tropic (Nice et al., 2013). These results suggest that not all viruses can stimulate enhanced epithelial proliferation, perhaps due to differences in tissue tropism, viral pathogenesis and/or virus-encoded pathogen associated molecular patterns (PAMPs). In humans, host factors may also play a role in the extent of induced proliferation, as genetic differences can affect immune responses to pathogens, including the Type I IFN response (Lee et al., 2014). Since chronic viral infection clearly has a systemic effect on host physiology, and all individuals possess a collection of persistent viruses as their virome, the use of mouse models of chronic viral infections may uncover new biology.

Type I IFNs have been generally considered to be pro-apoptotic and anti-proliferative, but the vast majority of these studies were performed with direct administration of these cytokines onto cells *in vitro* (Chawla-Sarkar et al., 2003; Maher et al., 2007; Tanaka et al., 1998).

Our results show that the effects of Type I IFNs *in vivo* are more complex, as Type I IFNs do not directly stimulate either apoptosis or proliferation of primary intestinal epithelial cells *in vitro*. These findings are in stark contrast with recent studies showing that Type II IFN, IFNγ, directly mediates intestinal epithelial cell death *in vitro* and *in vivo* (Farin et al., 2014; Moon et al., 2013).

We found that the effects of Type I IFN on epithelial proliferation are indirect through an additional cell type that includes macrophages. We propose that macrophages can act as a relay. Because of their widespread distribution, these cells are poised to synthesize information from multiple local and remote sources and then in turn instruct proximal epithelial cells. The use of an integrative relay enables the separation of signal from noise and allows for the amplification of additive weak signals. The pattern of foci of *Apol9a* expression in stromal and epithelial cells observed in the salivary gland and small intestine supports the concept of a central cell that spreads and amplifies signals to neighboring cells. This myeloid-epithelial circuit could be used by other cytokine signaling systems to modulate diverse epithelial functions. Our work extends a proposed role for macrophages in epithelial maintenance and repair by implicating Type I IFNs in this pathway (Farache et al., 2013). The host immune system may thus prime the epithelium for renewal and healing in response to additional damage.

We propose that *Apolipoprotein L9* is one of the mediators of this Type I IFN response directed towards epithelial progenitors. Relatively little is known about the Apolipoprotein L (ApoL) family. In humans, there are 6 known ApoLs, 5 of which are thought to be interferon-stimulated (Rusinova et al., 2013; Smith and Malik, 2009). In mice, there are as many as 14 apolipoprotein L members (Vanhollebeke and Pays, 2006). In contrast to other apolipoprotein families, only APOL1 has been implicated in lipid transport and metabolism to date (Albert et al., 2005; Duchateau et al., 2000; Duchateau et al., 1997). APOL1 also has pore-forming

trypanolytic activity against *Trypanosoma brucei*, and may be involved in the autophagy pathway (Perez-Morga et al., 2005; Vanhamme et al., 2003; Wan et al., 2008). In addition, APOL1 and APOL6 have been implicated in mediating cell death (Liu et al., 2005; Wan et al., 2008), while APOL2 was shown to be protective against IFNγ-induced cytotoxicity (Liao et al., 2011). Interestingly, increased expression of ApoLs has been observed in several cancers, including cervical and breast cancer (Ahn et al., 2004; Jung et al., 2005). Apol9a and Apol9b have the most protein homology with APOL3 (43% identity), but may share similar structural domains with the rest of the ApoL family. Apol9b has been implicated in anti-viral protection in L929 cells and primary neurons, but the extent and mechanism of such protection was unclear (Kreit et al., 2014). In this report, we show that Apol9a can be secreted and promotes epithelial proliferation. Since there are hundreds of ISGs that can be induced in a given cell type, it is unlikely that Apol9a and b are the sole mediators of Type I IFN-dependent epithelial proliferation. Other ISGs may have redundant functions. Nonetheless, Apol9a/b and the ApoL family are ISGs that warrant further study in the context of homeostasis and during viral infection.

We show that Apol9a expression can enhance activation of the ERK pathway and in turn proliferation. The connection between the ERK pathway and proliferation is well supported by previous studies, which show that ERK activation promotes cell cycle progression and cellular differentiation (Rubinfeld and Seger, 2005; Shaul and Seger, 2007; Zhang and Liu, 2002). Sustained ERK activation activates cyclin D1 expression and decreases CDK inhibitor levels to allow cells to pass the G_1 restriction point and enter the S phase of the cell cycle (Rubinfeld and Seger, 2005). Thus, an increase in ERK activation would be able to increase the rate of cell cycling.

Modulation of the ERK pathway would allow for an additional level of control of proliferation in epithelial organs beyond Wnt signaling, which is required for the maintenance of stem and progenitor cells (Haegebarth and Clevers, 2009; Reya and Clevers, 2005). Wnt ligands bind to their receptor complex and trigger the localization of b-catenin to the nucleus, where it associates with transcription factors that activate multiple target genes to promote a baseline rate of self-renewal and proliferation (Reya and Clevers, 2005). The source of Wnts is thought to be local non-epithelial mesenchymal cells and, in the intestine, also Paneth cells (Farin et al., 2012). In contrast, Type I IFN signaling can generate a signal at the systemic level. Downstream activation of the ERK pathway could then increase the normal rate of cell cycling in stem and progenitor cells. We propose that Type I IFNs provide additional control of epithelial proliferation and healing under non-homeostatic conditions of infection and injury.

Finally, many human conditions are associated with elevated Type I IFN signatures, similar to our observations in the *Irgm1*$^{-/-}$ mouse. For example, recombinant Type I IFN treatment is used for a variety of disorders, including multiple sclerosis, hepatitis C, and some malignancies (Ferrantini et al., 2007; Pawlotsky, 2014; Verweij and Vosslamber, 2013). Morever, upregulation of Type I IFNs is associated with the Type I Interferonopathies, a group of Mendelian disorders,(Crow, 2011; Rice et al., 2014a), as well as Systemic Lupus Erythematosus (SLE) (Di Domizio and Cao, 2013; Kirou and Gkrouzman, 2013; Lichtman et al., 2012). These diseases, which include Aicardi-Goutieres Syndrome (AGS) and spondyloenchondrodysplasia (SPENCD) are proposed to arise from either i) inappropriate activation of the Type I IFN response or ii) inadequate negative regulation of Type I IFN production (Crow, 2011). While the molecular bases of some cases of Type I Interferonopathy are known, many cases remain genetically uncharacterized. It would be interesting to determine

whether there are gene changes in human IRGM in these cases that are linked with elevated Type I IFN. In addition, we have only limited understanding of the role of Type I IFNs on disease pathogenesis and progression. Our findings here suggest that elevated Type I IFNs may not be sufficient to cause the severe autoimmunity seen in SLE, AGS, and SPENCD. We did not observe the abnormal skin, brain, or bone dysplasias typically seen in these conditions in Irgm1-deficient mice (results not shown). Instead, we observed increased epithelial turnover, with both augmented cell proliferation and cell death. It is possible that this elevated turnover could increase the risk for exposure of cell contents, such as nucleic acids, to the immune system. Additional genetic or environmental contributions could then trigger autoimmunity to the cellular components. Our findings show that constitutively elevated Type I IFNs can promote systemic epithelial proliferation and cell death, thus expanding our knowledge of the host response during infection and autoimmunity.

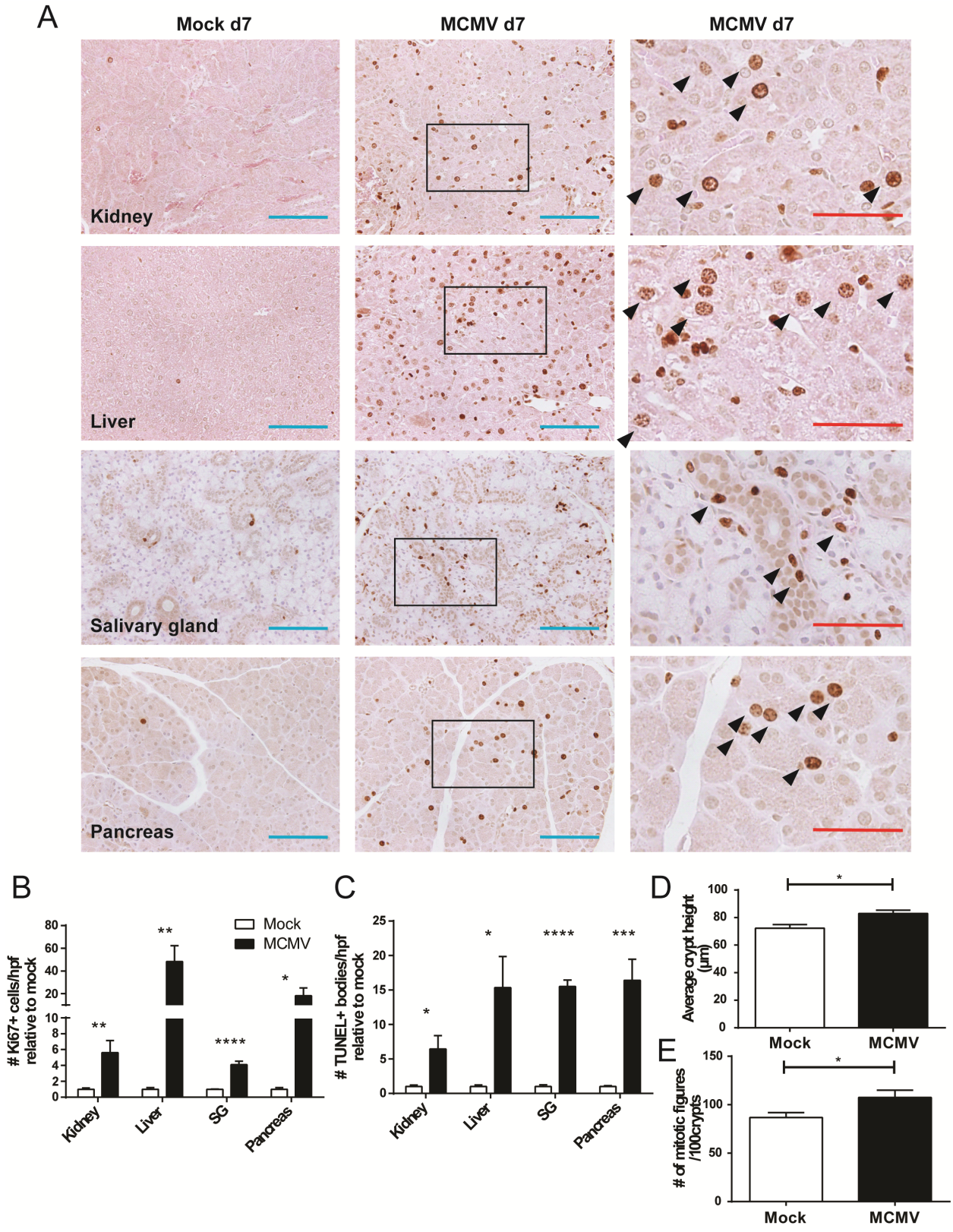

Figure 3.1. MCMV infection promoted epithelial turnover in multiple organs.

Figure 3.1. MCMV infection promoted epithelial turnover in multiple organs. A) Representative immunohistochemistry for Ki67 in salivary gland (SG), exocrine pancreas, kidney and liver of mock-infected mice or mice infected with $5x10^4$ pfu MCMV (Smith strain), d7 after intraperitoneal (i.p.) infection. Blue bars indicate 100μm, red bars measure 50μm. Black boxes indicate insets (right-most column). Black arrowheads show examples of Ki67+ epithelial cells that would be counted. B-C) Graph of the average number ± standard error of the mean (SEM) of B) Ki67+ epithelial cells per high power field (hpf, 400X) and C) TUNEL+ bodies/hpf relative to mock-infected animals. For B), approximately 25 hpf were quantified per organ and only epithelial cells were counted, and for C), approximately 50 hpf per organ were quantified. Graph of D) average crypt height and E) average number of mitotic figures ± SEM of 100 crypts in mock- and MCMV-infected mice. Lengths of crypts were measured from histological slides using ImageJ software. Mitotic figures were counted manually. For B) to E), mock-infected n=6 mice, MCMV-infected n=5 mice. *$p<0.05$; **$p<0.01$; ***$p<0.001$; ****$p<0.0001$ by Student's *t* test for each organ.

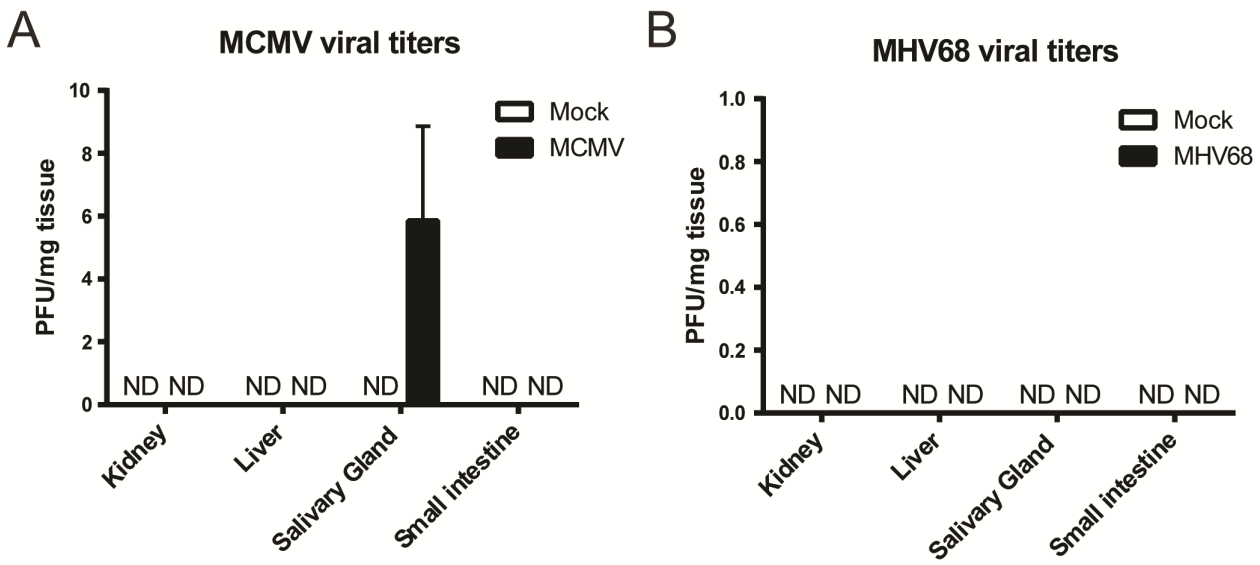

Figure 3.2. Viral titers in MCMV- and MHV68-infected mice. A) Graph of average plaque forming units (PFU)/mg of tissue ± standard deviation (SD) of kidney, liver, salivary gland and small intestine of mock-infected and MCMV-infected mice 7 days after i.p. infection with $5x10^4$ PFU MCMV (Smith strain). MCMV-infected n=5 mice, mock-infected n=6 mice. ND = not detected. The limit of detection for this plaque assay was 40 PFU/organ. B) Graph of average PFU/mg of tissue ± SD of kidney, liver, salivary gland and small intestine of mock-infected and MCMV-infected mice 16 days after i.p. infection with $1x10^6$ pfu MHV68. MHV68-infected n=4 mice, mock-infected n=4 mice. ND = not detected. The limit of detection for this plaque assay was 100 PFU/organ.

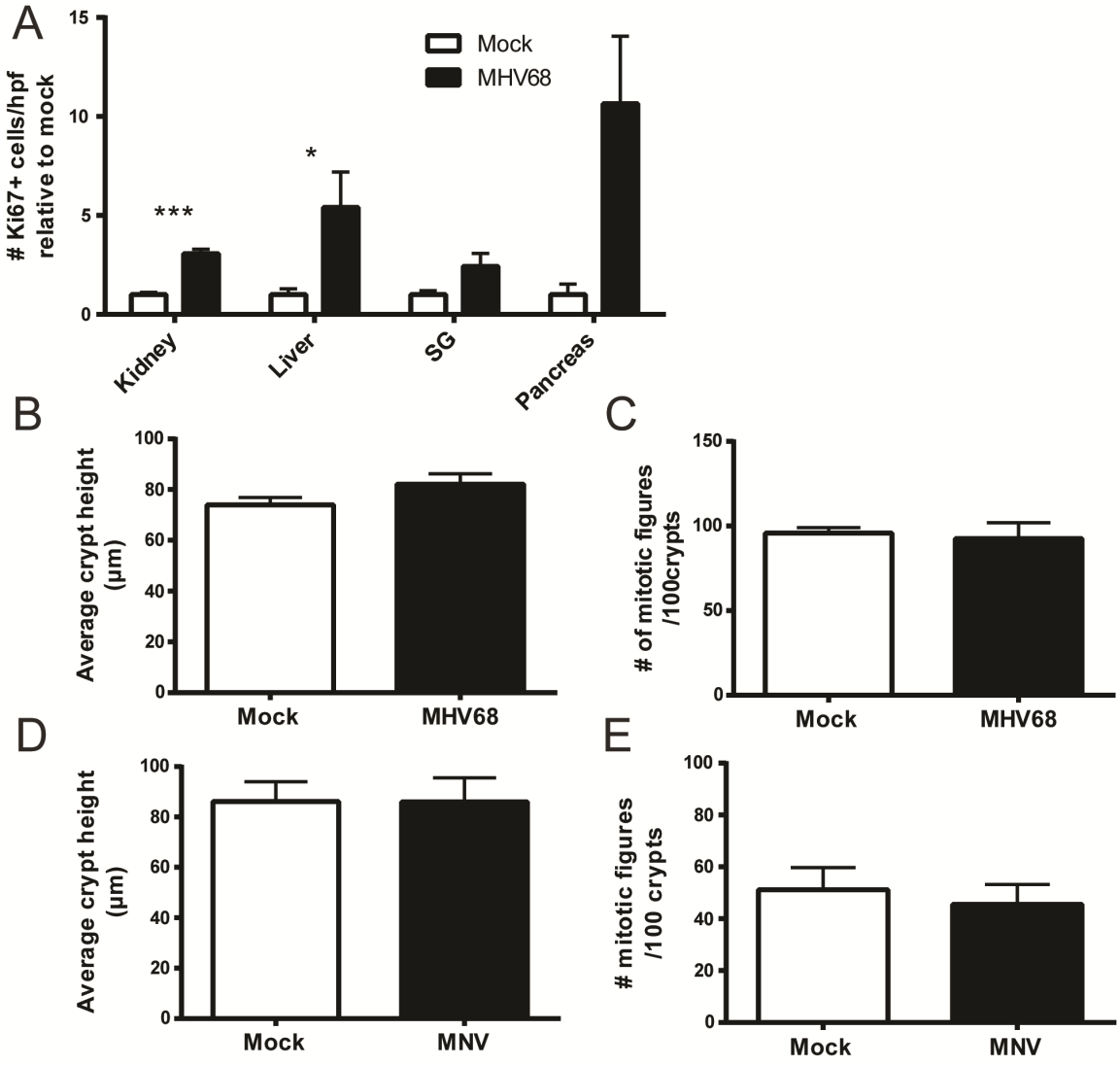

Figure 3.3. Different effects of MCMV, MHV68 and MNV on epithelial proliferation.

Figure 3.3. Different effects of MCMV, MHV68 and MNV on epithelial proliferation.

A) Graph of the average number ± SEM of Ki68+cells/high power field (400X; hpf) relative to mock infected animals in kidney, liver, SG and pancreas of mock-infected mice (n=3-4 mice) and MHV68-infected mice (n=3-4mice) 16 days after i.p. infection with $1x10^6$ pfu MHV68. Approximately 25 hpf were counted per organ. *$p<0.05$; ***$p<0.001$ by Student's *t* test for each organ. Graph of B) average crypt height and C) average number of mitotic figures ± SEM of 100 crypts of the small intestine in mock-infected (n=4 mice) and MHV68-infected mice (n=4 mice) 16 days after i.p. infection with $1x10^6$ pfu MHV68. Averages are not significantly different by Student's *t* test. Graph of D) average crypt height and E) average number of mitotic figures ± SEM of 100 crypts of the small intestine in mock-infected (n=6 mice) and MNV-infected mice (n=6 mice) 7 days after oral infection with persistent $3x10^7$pfu MNV (CR6 strain). Averages are not significantly different by Student's *t* test.

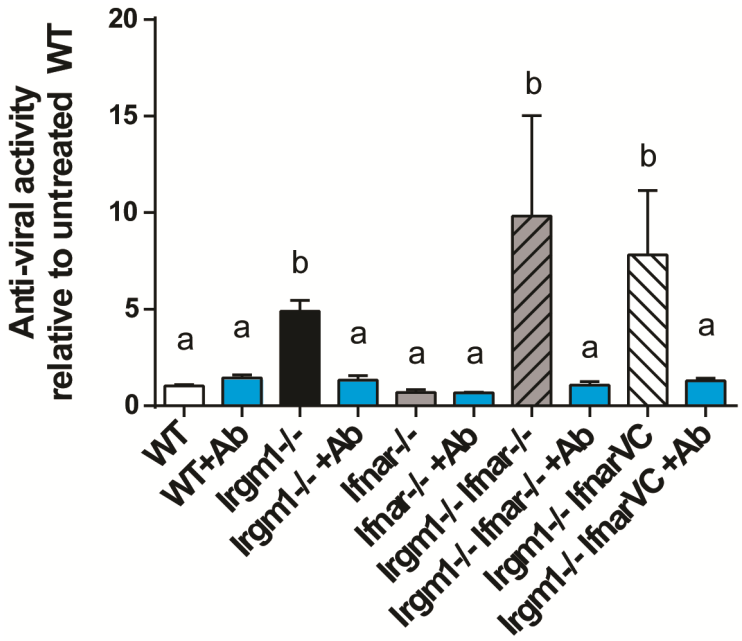

Figure 3.4. Antiviral activity of serum from various mouse strains. Graph of antiviral activity of serum from WT (n=12 mice), *Irgm1*$^{-/-}$ (n=16 mice), *Ifnar*$^{-/-}$ (n=4 mice), *Irgm1*$^{-/-}$*Ifnar*$^{-/-}$ (n=5 mice), and *Irgm1*$^{-/-}$*IfnarVC* (n=2 mice) mice. Blue bars indicate the addition of anti-Ifnar antibody (Ab). Means ± SEM relative to untreated WT samples are shown. Means with significant differences are indicated with different letters by uncorrected Fisher's LSD test.

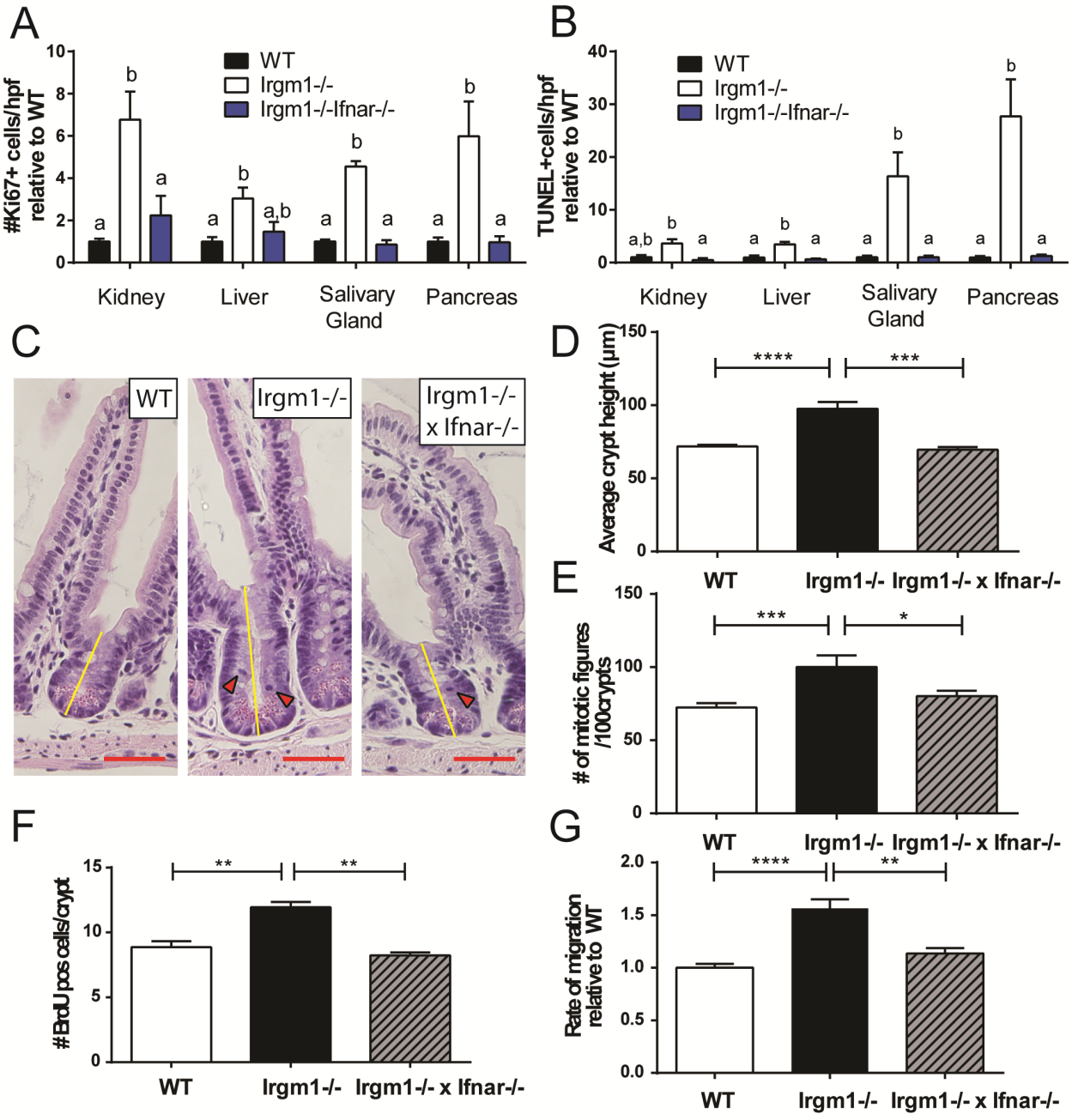

Figure 3.5. Elevated Type I IFNs in *Irgm1*$^{-/-}$ mice promoted enhanced epithelial turnover.

Figure 3.5. Elevated Type I IFNs in *Irgm1*$^{-/-}$ mice promoted enhanced epithelial turnover. A) Quantification of the average number of Ki67+cells/hpf ± SEM. n=6-11 mice per genotype. B) Quantification of average number of TUNEL-positive cells per hpf ± SEM. n=5-10 mice per genotype. For A) and B), approximately 50 hpfs were examined per organ. For each organ, means with different letters are significantly different ($p<0.05$) by Tukey's multiple comparisons test. C) Representative histology of small intestinal crypts of WT, *Irgm1*$^{-/-}$ and *Irgm1*$^{-/-}$*Ifnar*$^{-/-}$ mice. Red bar = 50μm. Yellow bars delineate the height of a crypt; red arrowheads mark mitotic figures. Graph of D) average crypt height and E) average number of mitotic figures ± SEM of 100 crypts in WT, *Irgm1*$^{-/-}$, and *Irgm1*$^{-/-}$*Ifnar*$^{-/-}$ mice. Length of crypts was measured from histological slides using ImageJ software. Mitotic figures were counted manually. WT n=23 mice, *Irgm1*$^{-/-}$ n=18 mice, *Irgm1*$^{-/-}$*Ifnar*$^{-/-}$ n=18 mice from 4 independent experiments. F) Quantification of the average number ± SEM of BrdU-positive cells per crypt. Mice were injected with BrdU 1h before sacrifice. Immunofluorescent staining against BrdU was performed on histological slides and the number of BrdU-positive cells was counted over an average number of 50 crypts. WT n=3 mice, *Irgm1*$^{-/-}$ n=3 mice, *Irgm1*$^{-/-}$*Ifnar*$^{-/-}$ n=2 mice. **$p<0.01$ by Tukey's multiple comparisons test. G) Graph of the average migration rate ± SEM of small intestinal epithelial cells in WT, *Irgm1*$^{-/-}$ and *Irgm1*$^{-/-}$ *Ifnar*$^{-/-}$ mice, calculated relative to WT for 100 villi/mouse using a 2-color thymidine analog experiment. WT n=11 mice, *Irgm1*$^{-/-}$ n=17 mice, *Irgm1*$^{-/-}$*Ifnar*$^{-/-}$ n=9 mice from 4 independent experiments.

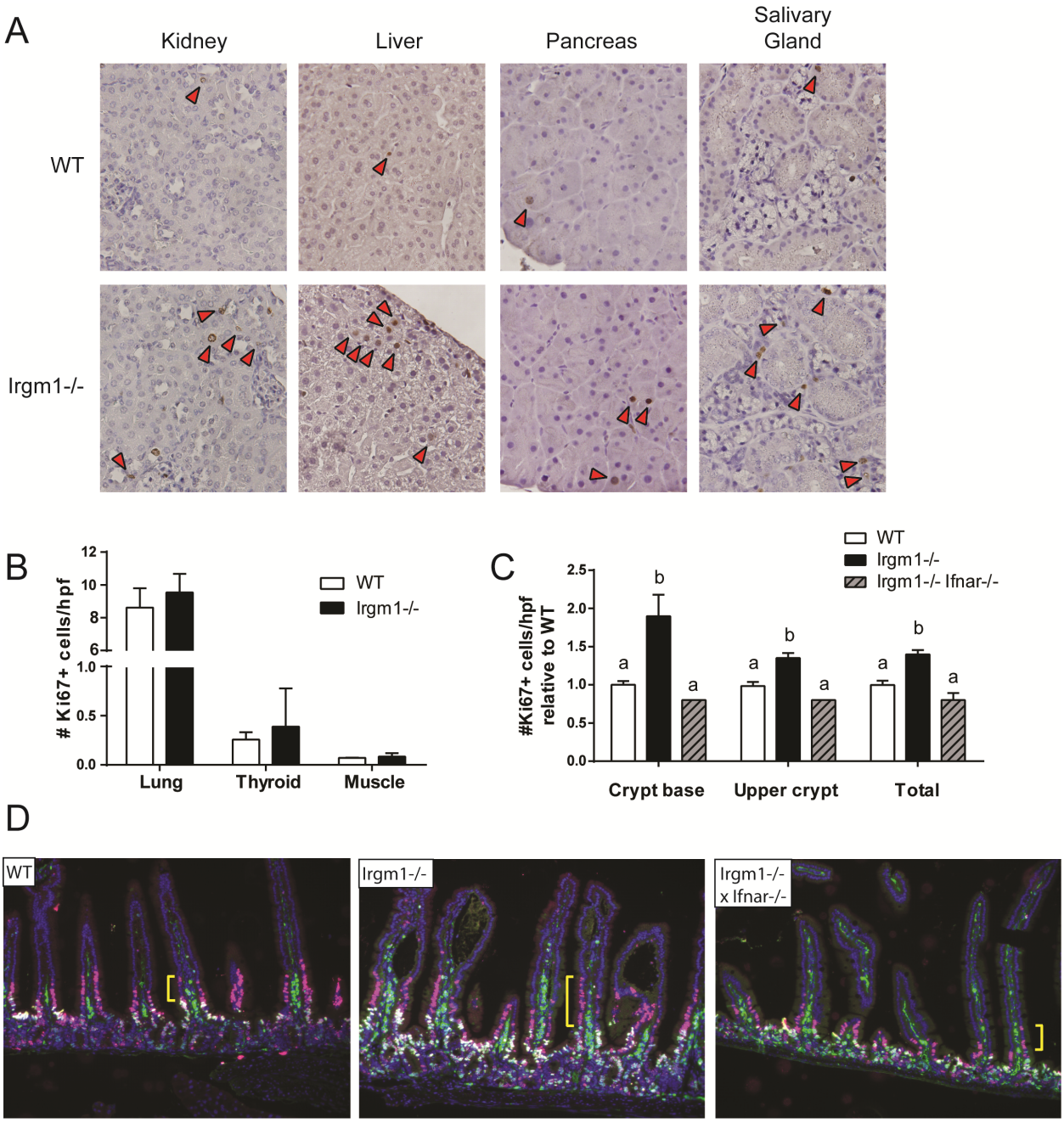

Figure 3.6. Further evidence that elevated Type I IFNs in *Irgm1*$^{-/-}$ mice promoted enhanced epithelial turnover.

Figure 3.6. Further evidence that elevated Type I IFNs in *Irgm1*$^{-/-}$ mice promoted enhanced epithelial turnover. A) Representative histology of Ki67 immunohistochemistry of kidney tubules, liver hepatocytes, pancreatic acinar cells, and submandibular salivary mucinous and serous glands of *Irgm1*$^{-/-}$ and WT mice. Red arrowheads indicate cells stained with Ki67. All images taken at 200X magnification. B) Quantification of the average number of Ki67-positive cells per high power field (400X) ± SEM in lung epithelium, thyroid gland epithelium, and skeletal muscle cells. N=2-3 mice per genotype per organ. C) Graph of the average number ± SEM of Ki67-positive cells per crypt base region (stem cell compartment), upper crypt region (transit-amplifying compartment), or total crypt relative to WT. WT n=6 mice, *Irgm1*$^{-/-}$ n=6 mice, *Irgm1*$^{-/-}$*Ifnar*$^{-/-}$ n=2 mice. 20-50 crypts were counted per mouse. For each crypt region, different letters indicate means with significant differences by Tukey's multiple comparisons test. D) Representative immunofluorescent images of CldU and IdU stained small intestinal sections. Red – CldU, Green – IdU, Blue – nuclei. CldU was injected 36h prior to sacrifice and IdU was injected 24hrs prior to sacrifice. Yellow bar shows the distance cells have migrated in 12h. Images taken at 200Xmagnification.

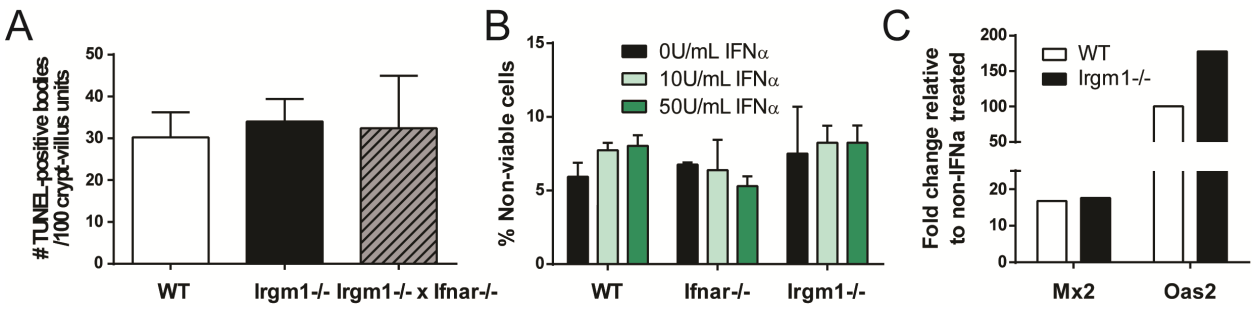

Figure 3.7. Type I IFN-dependent enhanced turnover in *Irgm1*$^{-/-}$ mice was not due to increased cell death. A) Graph of the average number ± SEM of TUNEL-positive bodies per 100 crypts. WT n=10 mice, *Irgm1*$^{-/-}$ n=12 mice, *Irgm1*$^{-/-}$ *Ifnar*$^{-/-}$ n=10 mice. B) Graph of the average percentage ± SEM of non-viable intestinal crypt cells after 24h incubation with 0, 10UmL, and 50U/mL of recombinant murine IFNαA. WT, *Ifnar1*$^{-/-}$ and *Irgm1*$^{-/-}$ intestinal epithelial cells were used. The percentages of non-viable cells were measured by Sytox 7'AAD dead cell nucleic acid stain. P=0.3412 by ordinary ANOVA. N=2 replicates each group from 2 independent experiments. C) Graph of the fold change in mRNA expression of Mx2 and Oas2 in WT and *Irgm1*$^{-/-}$ intestinal epithelial crypt cultures after addition of 2.5U/mL IFNα for 24h. The expression of Mx2 and Oas2 relative to non-IFNα treated cells for each genotype is shown.

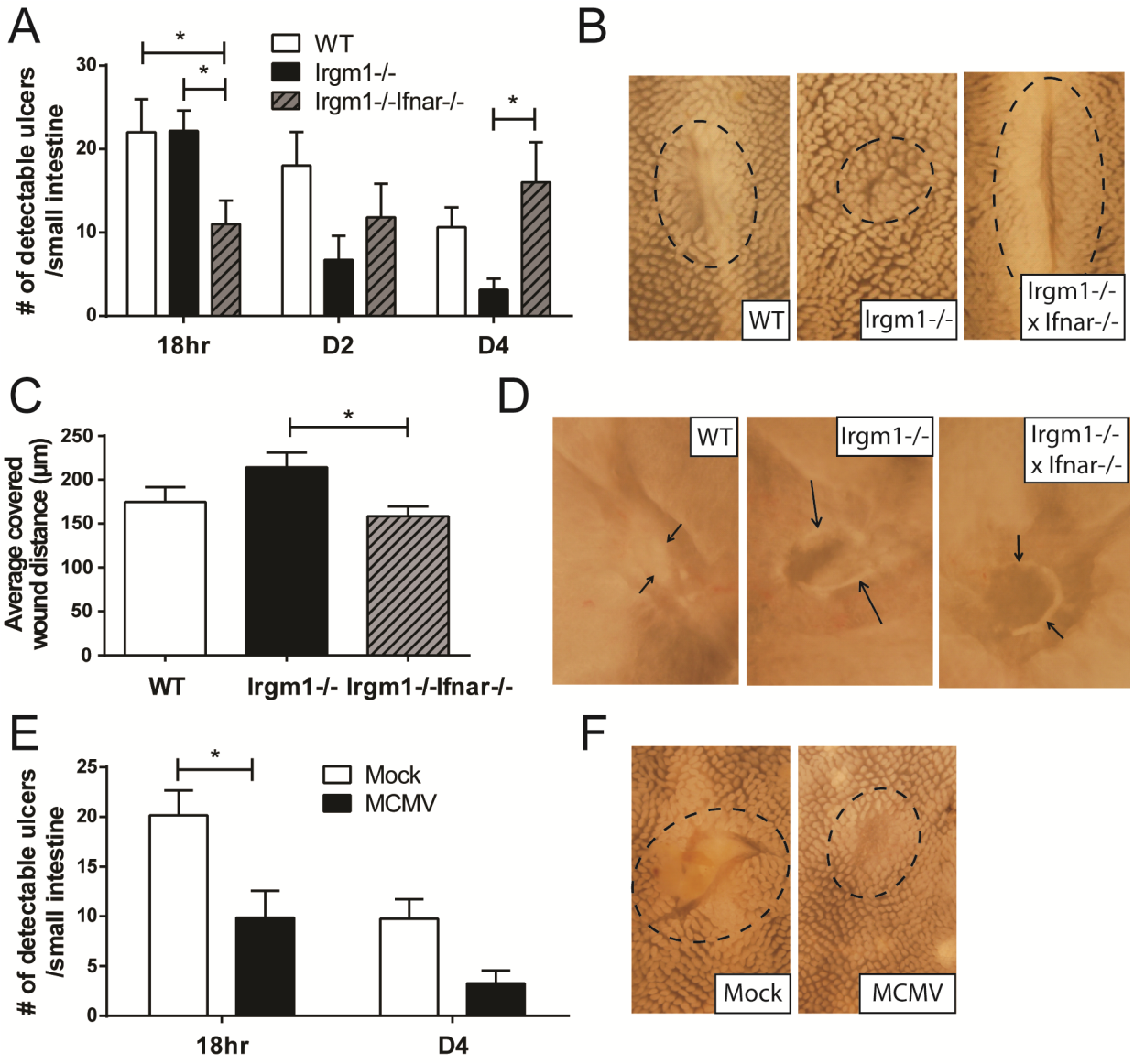

Figure 3.8. Viral infection and Type I IFNs changed response to diclofenac-induced wound healing.

Figure 3.8. Viral infection and Type I IFNs changed response to diclofenac-induced wound healing. A) Graph of the average number ± SEM of detectable ulcers per small intestine 18hr, 2 days (D2), and 4 days (D4) after i.p. injection of 60mg/kg dicloflenac sodium salt in sterile PBS. N=3-8 mice per genotype per day. Results from 5 independent experiments. *p<0.05 by Tukey's multiple comparisons test. B) Representative whole mount images of formalin-fixed small intestinal wounds of WT, *Irgm1*$^{-/-}$ and *Irgm1*$^{-/-}$*Ifnar*$^{-/-}$ mice 4 days after diclofenac injection. Dotted black lines outline the wound. All images at 32X. C) Graph of the average distance covered by WAE cells 4 days after colonic biopsy wounding. Quantification was performed blinded on whole mount images of formalin-fixed wounds using Image J software. 10 measurements per wound were averaged. WT n=8 wounds in 4 mice, *Irgm1*$^{-/-}$ n=12 wounds in 4 mice, *Irgm1*$^{-/-}$*Ifnar*$^{-/-}$ n=9 wounds in 3 mice. D) Representative whole mount images at 90X magnification of colonic biopsy wounds 4 days after wounding. Black arrows delineate the distance migrated by WAE cells. E) Graph of the average number ± SEM of detectable ulcers per small intestine 18hr, and 4 days (D4) after i.p. injection of 60mg/kg dicloflenac sodium salt in sterile PBS. Diclofenac was administered 4 days after mock infection or infection with $5x10^4$ PFU MCMV (Smith strain). Mock 18hr n=6 mice, D4 n=4 mice; MCMV-infected 18hr n=7 mice, D4 n=4 mice. *p<0.05 by Tukey's multiple comparisons test. F) Representative whole mount images at 32X magnification of small intestinal wounds 18hr after diclofenac injection in mock- and MCMV-infected mice. Dotted black lines outline the wound.

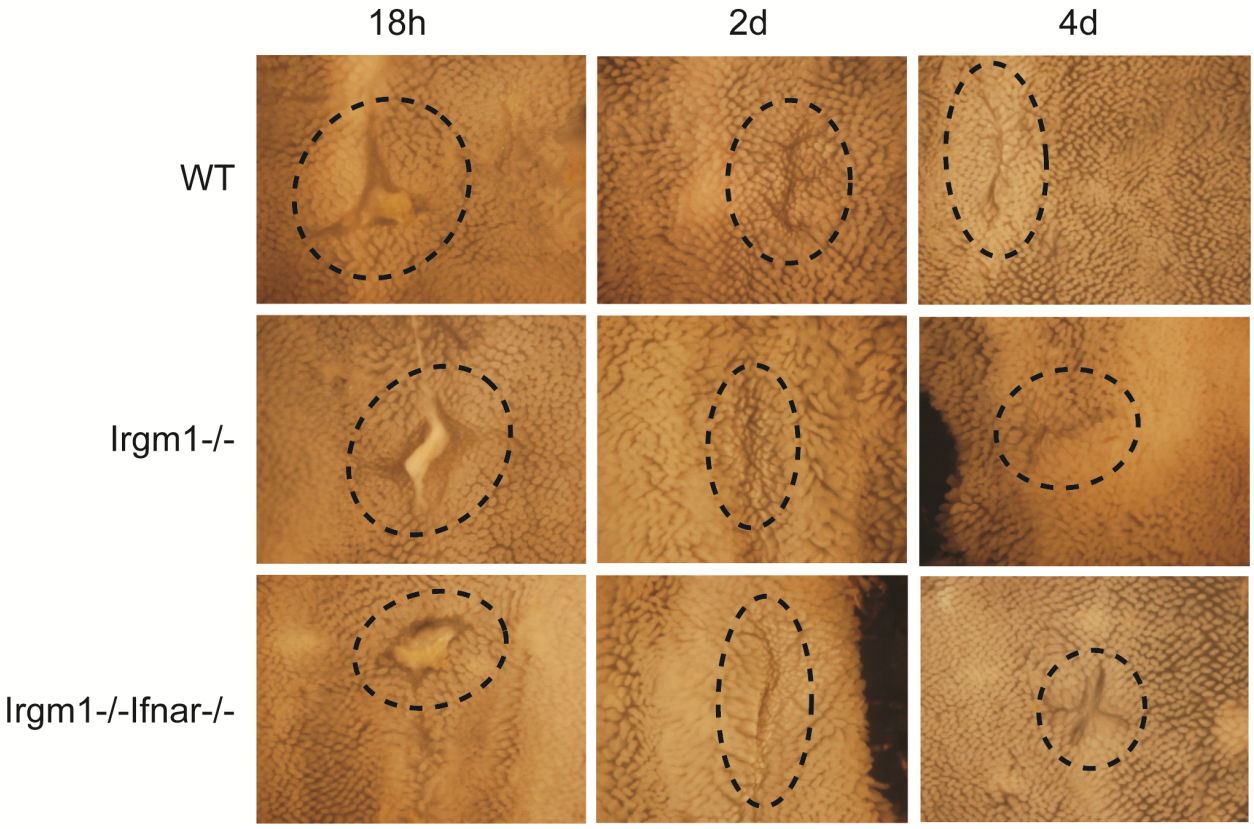

Figure 3.9. *Irgm1*$^{-/-}$ mice had enhanced wound healing dependent on Type I IFN signaling. Representative whole mount images of formalin-fixed small intestinal wounds of WT, *Irgm1*$^{-/-}$ and *Irgm1*$^{-/-}$*Ifnar*$^{-/-}$ mice 18h, 2d and 4d after injection of 60mg/kg diclofenac sodium salt in sterile PBS. Images are shown for 1 mouse each genotype each day at 32X magnification. Dotted black lines outline the wounds.

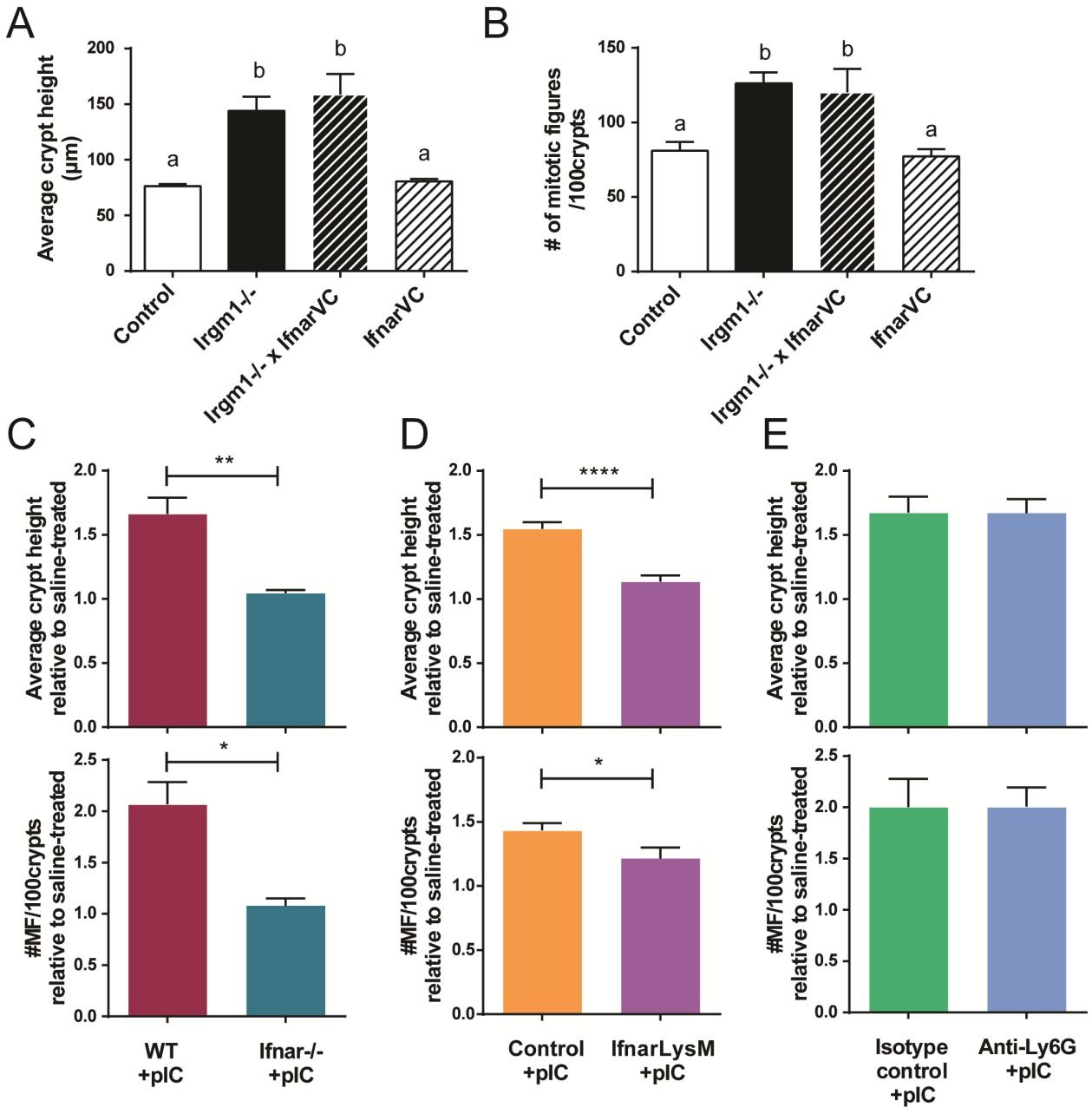

Figure 3.10. Type I IFNs signaled through macrophages to indirectly promote epithelial turnover.

Figure 3.10. Type I IFNs signaled through macrophages to indirectly promote epithelial turnover. A-B) Graph of A) the average crypt height and B) the average number of mitotic figures of 100 crypts ± SEM in control (n=9 mice), *Irgm1*$^{-/-}$ (n=8 mice), *Irgm1*$^{-/-}$*IfnarVC* (n=7 mice), and *IfnarVC* (n=6 mice) mice. Control mice were *Irgm1*$^{+/+}$*Ifnar*$^{f/f}$*-VillinCre* negative. Means with different letters are significantly different by Tukey's multiple comparisons test. C) Graph of the average crypt height and average number of mitotic figures (MF)/100 crypts ± SEM in WT and *Ifnar*$^{-/-}$ mice injected i.p. with saline or 5mg/kg polyI:C for 4 days. WT n=13 mice for each treatment; *Ifnar*$^{-/-}$ n=5 mice for each treatment. D) Graph of the average crypt height and average number of MF/100 crypts ± SEM in control and *IfnarLysM* mice injected i.p. 5mg/kg polyI:C for 4 days. Control: saline n=9 mice, polyI:C n=11 mice. *IfnarLysM*: saline n=7 mice, polyI:C n=8 mice. Control mice were *Ifnar*$^{f/f}$*-LysMCre* negative. Results compiled from 3 independent experiments. E) Graph of the average crypt height and average number of MF/100crypts ± SEM in WT mice treated with isotype control (saline n=5 mice, polyI:C n=6 mice) or anti-Ly6G (saline n=6 mice, polyI:C n=6 mice). Results compiled from 2 independent experiments. For C) to E), the averages ± SEM relative to saline-treated mice are shown. *p<0.05; **p<0.01; ****p<0.0001 by Student's *t* test.

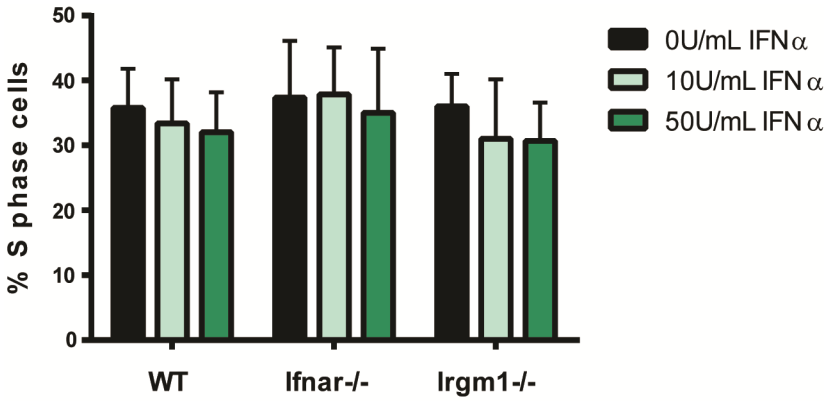

Figure 3.11. IFNα did not directly increase proliferation of epithelial cells *in vitro*. A) Quantification of the average percentage ± SEM of S phase cells after 24h incubation with 0, 10UmL, and 50U/mL of recombinant murine IFNαA. WT, *Ifnar1*$^{-/-}$ and *Irgm1*$^{-/-}$ intestinal epithelial cells were used. Percent S-phase cells were measured by EdU incorporation assay. P=0.7813 by ordinary ANOVA. N=2 replicates each group from 2 independent experiments.

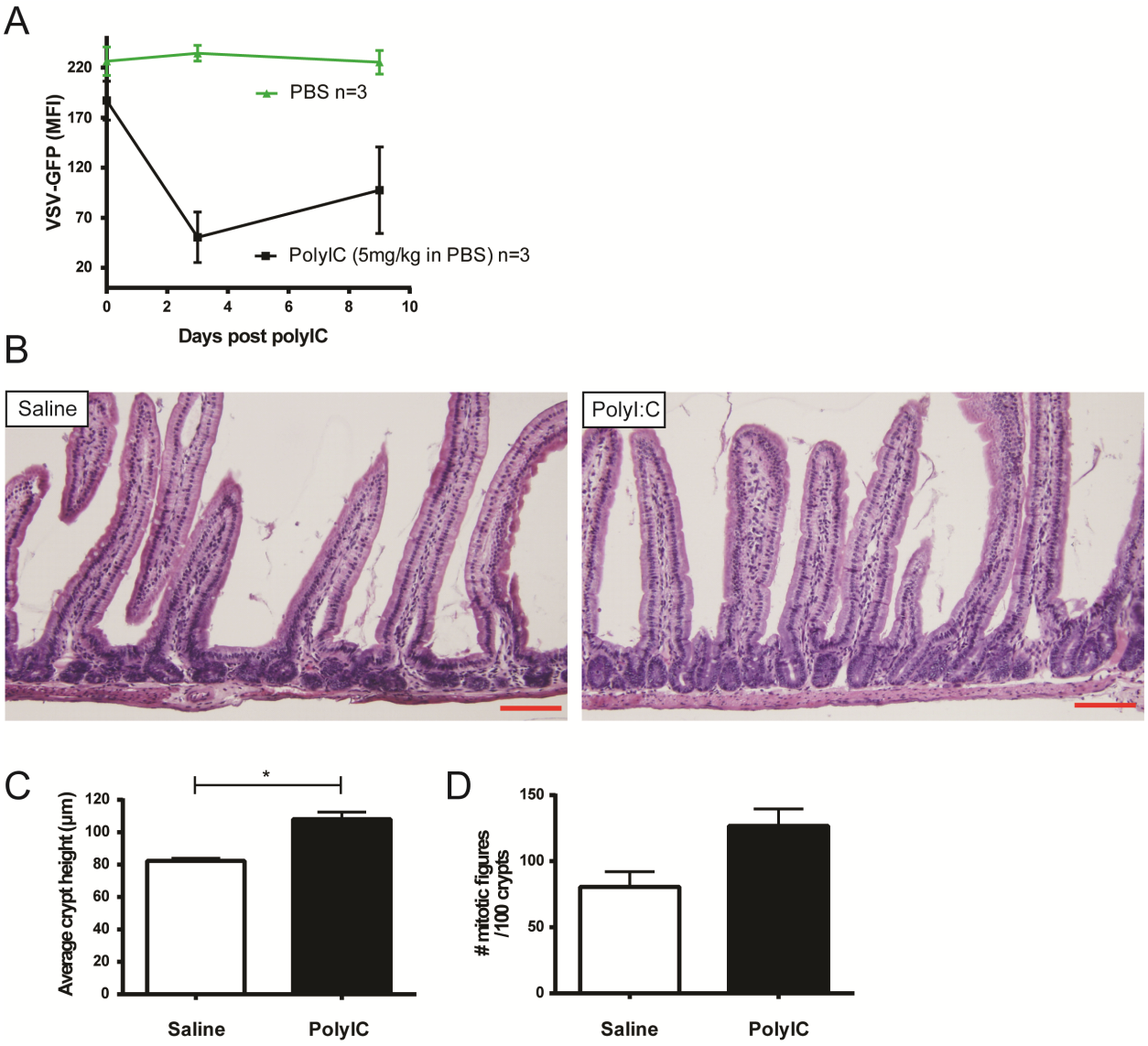

Figure 3.12. PolyI:C injection induced Type I IFNs and promoted epithelial proliferation in WT and *IfnarVC* mice.

Figure 3.12. PolyI:C injection induces Type I IFNs and promote epithelial proliferation in WT and *IfnarVC* mice. A) Graph of average MFI ± SD as a measure of anti-viral activity in serum of polyI:C-injected or saline-injected WT mice over time. N=3 mice each group. Mice were injected daily with 5mg/kg polyI:C or saline and serum samples taken at 0, 3 and 9 days. Serum was assayed for the ability to inhibit VSV-GFP infection in L929 cells in the bioassay system. B) Representative histology of WT mice injected with saline or 5mg/kg polyI:C daily for 4 consecutive days and sacrificed on day 5. Yellow bars delineate the height of a crypt; red bars =100μm. C-D) Quantification of C) the average crypt height ± SEM and D) the average number of mitotic figures/100crypts ± SEM in saline-injected and polyI:C-treated *IfnarVC* mice. Saline n=2 mice, polyI:C n=3 mice. *$p<0.05$ by Student's *t* test.

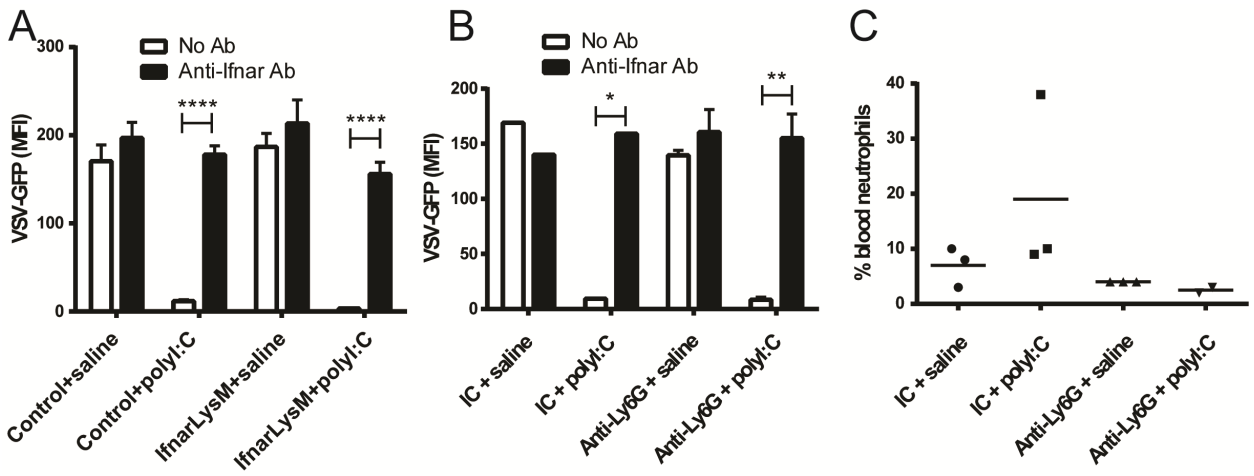

Figure 3.13. Control information for IfnarLysM and neutrophil depletion experiments. A-B) Graphs of antiviral activity present in serum of A) Control and *IfnarLysM* mice (saline n=4 mice, polyI:C n=5 mice for each genotype) and B) neutrophil-depleted mice (isotype control (IC) n=1 mouse each treatment, neutrophil-depleted n=2 mice each treatment). 500ug/mouse of anti-Ly6G antibody or rat IgG2 IC was give i.p. to mice on days -1 and 3 during 4 days of i.p. polyI:C administration to WT mice. *$p<0.05$; **$p<0.01$; ****$p<0.0001$ by Sidak's multiple comparisons test. C) Graph of the percentage of blood neutrophils after administration of depleting antibody. The percent of white blood cells that were neutrophils in whole blood were counted manually by blood smear. Representative experiment out of 2 independent experiments shown.

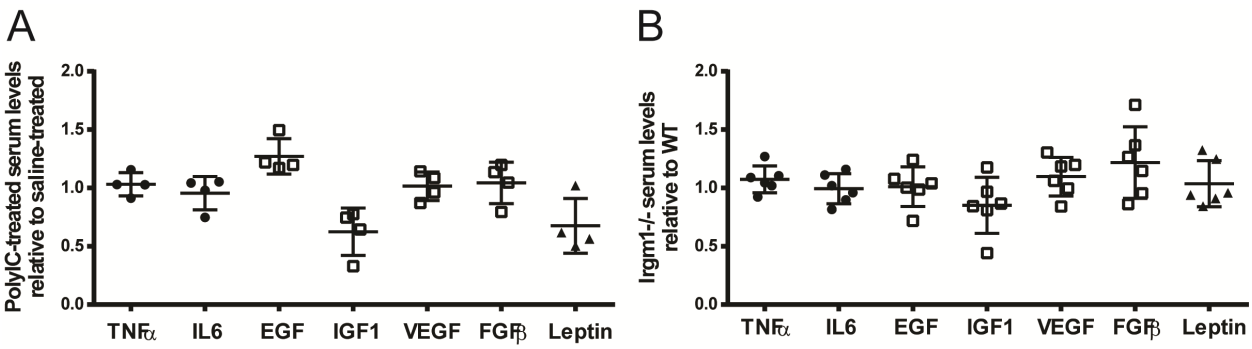

Figure 3.14. Levels of multiple growth factors were unchanged between mice with elevated Type I IFNs and controls. A-B) Graph of the serum levels of multiple known growth factors measured by ELISA in A) saline-treated (4 pools of 2-3 mice, 10 mice total) and polyI:C-treated WT mice (4 pools of 2-3 mice, 9 mice total), and B)WT (6 pools of 1-5 mice, 13 mice total) and *Irgm1*$^{-/-}$ mice (6 pools of 1-6 mice, 14 mice total).

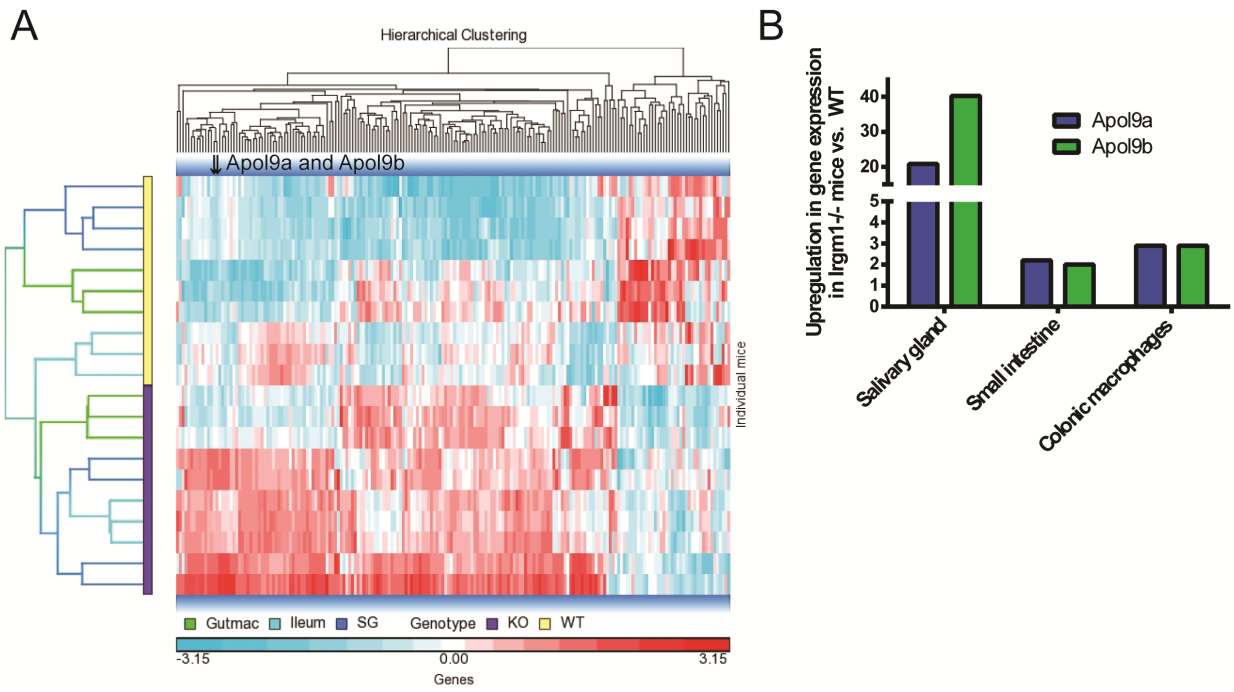

Figure 3.15. Microarray analysis revealed *Apol9a/b* upregulation in *Irgm1*$^{-/-}$ macrophages and tissues. A) Heat map of genes that significantly differed in expression in salivary gland, small intestine, and isolated macrophages between *Irgm1*$^{-/-}$ mice and WT mice, with $p<0.05$ by ANOVA (463 genes), displayed after hierarchical clustering. Whole genome microarray analysis was performed on samples from 3 to 4 mice per genotype per tissue. Rows represent mice and columns represent genes. Black arrows indicate the location of *Apol9a* and *Apol9b*. B) Graph of the fold change in *Apol9a* and *Apol9b* gene expression in *Irgm1*$^{-/-}$ mice relative to WT mice in the three microarrays.

Gene Name	Protein name	Fold change (Macrophages)	P value	Cellular component (Gene Ontology)	Fold change (Salivary gland)	Fold change (Small intestine)
Rtp4	Receptor transporting protein 4	3.02	0.0098	Membrane	8.14	3.77
Apol9b	Apolipoprotein L 9b	2.95	0.0057	Extracellular region	40.13	1.98
Apol9a	Apolipoprotein L 9a	2.92	0.0056	Extracellular region	20.79	2.18
Slc12a2	Solute carrier family 12 member 2	2.76	0.0032	Membrane	0.71	0.96
Cldn14	Claudin 14	2.25	0.0061	Cell membrane	0.60	0.87
Cldn2	Claudin 2	2.12	0.0014	Cell membrane	0.80	1.59
Slc12a8	Solute carrier family 12 member 8	2.10	0.0085	Membrane	0.67	0.98

Table 3.1. Membrane-associated and secreted factors upregulated in *Irgm1*$^{-/-}$ colonic macrophages and tissues. Table of genes upregulated >2-fold with p-value <0.01 by ANOVA in whole genome microarray analysis of *Irgm1*$^{-/-}$ colonic macrophages compared to WT (3 to 4 mice per genotype per tissue). Cellular component was determined by Gene Ontology (GO) analysis. The fold change in salivary gland and distal small intestine is shown for each factor.

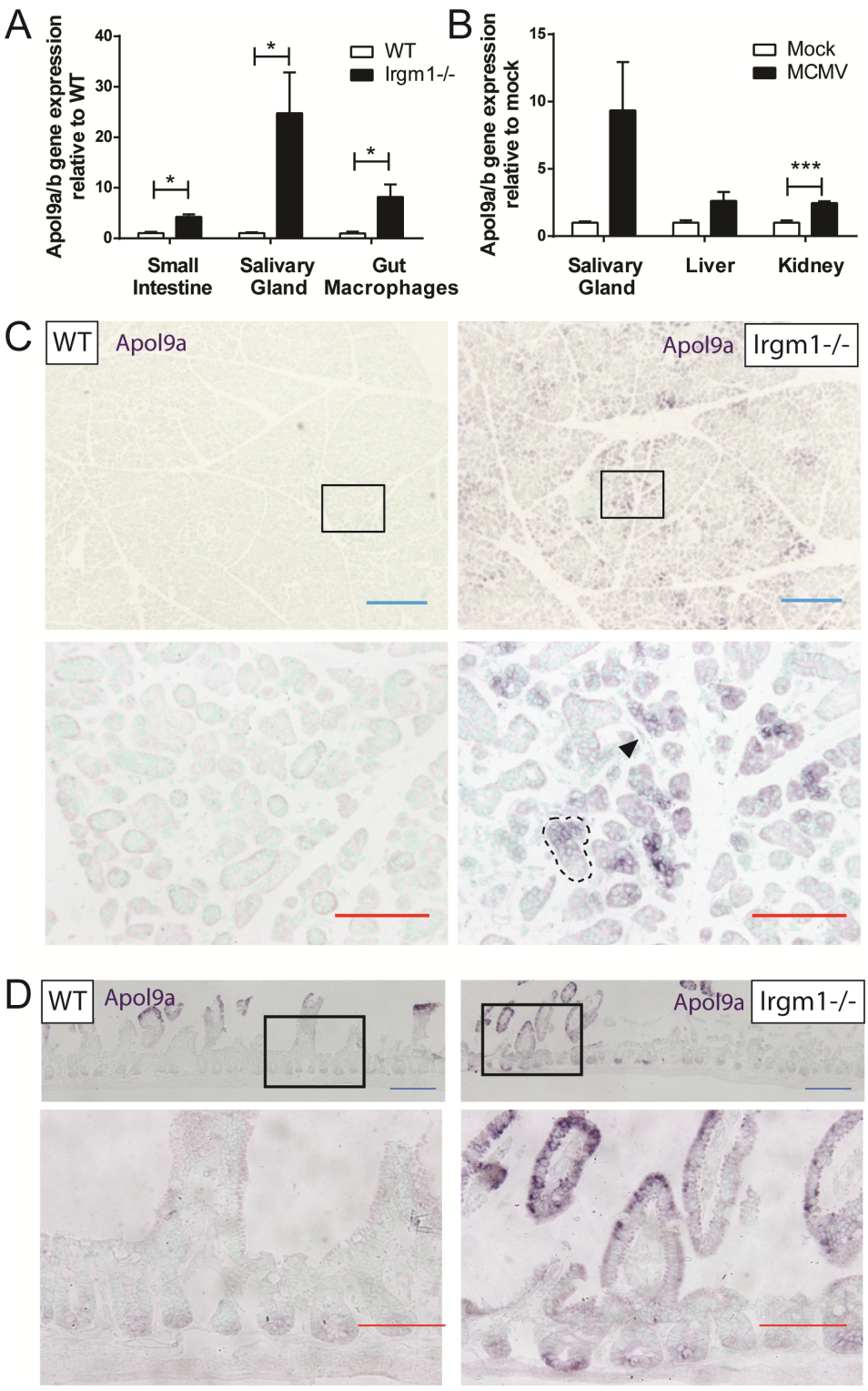

Figure 3.16. The interferon-stimulated genes *Apolipoprotein L9a* and *b* were elevated in stromal and epithelial cells of *Irgm1*$^{-/-}$ and MCMV-infected mice.

Figure 3.16. The interferon-stimulated genes *Apolipoprotein L9a* and *b* were elevated in stromal and epithelial cells of *Irgm1*$^{-/-}$ and MCMV-infected mice. A) Quantification of the average expression ± SEM of *Apol9a/b* mRNA in *Irgm1*$^{-/-}$ small intestine, salivary gland and isolated colonic macrophages relative to WT tissue as measured by qRT-PCR. N=3 mice per genotype. Primers were designed to amplify both *Apol9a* and *b*. *p<0.05 by Student's *t* test for each organ. B) Quantification of the average expression ± SEM of *Apol9a/b* mRNA in MCMV-infected salivary gland, liver and kidney relative to mock-infected tissue as measured by qRT-PCR. Mock-infected n=3 mice, MCMV-infected n=5 mice. ***p<0.001 by Student's *t* test for each organ. C) Representative *in situ* hybridization images for *Apol9a* in WT and *Irgm1*$^{-/-}$ salivary gland. *Apol9a* expression is indicated by dark purple staining. Lower images are insets (area within the black box) of upper images. Blue bar indicates 200μm, red bar indicates 100μm. Black arrowhead indicates an *Apol9a*-positive stromal cell. Dashed black lines outline an *Apol9a*-positive epithelial gland. D) Representative Apol9a *in situ* hybridization images of WT and *Irgm1*$^{-/-}$ small intestine. Black box indicates area of inset (lower images). Black box in *Irgm1*$^{-/-}$ section shows a focus of Apol9a expression. Blue bars indicate 200μm; red bars indicate 100μm.

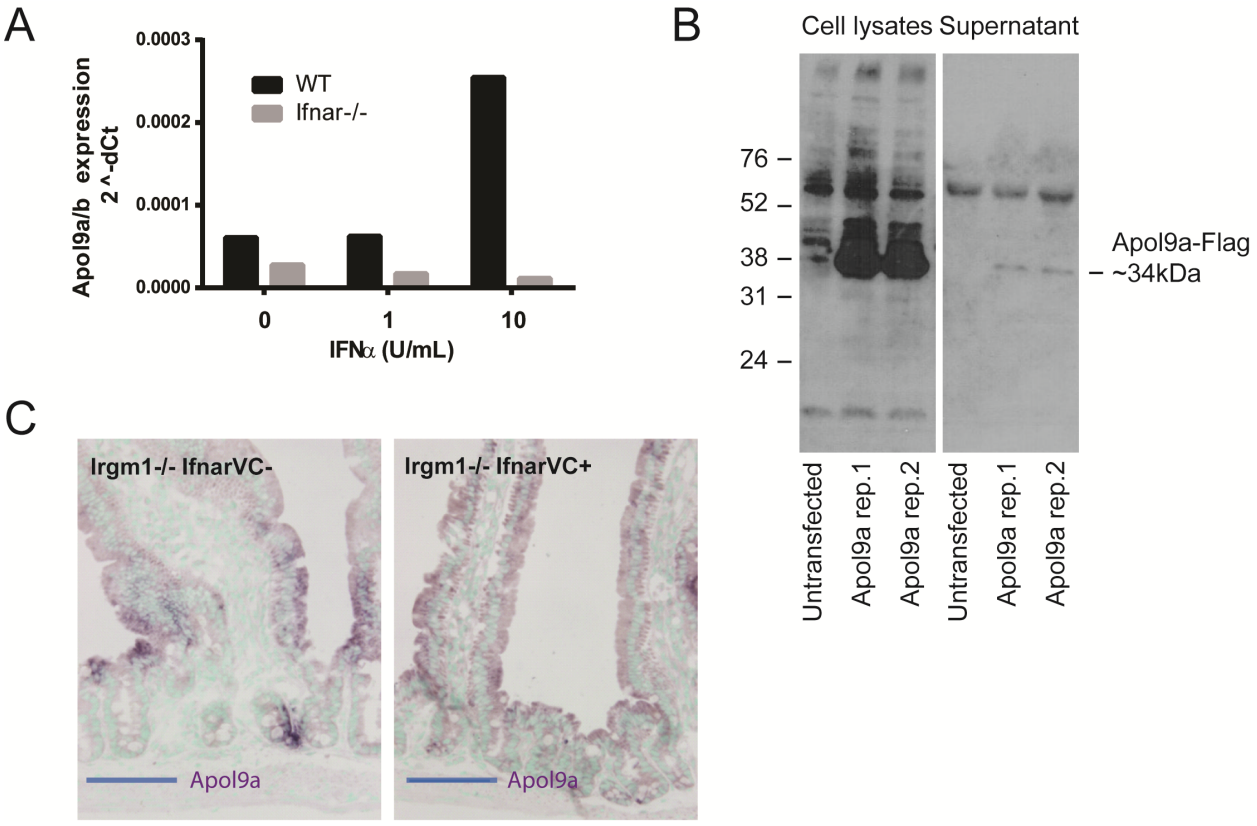

Figure 3.17. Apol9a was stimulated by Type I IFNs, can be secreted, and can be indirectly stimulated. A) Graph of *Apol9a/b* mRNA expression in WT and *Ifnar*$^{-/-}$ bone marrow-derived macrophages stimulated with 0U/mL, 1U/mL, and 10U/mL of recombinant murine IFNαA for 8h. WT n=1, *Ifnar*$^{-/-}$ n=1. 2^-dCt values were calculated relative to GAPDH expression. Primers were constructed to amplify both *Apol9a* and *Apol9b.* B) Anti-Flag immunoblot of cell lysates and supernatant of 293FT cells overexpressing Apol9a-Flag. Supernatant was concentrated 5X after harvesting. 2 separate replicates shown, along with untransfected 293FT cells. C) Representative images of *in situ* hybridization of *Apol9a* in *Irgm1*$^{-/-}$ *VC-* and *Irgm1*$^{-/-}$ *VC+* small intestine. *Apol9a* expression is indicated by dark purple staining. Length of blue bar indicates 100μm.

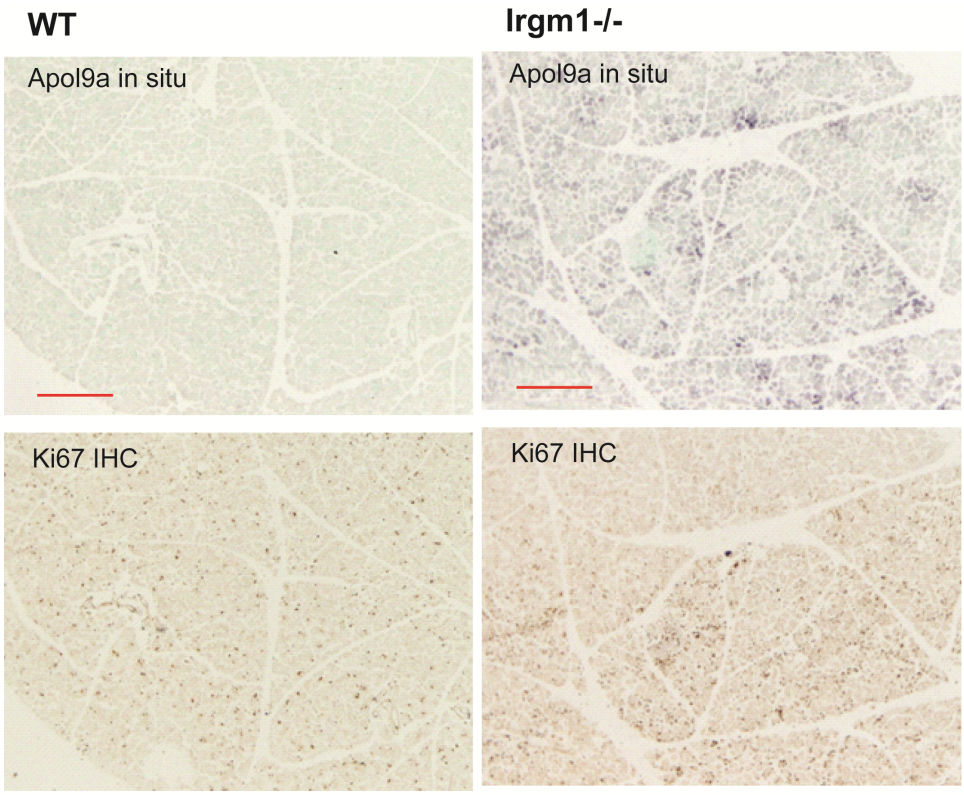

Figure 3.18. Apol9a expression correlated with Ki67 expression in salivary gland.

Representative serial sections of Apol9a *in situ* hybridization and Ki67 immunohistochemistry (IHC) of WT and *Irgm1*$^{-/-}$ salivary gland. Red bar indicates 200μm.

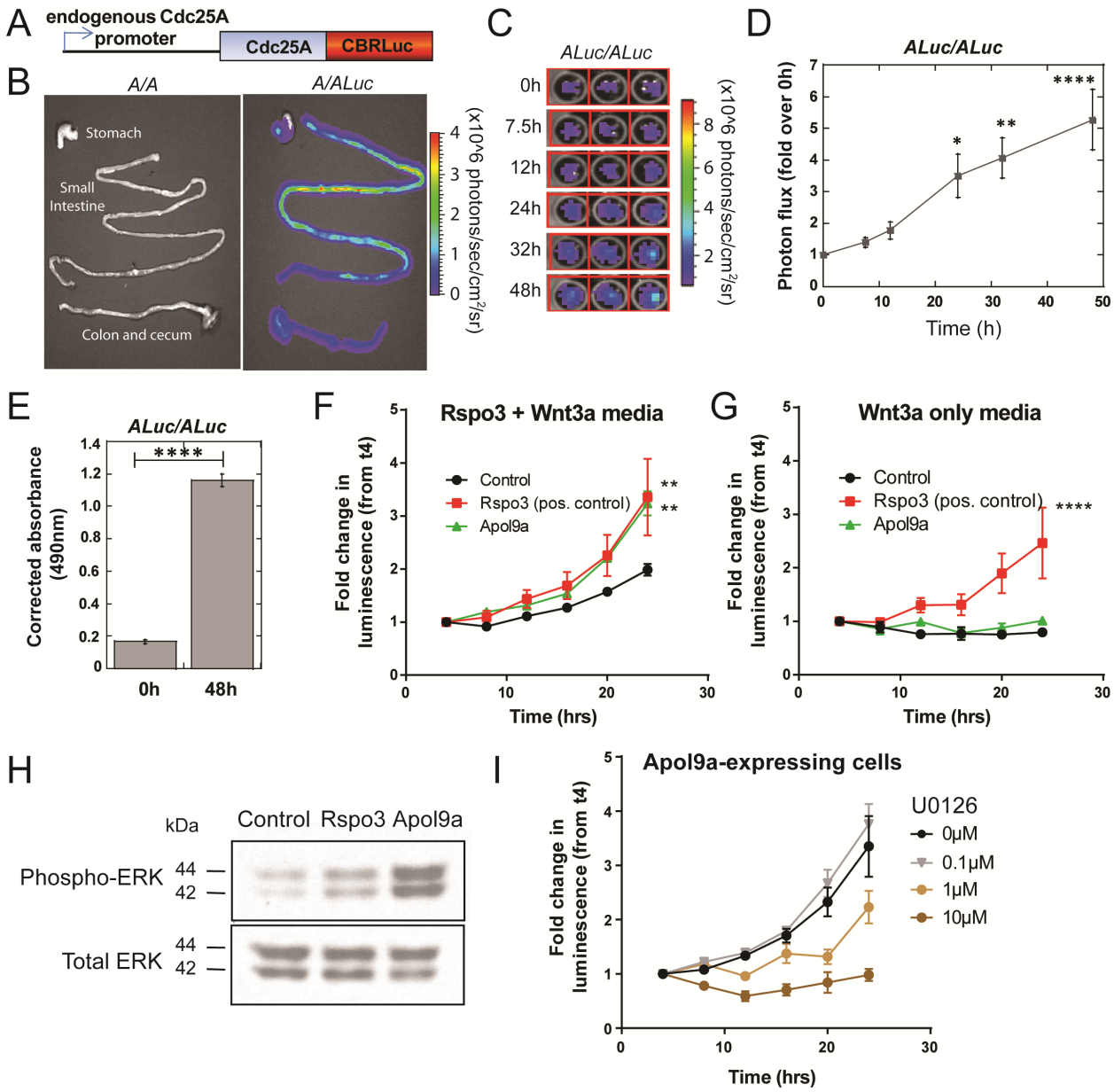

Figure 3.19. Apol9a augmented epithelial proliferation through ERK1/2 activation.

Figure 3.19. Apol9a augmented epithelial proliferation through ERK1/2 activation. A) Schematic representation of Cdc25A-CBRLuc fusion protein expressed in the endogenous *Cdc25A* locus. B) Gray scale photograph and bioluminescence image of gastrointestinal tract of wild-type mice (*A/A*) and knock-in mice that were heterozygous (*A/Luc)* for the Cdc25A-CBRLuc fusion protein. Mice were injected intraperitoneally with D-luciferin, sacrificed and the indicated organs were isolated and subjected to bioluminescence imaging *ex vivo*. Photon flux is indicated by the pseudocolored heatmap. C) Bioluminescence image of Cdc25A-CBRLuc-expressing colonic epithelial cell growth over time. Colonic crypts were isolated from knock-in mice that were homozygous (*ALuc/ALuc*) for the Cdc25A-CBRLuc fusion protein and colonic epithelial spheroid cultures were established. 16h later, fresh media containing D-luciferin was added (t = 0h) and bioluminescence was measured 0h, 7.5h, 12h, and 24h later. Fresh media with D-luciferin was replaced at 24 h post imaging and bioluminescence was measured 32h and 48h later. D) Graph shows the average fold change in bioluminescence (photon flux) relative to 0h after addition of D-luciferin substrate. n = 6 wells from two independent experiments were measured and data are presented as mean ± SEM. *p<0.05, **p<0.01. ****p<0.001 as measured by Dunnett's multiple comparison test. E) Plot of the average absorbance at 490nm obtained by MTS assay of Cdc25A-CBRLuc expressing colonic epithelial spheroid cultures at 0h and 48h of growth. Absorbance was corrected by subtracting background absorbance (media only). Triplicate samples were measured and data are presented as mean ± SEM. Asterisks indicate ****p<0.001 as measured by Student's *t* test. F-G) Graph of the fold change in luminescence during a 24h period after addition of D-luciferin in Cdc25A-CBRLuc intestinal spheroid cultures cultured with F) media containing Rspo3 and Wnt3a or G) Wnt3a only. Cells express Rspo3, Apol9a, or a negative control. The average fold change in luminescence relative to luminescence

measured at 4h, ± SEM, of 3 independent experiments is shown, with 12-18 replicates per cell line per experiment. F) p=0.0389 by repeated measures 2-way ANOVA. G) p= 0.0574 by repeated measures 2-way ANOVA. Asterisks indicate **p<0.01 and ****p<0.0001at 24h only by Dunnett's multiple comparisons test with comparison to control cells. H) Western blot of phosphorylated and total ERK1/2 (p42 and p44) of cells expressing a negative control, Rspo3, or Apol9a. Background-subtracted representative image from 3 independent experiments is shown. I) Graph of the fold change in luminescence measured during a 24h period after addition of D-luciferin and differing concentrations of MEK inhibitor U0126 in Apol9a-expressing Cdc25A-CBRLuc intestinal spheroid cultures. The average fold change in luminescence relative to luminescence measured at 4h, ± SEM, of 2 independent experiments is shown, with 3 replicates per dose per experiment. P=0.0066 by repeated measures 2-way ANOVA.

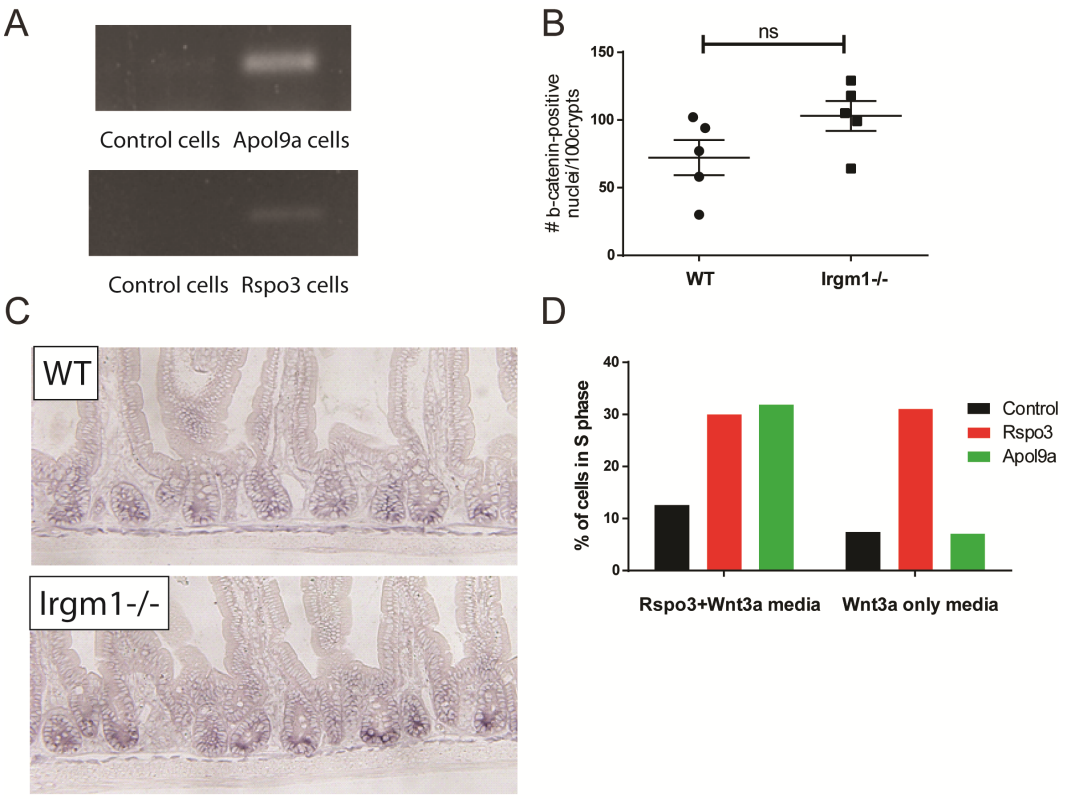

Figure 3.20. Apol9a did not increase epithelial proliferation by enhancing Wnt activation.

A) Gel image of PCR products from Apol9a PCR amplification (30 cycles) from cDNAs generated from small intestinal epithelial cells expressing a control construct or Apol9a and gel image of PCR products from Rspo3 PCR amplification (40 cycles) from cDNAs from small intestinal epithelial cell cultures expressing either a control construct or Rspo3. B) Quantification of the number of β-catenin-positive nuclei per 100 crypts in WT (n=5 mice) and *Irgm1*$^{-/-}$ (n=5 mice) small intestinal tissue after immunohistochemistry staining for β-catenin. C) Representative images of *Axin2* localization by *in situ* hybridization in WT and *Irgm1*$^{-/-}$ small intestinal sections. D) Quantification of the percentage of S phase cells of small intestinal epithelial cells expressing Apol9a, Rspo3, and control after plating in Rspo3+Wnt3a media or Wnt3a only media for 24h. EdU was then added for 2h, and the percentage of EdU positive cells (S-phase cells) was measured by flow cytometry.

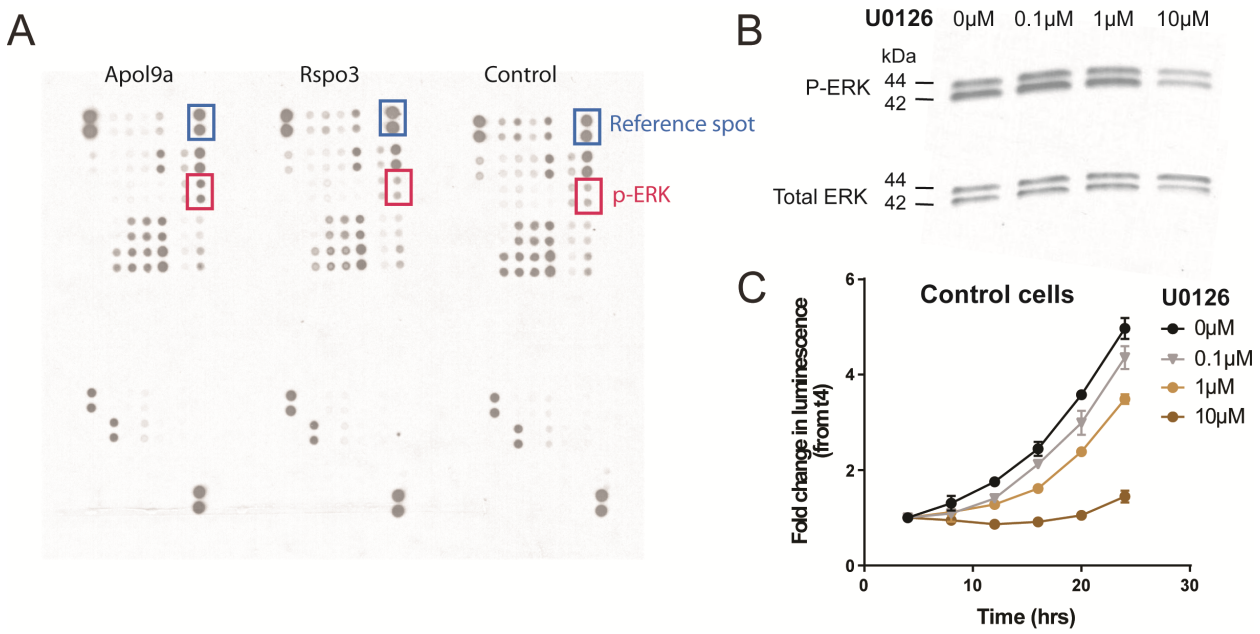

Figure 3.21. Apol9a was associated with activated ERK, and inhibition of ERK activation decreased epithelial proliferation. A) Background-subtracted image of phospho-kinase dot blot array of cell lysates from control, Rspo3, and Apol9a-expressing intestinal epithelial cells. In this commercially available kit, antibodies against phosphorylated kinase targets were dotted onto the array membrane in duplicate before incubation with cell lysates. Red boxes outline dot blot corresponding to phosphorylated ERK1/2, while blue boxes outline reference spots. B) Background-subtracted image of immunoblot detecting phosphorylated ERK1/2 (P-ERK) and total ERK from cell lysates of control small intestinal epithelial cells incubated with increasing concentration of MEK inhibitor U0126 for 24h immediately after passage. C) Graph of the fold change in luminescence measured during a 24h period after addition of D-luciferin and differing concentrations of MEK inhibitor U0126 in control Cdc25A-FLuc intestinal spheroid cultures. The average fold change in luminescence relative to luminescence measured at 4h, ± SEM, of 2 independent experiments is shown, with 3 replicates per dose per experiment. P=0.0006 by repeated measures 2-way ANOVA.

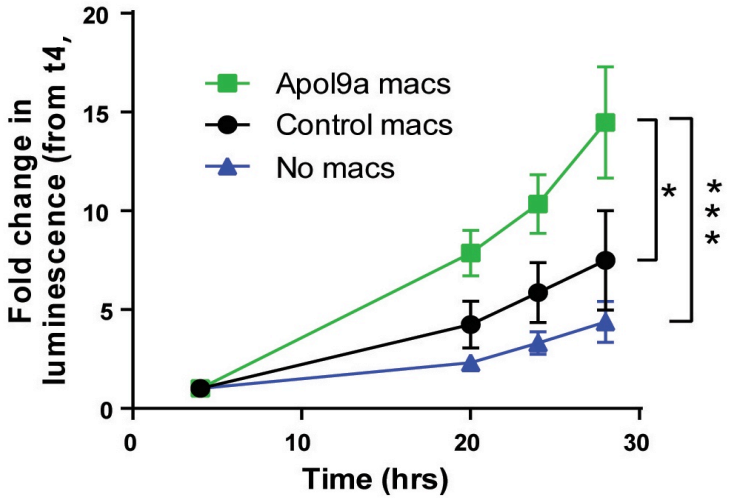

Figure 3.22. Macrophages promoted epithelial proliferation in *trans* via Apol9a expression. Graph of the fold change in luminescence measured during a 28h period after addition of D-luciferin of Cdc25A-CBRLuc intestinal spheroid cultures cultured with WT macrophages expressing Apol9a or a control construct, or without macrophages. The average fold change in luminescence relative to luminescence measured at 4h, ± SEM, of 3 ind. expts. is shown, with 4-5 technical replicates per experiment. P=0.0297 by repeated measures 2-way ANOVA. *p<0.05, ***p<0.001 at 24hrs only by Sidak's multiple comparisons test.

CHAPTER 4:

Summary and Future Directions

SUMMARY

These studies demonstrated that the immune response to viral infection can have broad effects on host physiology. These findings are schematized in **Figure 4.1.** Specifically, we showed that infection with chronic, systemic herpesviruses increased epithelial turnover in multiple organs. Infection with a local RNA virus, MNV, did not increase epithelial turnover in the intestine where it is tropic. I hypothesized that this effect was due to the innate anti-viral cytokines Type I IFNs. However, studying Type I IFN responses in a viral infection model is difficult, as loss of these cytokines can result in uncontrolled viral replication, morbidity, and mortality. To this end, I employed a mouse model with persistently elevated Type I IFNs even in the absence of exogenous viral infection, the *Irgm1*$^{-/-}$ mouse.

I found that *Irgm1*$^{-/-}$ mice had elevated Type I IFNs in the lung and serum, starting as early as 7 days after birth and up to at least 17 weeks of age. IFNα in particular was increased in the serum of *Irgm1*$^{-/-}$ mice. A complete loss of Irgm1 was required to promote Type I IFN production, as *Irgm1*$^{+/-}$ mice had levels of IFNs similar to WT controls. I verified that the Type I IFNs were functional, since they induced ISG expression in multiple organs. *Irgm1*$^{-/-}$ mice were protected against influenza A infection, likely due to a primed antiviral response. Investigation of lung histology revealed the presence of aggregates of mixed immune cells (T and B cells, dendritic cells, macrophages) in *Irgm1*$^{-/-}$ mice even without influenza infection. The formation of these aggregates was dependent on Type I IFN signaling. These aggregates may have played a role in antiviral defense against flu infection in Irgm1-deficient animals.

I next attempted to determine the source of increased Type I IFN production in *Irgm1*$^{-/-}$ mice. IFNα and IFNβ1 transcripts were unchanged in multiple organ homogenates of *Irgm1*$^{-/-}$ and WT mice. Irgm1-deficient bone marrow-derived dendritic cells and intestinal epithelial cells

had similar sensitivity to polyI:C stimulation compared to WT cells. Bone marrow cells from *Irgm1*$^{-/-}$ and WT mice had comparable surface expression of the Type I IFN receptor Ifnar. I found that T and B cells and thus the adaptive immune system were not required for enhanced production of Type I IFNs in Irgm1-deficient animals, but that liver macrophages played a role in this process. Finally, I established that broad-spectrum antibiotic treatment did not diminish increased Type I IFN levels in *Irgm1*$^{-/-}$ mice. Together, these results revealed a previously unreported role for Irgm1 in macrophages in the negative regulation of Type I IFN production.

The *Irgm1*$^{-/-}$ mouse also enabled the exploration of the impact of Type I IFNs on host physiology. Similar to what I observed in herpesvirus infection, *Irgm1*$^{-/-}$ mice also had increased epithelial turnover in multiple organs. Using *Irgm1*$^{-/-}$*Ifnar*$^{-/-}$ mice, I verified that this effect was dependent on Type I IFN signaling. Accelerated turnover was not universal, as there was no increased proliferation in lung epithelium, thyroid epithelium, or skeletal muscle. Increased proliferation, not cell death, seemed to be the primary driver of increased turnover. Notably, Type I IFNs promoted enhanced healing in two different models of wound repair in *Irgm1*$^{-/-}$ mice. I discovered that Type I IFNs did not act directly on the epithelial cells to promote turnover. Instead, Type I IFN signaling through macrophages was important for this process. I used a microarray screening approach to determine novel candidates that could promote epithelial proliferation. I found that the ISGs *Apolipoprotein L9a* and *b* were elevated in *Irgm1*$^{-/-}$ mice and also virally-infected animals. Finally, expression of *Apol9a* in intestinal epithelial cells could increase proliferation through enhanced ERK activation. These findings demonstrate a novel role for Type I IFNs in modulating epithelial turnover through the function of previously uncharacterized ISGs (**Figure 4.1**).

FUTURE DIRECTIONS

Determine the mechanism by which Irgm1 negatively regulates Type I IFN production

Chapter 2 describes the elevation of Type I IFNs in *Irgm1*$^{-/-}$ mice, but what causes this increase is unclear. Based on our preliminary results and prior reports in the literature, I hypothesize that Irgm1 functions to regulate sensing of intracellular nucleic acid debris in tissue macrophages.

Our preliminary evidence suggested that hepatic macrophages play a role in the production of Type I IFNs in *Irgm1*$^{-/-}$ mice. To support our findings using clodronate liposomes to deplete liver macrophages, we are currently generating an *Irgm1*$^{flox/flox}$ mouse. This line can then be crossed to a LysM-Cre line to knock out Irgm1 in macrophages and granulocytes only. If Irgm1 acts in macrophages to negatively regulate Type I IFN production, these *Irgm1*$^{flox/flox}$ *LysM-Cre* animals should still have elevations in systemic Type I IFNs. If instead Irgm1 acts through an alternative or additional cell type, Type I IFN levels should be similar to controls. In this latter case, the *Irgm1*$^{flox/flox}$ mouse can be crossed to different Cre lines to find the relevant cell type.

To verify that Irgm1-deficient Kupffer cells produce increased Type I IFNs, we could isolate liver macrophages from WT and *Irgm1*$^{-/-}$ mice and assess mRNA expression and protein production of Type I IFNs. I predict that Type I IFN expression would be enhanced in *Irgm1*$^{-/-}$ liver macrophages, either at baseline and/or upon addition of polyI:C or other stimuli. We could also assess the localization of Type I IFN production *in vivo* using *in situ* hybridization for IFNα and anti-IFNα antibodies. Co-localization with liver macrophages would demonstrate that these cells are the source of Type I IFNs.

The next step would be to determine a molecular mechanism for enhanced Type I IFN production in liver macrophages. First, the location of Irgm1 within the cell should be determined. Previous studies have shown Irgm1 localization onto the Golgi membrane as well as late endosomal and lysosomal compartments in IFNγ-treated cells (Martens et al., 2004; Zhao et al., 2010). These studies were conducted in L929 fibroblasts, TIB-75 hepatocytes, RAW264.7 macrophages, and murine embryonic fibroblasts (MEFs). It would be informative to see if Irgm1 also localizes in a similar manner in primary Kupffer cells, and if it co-localizes with membrane-bound IFN regulators such as STING and MAVS. Binding of Irgm1 to these proteins or associated protein complexes could be determined by co-immunoprecipitation. Such co-localization would suggest that Irgm1 could regulate the production of Type I IFNs through these adaptors of nucleic acid-sensing pathways. Kupffer cells in particular would have a high burden of intracellular nucleic acids due to their function in clearing erythrocyte nuclei, apoptotic bodies, and other debris.

It is also possible that Irgm1 functions by a completely different, unknown mechanism. In this case, it would be informative to determine novel protein interactions by co-immunoprecipitation and mass spectroscopy. Whole genome microarray or RNA-seq analysis of the Type I IFN-producing cell in *Irgm1*$^{-/-}$ and WT mice could also be performed.

Clarify viral contributions to increased epithelial turnover

An additional point of interest is that some but not all viruses can induce increased epithelial turnover. We found that MCMV and MHV68, two DNA herpesviruses, could increase epithelial turnover, whereas MNV, an RNA virus, could not. One explanation could be that different viruses induce or inhibit varying levels of Type I IFNs. Viruses that induce higher

levels of interferons may be able to promote greater levels of epithelial proliferation. To test this, we could measure Type I IFN levels at multiple time points after infection with MCMV, MHV68 and MNV. Additional viral types could be tested to further elucidate whether certain classes of viruses stimulate epithelial turnover. It may be that a systemic viral infection is required to promote epithelial proliferation (as observed in MCMV and MHV68 infection), compared to an isolated infection (seen in MNV infection). A further advantage of using these murine viruses is that viral mutants can be generated to test whether certain viral components are required to produce a response.

In addition, we only examined epithelial turnover at one time point for each virus, day 7 after infection for MNV and MCMV, and day 16 for MHV68. These time points were chosen as they were the time when these viruses are establishing persistent chronic infection (Munks et al., 2006; Nice et al., 2013; Tibbetts et al., 2003). However, it would also be important to look at epithelial turnover at other times, including the earlier acute phase and later during chronic infection.

Distinguish differences in epithelial organs that result in discrepant proliferative responses to Type I IFNs

One notable finding was that not all epithelial organs had proliferative responses to Type I IFN stimulation. Increased turnover was observed in small intestine, kidney, salivary gland, liver, and pancreatic epithelia, but not lung or thyroid epithelia, nor skeletal muscle of *Irgm1*$^{-/-}$ mice. It would be interesting to extend these findings to other organs, including epithelial organs such as skin, esophagus, uterus, and bladder, as well as non-epithelial organs including cardiac muscle, smooth muscle, neuronal tissue, and adipose tissue. Intriguingly, a glandular

organization is shared among those epithelial organs examined so far that had increased turnover in *Irgm1*$^{-/-}$ mice. By investigating additional tissues, patterns may be distinguished that could aid in our understanding of this phenomenon.

We found that, at least in the case of the small intestine, Type I IFNs signaled indirectly through macrophages to promote increased epithelial turnover. It could be that there are differences in the tissue macrophage populations that reside in the disparate organs, resulting in some that promote turnover in response to Type I IFNs, and some that do not. The macrophages in these tissues could be isolated and compared by flow cytometry and/or microarray analysis to identify these differences. The tissue localization of the macrophages could also play a role in determining epithelial responses. In the tissue types that had increased epithelial proliferation, macrophages are situated between and around the glandular epithelium. This close proximity may enable the macrophages to influence the surrounding epithelial cells. *In vitro* primary macrophage-epithelial co-culture experiments would be valuable in dissecting out these interactions.

Characterize the function of Apolipoprotein L9a/b

Finally, this project demonstrates that *Apolipoprotein L9a* and *b*, highly homologous interferon-stimulated genes, are involved in Type I IFN-induced epithelial turnover by enhancing ERK activation. However, many questions remain regarding the localization, function, and protein interactions of these proteins.

We are currently generating an *Apol9a/b* knockout mouse using the CRISPR/Cas9 system. Once obtained, this knockout will allow in depth loss-of-function studies into the role of Apol9a/b in viral infection, epithelial turnover, and potentially undiscovered physiological

processes. Initial characterization of the knockout, if it is not embryonic lethal, should consist of a careful gross and histological examination of conventionally raised animals without additional challenge. The *Apol9a/b* knockout mouse could be administered polyI:C injections and/or crossed with the *Irgm1*$^{-/-}$ mouse line to determine whether Apol9a/b is absolutely necessary for increased epithelial proliferation in response to Type I IFNs. One previous study suggested a role for Apol9b in anti-viral protection in neurons (Kreit et al., 2014). It would thus be informative to infect *Apol9a/b* knockout mice with different viruses and examine not only the epithelial proliferative response, but also the antiviral immune response.

In the shorter term, *Apol9a/b* knockdown primary epithelial cell lines could be created. This would allow for examination of epithelial responses *in vitro.* For example, preliminary evidence suggests that co-culture of bone marrow-derived macrophages with intestinal epithelial cells enhances epithelial proliferation (**Figure 4.2**). Knocking down *Apol9a/b* in the epithelial cells would uncover whether these ISGs are necessary for epithelial proliferation under stimulative conditions. It would also be interesting to determine whether *Apol9a/b* expression under baseline conditions is also necessary for epithelial proliferation.

An additional question is where Apol9a/b is localized within the cell and whether it is secreted. Our preliminary evidence suggests that Apol9a can be secreted from 293FT cells. However, whether this is true in a macrophage cell line or primary macrophages and epithelial cells is unclear. To this end, a Flag-tagged Apol9a construct could be expressed within these cell types. Immunofluorescence against the Flag-tag could localize Apol9a within the cell. Alternatively, cell fractionation and immunoblotting against various cellular compartments could be performed. Cells could be cultured and supernatant immunoblotted for secreted Apol9a. In addition, it may be prudent to generate a few antibodies against Apol9a and b, which are

currently not commercially available. This would prevent mislocalization or inhibition of function due to the Flag-tag.

Whether or not Apol9a/b is secreted, co-immunoprecipitation and mass spectroscopy could be used to identify its binding partner(s). It would be interesting to determine whether Apol9a/b interacts directly with ERK or if there are adaptors or intermediate signaling proteins that are involved. Findings regarding Apol9a/b could extend further to other members of the Apolipoprotein L family, of which little is currently known.

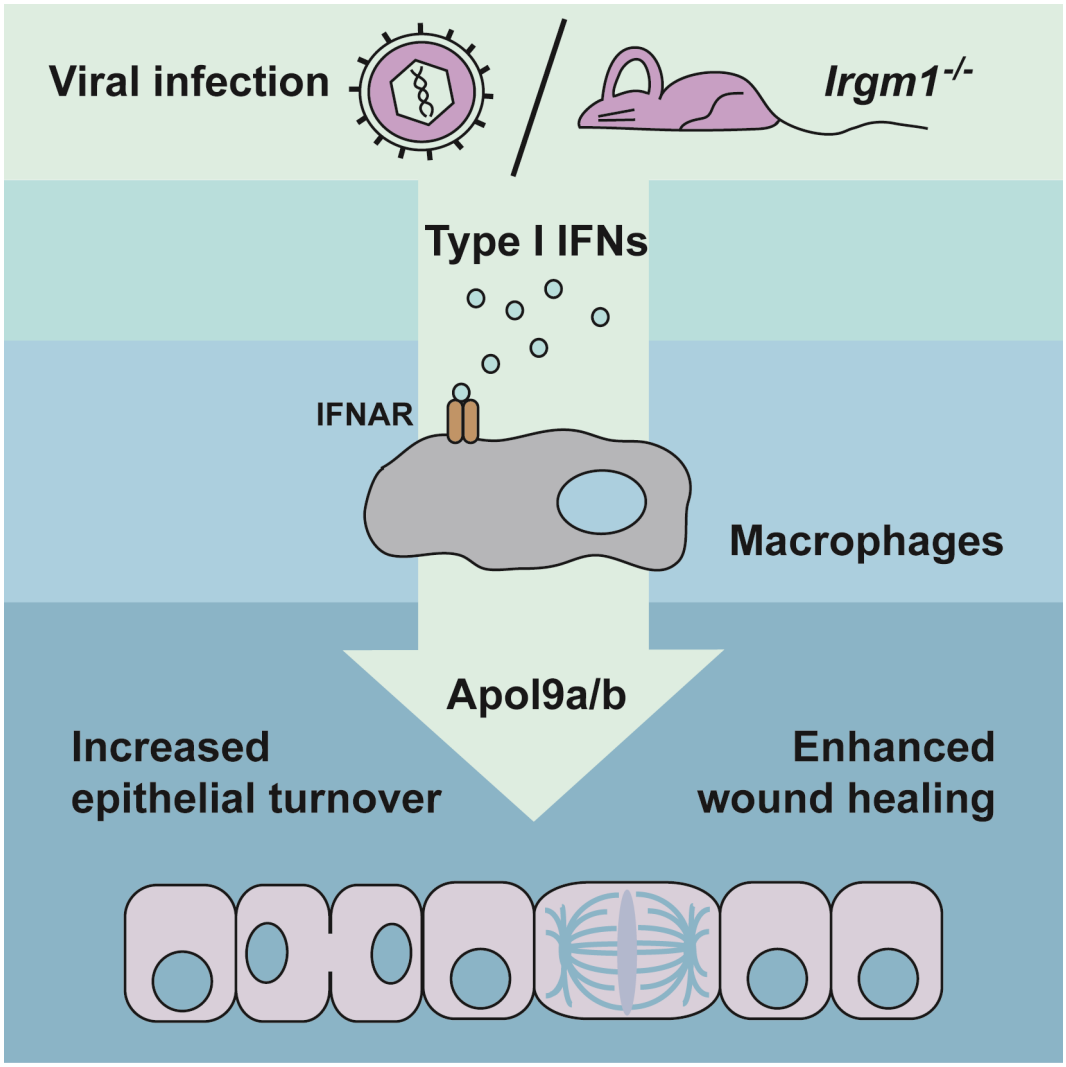

Figure 4.1. Model of Type I IFN induction of increased epithelial turnover. Type I IFNs are elevated in both viral infection and in mice lacking Irgm1. These cytokines signal through macrophages, stimulating expression of *Apol9a/b* and promoting *Apol9a/b* expression in epithelial cells themselves. Epithelial cell proliferation and cell death is increased, resulting in enhanced wound healing.

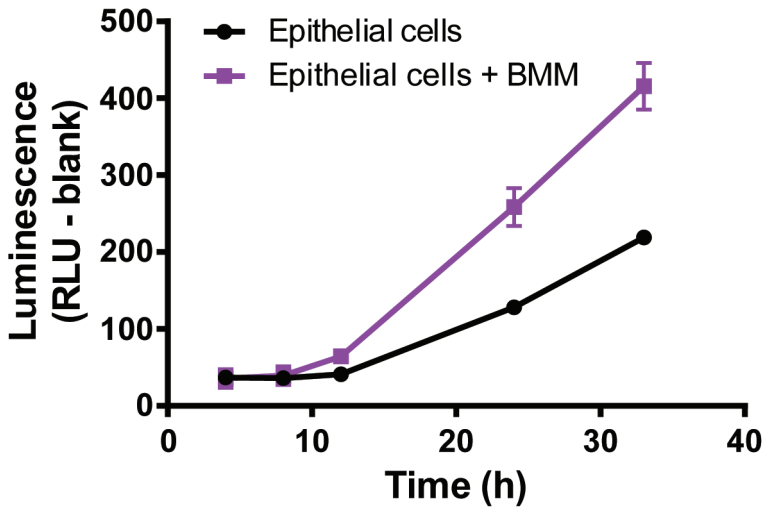

Figure 4.2. Co-culture with macrophages increased proliferation of epithelial cells. Graph of average luminescence of Cdc25A-CBRLuc small intestinal epithelial spheroid cells as measured by blank-subtracted relative light units (RLU). Spheroid cells were trypsinized and plated in 96-well plates either with bone marrow-derived macrophages (BMM) (n=2 sets of BMM from 2 mice, 4 technical replicates) or without co-culture (4 technical replicates). All cells were plated in Matrigel and covered with 100μL of 50% L-WRN conditioned media and ROCK inhibitor. Luminescence was measured at 4, 8, 12, 24 and 33 hours after plating using a plate reader.

REFERENCES

Ablasser, A., Bauernfeind, F., Hartmann, G., Latz, E., Fitzgerald, K.A., and Hornung, V. (2009). RIG-I-dependent sensing of poly(dA:dT) through the induction of an RNA polymerase III-transcribed RNA intermediate. Nat Immunol *10*, 1065-1072.

Abt, M.C., Osborne, L.C., Monticelli, L.A., Doering, T.A., Alenghat, T., Sonnenberg, G.F., Paley, M.A., Antenus, M., Williams, K.L., Erikson, J.*, et al.* (2012). Commensal bacteria calibrate the activation threshold of innate antiviral immunity. Immunity *37*, 158-170.

Ahn, W.S., Bae, S.M., Lee, J.M., Namkoong, S.E., Han, S.J., Cho, Y.L., Nam, G.H., Seo, J.S., Kim, C.K., and Kim, Y.W. (2004). Searching for pathogenic gene functions to cervical cancer. Gynecol Oncol *93*, 41-48.

Albert, T.S., Duchateau, P.N., Deeb, S.S., Pullinger, C.R., Cho, M.H., Heilbron, D.C., Malloy, M.J., Kane, J.P., and Brown, B.G. (2005). Apolipoprotein L-I is positively associated with hyperglycemia and plasma triglycerides in CAD patients with low HDL. J Lipid Res *46*, 469-474.

Alexopoulou, L., Holt, A.C., Medzhitov, R., and Flavell, R.A. (2001). Recognition of double-stranded RNA and activation of NF-kappaB by Toll-like receptor 3. Nature *413*, 732-738.

Arbuckle, M.R., McClain, M.T., Rubertone, M.V., Scofield, R.H., Dennis, G.J., James, J.A., and Harley, J.B. (2003). Development of autoantibodies before the clinical onset of systemic lupus erythematosus. N Engl J Med *349*, 1526-1533.

Arimori, Y., Nakamura, R., Yamada, H., Shibata, K., Maeda, N., Kase, T., and Yoshikai, Y. (2013). Type I interferon limits influenza virus-induced acute lung injury by regulation of excessive inflammation in mice. Antiviral Res *99*, 230-237.

Ashida, H., Ogawa, M., Kim, M., Mimuro, H., and Sasakawa, C. (2012). Bacteria and host interactions in the gut epithelial barrier. Nat Chem Biol *8*, 36-45.

Asselin-Paturel, C., and Trinchieri, G. (2005). Production of type I interferons: plasmacytoid dendritic cells and beyond. J Exp Med *202*, 461-465.

Auerbuch, V., Brockstedt, D.G., Meyer-Morse, N., O'Riordan, M., and Portnoy, D.A. (2004). Mice lacking the type I interferon receptor are resistant to Listeria monocytogenes. J Exp Med *200*, 527-533.

Bahari, G., Hashemi, M., Taheri, M., Naderi, M., Eskandari-Nasab, E., and Atabaki, M. (2012). Association of IRGM Polymorphisms and Susceptibility to Pulmonary Tuberculosis in Zahedan, Southeast Iran. ScientificWorldJournal *2012*, 950801.

Barton, E.S., Lutzke, M.L., Rochford, R., and Virgin, H.W.t. (2005). Alpha/beta interferons regulate murine gammaherpesvirus latent gene expression and reactivation from latency. J Virol *79*, 14149-14160.

Bekpen, C., Hunn, J.P., Rohde, C., Parvanova, I., Guethlein, L., Dunn, D.M., Glowalla, E., Leptin, M., and Howard, J.C. (2005). The interferon-inducible p47 (IRG) GTPases in vertebrates: loss of the cell autonomous resistance mechanism in the human lineage. Genome Biol *6*, R92.

Bekpen, C., Marques-Bonet, T., Alkan, C., Antonacci, F., Leogrande, M.B., Ventura, M., Kidd, J.M., Siswara, P., Howard, J.C., and Eichler, E.E. (2009). Death and resurrection of the human IRGM gene. PLoS Genet *5*, e1000403.

Belgnaoui, S.M., Paz, S., and Hiscott, J. (2011). Orchestrating the interferon antiviral response through the mitochondrial antiviral signaling (MAVS) adapter. Curr Opin Immunol *23*, 564-572.

Bellizzi, A., Anzivino, E., Rodio, D.M., Palamara, A.T., Nencioni, L., and Pietropaolo, V. (2013). New insights on human polyomavirus JC and pathogenesis of progressive multifocal leukoencephalopathy. Clin Dev Immunol *2013*, 839719.

Bhinder, G., Sham, H.P., Chan, J.M., Morampudi, V., Jacobson, K., and Vallance, B.A. (2013). The Citrobacter rodentium mouse model: studying pathogen and host contributions to infectious colitis. J Vis Exp, e50222.

Blanpain, C., Horsley, V., and Fuchs, E. (2007). Epithelial stem cells: turning over new leaves. Cell *128*, 445-458.

Boehm, U., Guethlein, L., Klamp, T., Ozbek, K., Schaub, A., Futterer, A., Pfeffer, K., and Howard, J.C. (1998). Two families of GTPases dominate the complex cellular response to IFN-gamma. J Immunol *161*, 6715-6723.

Botto, M., Dell'Agnola, C., Bygrave, A.E., Thompson, E.M., Cook, H.T., Petry, F., Loos, M., Pandolfi, P.P., and Walport, M.J. (1998). Homozygous C1q deficiency causes glomerulonephritis associated with multiple apoptotic bodies. Nat Genet *19*, 56-59.

Botto, M., Kirschfink, M., Macor, P., Pickering, M.C., Wurzner, R., and Tedesco, F. (2009). Complement in human diseases: Lessons from complement deficiencies. Mol Immunol *46*, 2774-2783.

Boutros, R., Dozier, C., and Ducommun, B. (2006). The when and wheres of CDC25 phosphatases. Curr Opin Cell Biol *18*, 185-191.

Brest, P., Lapaquette, P., Souidi, M., Lebrigand, K., Cesaro, A., Vouret-Craviari, V., Mari, B., Barbry, P., Mosnier, J.F., Hebuterne, X.*, et al.* (2011). A synonymous variant in IRGM alters a binding site for miR-196 and causes deregulation of IRGM-dependent xenophagy in Crohn's disease. Nat Genet.

Briggs, T.A., Rice, G.I., Daly, S., Urquhart, J., Gornall, H., Bader-Meunier, B., Baskar, K., Baskar, S., Baudouin, V., Beresford, M.W.*, et al.* (2011). Tartrate-resistant acid phosphatase deficiency causes a bone dysplasia with autoimmunity and a type I interferon expression signature. Nat Genet *43*, 127-131.

Brown, S.L., Riehl, T.E., Walker, M.R., Geske, M.J., Doherty, J.M., Stenson, W.F., and Stappenbeck, T.S. (2007). Myd88-dependent positioning of Ptgs2-expressing stromal cells maintains colonic epithelial proliferation during injury. J Clin Invest *117*, 258-269.

Brune, W., Hengel, H., and Koszinowski, U.H. (2001). A mouse model for cytomegalovirus infection. Curr Protoc Immunol *Chapter 19*, Unit 19 17.

Cadwell, K., Patel, K.K., Maloney, N.S., Liu, T.C., Ng, A.C., Storer, C.E., Head, R.D., Xavier, R., Stappenbeck, T.S., and Virgin, H.W. (2010). Virus-plus-susceptibility gene interaction determines Crohn's disease gene Atg16L1 phenotypes in intestine. Cell *141*, 1135-1145.

Cai, Q., and Sheng, Z.H. (2011). Uncovering the role of Snapin in regulating autophagy-lysosomal function. Autophagy *7*, 445-447.

Canny, S.P., Reese, T.A., Johnson, L.S., Zhang, X., Kambal, A., Duan, E., Liu, C.Y., and Virgin, H.W. (2014). Pervasive transcription of a herpesvirus genome generates functionally important RNAs. MBio *5*, e01033-01013.

Carrero, J.A., Calderon, B., and Unanue, E.R. (2004). Type I interferon sensitizes lymphocytes to apoptosis and reduces resistance to Listeria infection. J Exp Med *200*, 535-540.

Carrero, J.A., Calderon, B., and Unanue, E.R. (2006). Lymphocytes are detrimental during the early innate immune response against Listeria monocytogenes. J Exp Med *203*, 933-940.

Cesarman, E. (2014). Gammaherpesviruses and lymphoproliferative disorders. Annu Rev Pathol *9*, 349-372.

Chawla-Sarkar, M., Lindner, D.J., Liu, Y.F., Williams, B.R., Sen, G.C., Silverman, R.H., and Borden, E.C. (2003). Apoptosis and interferons: role of interferon-stimulated genes as mediators of apoptosis. Apoptosis *8*, 237-249.

Che, N., Li, S., Gao, T., Zhang, Z., Han, Y., Zhang, X., Sun, Y., Liu, Y., Sun, Z., Zhang, J.*, et al.* (2010). Identification of a novel IRGM promoter single nucleotide polymorphism associated with tuberculosis. Clin Chim Acta *411*, 1645-1649.

Cheng, C.S., Feldman, K.E., Lee, J., Verma, S., Huang, D.B., Huynh, K., Chang, M., Ponomarenko, J.V., Sun, S.C., Benedict, C.A.*, et al.* (2011). The specificity of innate immune responses is enforced by repression of interferon response elements by NF-kappaB p50. Sci Signal *4*, ra11.

Chiu, Y.H., Macmillan, J.B., and Chen, Z.J. (2009). RNA polymerase III detects cytosolic DNA and induces type I interferons through the RIG-I pathway. Cell *138*, 576-591.

Chong, K.T., Gresser, I., and Mims, C.A. (1983). Interferon as a defence mechanism in mouse cytomegalovirus infection. J Gen Virol *64 (Pt 2)*, 461-464.

Clausen, B.E., Burkhardt, C., Reith, W., Renkawitz, R., and Forster, I. (1999). Conditional gene targeting in macrophages and granulocytes using LysMcre mice. Transgenic Res *8*, 265-277.

Cliffe, L.J., Humphreys, N.E., Lane, T.E., Potten, C.S., Booth, C., and Grencis, R.K. (2005). Accelerated intestinal epithelial cell turnover: a new mechanism of parasite expulsion. Science *308*, 1463-1465.

Coers, J., Bernstein-Hanley, I., Grotsky, D., Parvanova, I., Howard, J.C., Taylor, G.A., Dietrich, W.F., and Starnbach, M.N. (2008). Chlamydia muridarum evades growth restriction by the IFN-gamma-inducible host resistance factor Irgb10. J Immunol *180*, 6237-6245.

Collazo, C.M., Yap, G.S., Sempowski, G.D., Lusby, K.C., Tessarollo, L., Woude, G.F., Sher, A., and Taylor, G.A. (2001). Inactivation of LRG-47 and IRG-47 reveals a family of interferon gamma-inducible genes with essential, pathogen-specific roles in resistance to infection. J Exp Med *194*, 181-188.

Colonna, M., Trinchieri, G., and Liu, Y.J. (2004). Plasmacytoid dendritic cells in immunity. Nat Immunol *5*, 1219-1226.

Creamer, B. (1967). The turnover of the epithelium of the small intestine. Br Med Bull *23*, 226-230.

Cross, M., Mangelsdorf, I., Wedel, A., and Renkawitz, R. (1988). Mouse lysozyme M gene: isolation, characterization, and expression studies. Proc Natl Acad Sci U S A *85*, 6232-6236.

Crow, M.K. (2014). Type I Interferon in the Pathogenesis of Lupus. J Immunol *192*, 5459-5468.

Crow, Y.J. (2011). Type I interferonopathies: a novel set of inborn errors of immunity. Ann N Y Acad Sci *1238*, 91-98.

Crow, Y.J., Hayward, B.E., Parmar, R., Robins, P., Leitch, A., Ali, M., Black, D.N., van Bokhoven, H., Brunner, H.G., Hamel, B.C.*, et al.* (2006a). Mutations in the gene encoding the 3'-5' DNA exonuclease TREX1 cause Aicardi-Goutieres syndrome at the AGS1 locus. Nat Genet *38*, 917-920.

Crow, Y.J., Leitch, A., Hayward, B.E., Garner, A., Parmar, R., Griffith, E., Ali, M., Semple, C., Aicardi, J., Babul-Hirji, R.*, et al.* (2006b). Mutations in genes encoding ribonuclease H2 subunits cause Aicardi-Goutieres syndrome and mimic congenital viral brain infection. Nat Genet *38*, 910-916.

David, M., Petricoin, E., 3rd, Benjamin, C., Pine, R., Weber, M.J., and Larner, A.C. (1995). Requirement for MAP kinase (ERK2) activity in interferon alpha- and interferon beta-stimulated gene expression through STAT proteins. Science *269*, 1721-1723.

Davies, L.C., Jenkins, S.J., Allen, J.E., and Taylor, P.R. (2013). Tissue-resident macrophages. Nat Immunol *14*, 986-995.

de Veer, M.J., Holko, M., Frevel, M., Walker, E., Der, S., Paranjape, J.M., Silverman, R.H., and Williams, B.R. (2001). Functional classification of interferon-stimulated genes identified using microarrays. J Leukoc Biol *69*, 912-920.

de Weerd, N.A., and Nguyen, T. (2012). The interferons and their receptors--distribution and regulation. Immunol Cell Biol *90*, 483-491.

de Weerd, N.A., Samarajiwa, S.A., and Hertzog, P.J. (2007). Type I interferon receptors: biochemistry and biological functions. J Biol Chem *282*, 20053-20057.

Deng, Y., and Tsao, B.P. (2010). Genetic susceptibility to systemic lupus erythematosus in the genomic era. Nat Rev Rheumatol *6*, 683-692.

DeSelm, C.J., Takahata, Y., Warren, J., Chappel, J.C., Khan, T., Li, X., Liu, C., Choi, Y., Kim, Y.F., Zou, W*., et al.* (2012). IL-17 mediates estrogen-deficient osteoporosis in an Act1-dependent manner. J Cell Biochem *113*, 2895-2902.

Di Domizio, J., and Cao, W. (2013). Fueling autoimmunity: type I interferon in autoimmune diseases. Expert Rev Clin Immunol *9*, 201-210.

Diamond, G., Legarda, D., and Ryan, L.K. (2000). The innate immune response of the respiratory epithelium. Immunol Rev *173*, 27-38.

Diebold, S.S., Kaisho, T., Hemmi, H., Akira, S., and Reis e Sousa, C. (2004). Innate antiviral responses by means of TLR7-mediated recognition of single-stranded RNA. Science *303*, 1529-1531.

Dixon, L.J., Barnes, M., Tang, H., Pritchard, M.T., and Nagy, L.E. (2013). Kupffer cells in the liver. Compr Physiol *3*, 785-797.

Dor, Y., Brown, J., Martinez, O.I., and Melton, D.A. (2004). Adult pancreatic beta-cells are formed by self-duplication rather than stem-cell differentiation. Nature *429*, 41-46.

Duchateau, P.N., Movsesyan, I., Yamashita, S., Sakai, N., Hirano, K., Schoenhaus, S.A., O'Connor-Kearns, P.M., Spencer, S.J., Jaffe, R.B., Redberg, R.F*., et al.* (2000). Plasma apolipoprotein L concentrations correlate with plasma triglycerides and cholesterol levels in normolipidemic, hyperlipidemic, and diabetic subjects. J Lipid Res *41*, 1231-1236.

Duchateau, P.N., Pullinger, C.R., Orellana, R.E., Kunitake, S.T., Naya-Vigne, J., O'Connor, P.M., Malloy, M.J., and Kane, J.P. (1997). Apolipoprotein L, a new human high density lipoprotein apolipoprotein expressed by the pancreas. Identification, cloning, characterization, and plasma distribution of apolipoprotein L. J Biol Chem *272*, 25576-25582.

Durbin, J.E., Fernandez-Sesma, A., Lee, C.K., Rao, T.D., Frey, A.B., Moran, T.M., Vukmanovic, S., Garcia-Sastre, A., and Levy, D.E. (2000). Type I IFN modulates innate and specific antiviral immunity. J Immunol *164*, 4220-4228.

Dutia, B.M., Allen, D.J., Dyson, H., and Nash, A.A. (1999). Type I interferons and IRF-1 play a critical role in the control of a gammaherpesvirus infection. Virology *261*, 173-179.

Edinger, A.L., and Thompson, C.B. (2004). Death by design: apoptosis, necrosis and autophagy. Curr Opin Cell Biol *16*, 663-669.

el Marjou, F., Janssen, K.P., Chang, B.H., Li, M., Hindie, V., Chan, L., Louvard, D., Chambon, P., Metzger, D., and Robine, S. (2004). Tissue-specific and inducible Cre-mediated recombination in the gut epithelium. Genesis *39*, 186-193.

Emmert-Buck, M.R., Bonner, R.F., Smith, P.D., Chuaqui, R.F., Zhuang, Z., Goldstein, S.R., Weiss, R.A., and Liotta, L.A. (1996). Laser capture microdissection. Science *274*, 998-1001.

Essers, M.A., Offner, S., Blanco-Bose, W.E., Waibler, Z., Kalinke, U., Duchosal, M.A., and Trumpp, A. (2009). IFNalpha activates dormant haematopoietic stem cells in vivo. Nature *458*, 904-908.

Farache, J., Zigmond, E., Shakhar, G., and Jung, S. (2013). Contributions of dendritic cells and macrophages to intestinal homeostasis and immune defense. Immunol Cell Biol *91*, 232-239.

Farin, H.F., Karthaus, W.R., Kujala, P., Rakhshandehroo, M., Schwank, G., Vries, R.G., Kalkhoven, E., Nieuwenhuis, E.E., and Clevers, H. (2014). Paneth cell extrusion and release of antimicrobial products is directly controlled by immune cell-derived IFN-gamma. J Exp Med *211*, 1393-1405.

Farin, H.F., Van Es, J.H., and Clevers, H. (2012). Redundant sources of Wnt regulate intestinal stem cells and promote formation of Paneth cells. Gastroenterology *143*, 1518-1529 e1517.

Faust, N., Varas, F., Kelly, L.M., Heck, S., and Graf, T. (2000). Insertion of enhanced green fluorescent protein into the lysozyme gene creates mice with green fluorescent granulocytes and macrophages. Blood *96*, 719-726.

Feng, C.G., Collazo-Custodio, C.M., Eckhaus, M., Hieny, S., Belkaid, Y., Elkins, K., Jankovic, D., Taylor, G.A., and Sher, A. (2004). Mice deficient in LRG-47 display increased susceptibility to mycobacterial infection associated with the induction of lymphopenia. J Immunol *172*, 1163-1168.

Feng, C.G., Weksberg, D.C., Taylor, G.A., Sher, A., and Goodell, M.A. (2008a). The p47 GTPase Lrg-47 (Irgm1) links host defense and hematopoietic stem cell proliferation. Cell Stem Cell *2*, 83-89.

Feng, C.G., Zheng, L., Jankovic, D., Bafica, A., Cannons, J.L., Watford, W.T., Chaussabel, D., Hieny, S., Caspar, P., Schwartzberg, P.L.*, et al.* (2008b). The immunity-related GTPase Irgm1 promotes the expansion of activated CD4+ T cell populations by preventing interferon-gamma-induced cell death. Nat Immunol *9*, 1279-1287.

Ferrantini, M., Capone, I., and Belardelli, F. (2007). Interferon-alpha and cancer: mechanisms of action and new perspectives of clinical use. Biochimie *89*, 884-893.

Foxman, E.F., and Iwasaki, A. (2011). Genome-virome interactions: examining the role of common viral infections in complex disease. Nat Rev Microbiol *9*, 254-264.

Friedman, C.S., O'Donnell, M.A., Legarda-Addison, D., Ng, A., Cardenas, W.B., Yount, J.S., Moran, T.M., Basler, C.F., Komuro, A., Horvath, C.M.*, et al.* (2008). The tumour suppressor CYLD is a negative regulator of RIG-I-mediated antiviral response. EMBO Rep *9*, 930-936.

Fujimori, S., Gudis, K., Takahashi, Y., Seo, T., Yamada, Y., Ehara, A., Kobayashi, T., Mitsui, K., Yonezawa, M., Tanaka, S.*, et al.* (2010). Distribution of small intestinal mucosal injuries as a result of NSAID administration. Eur J Clin Invest *40*, 504-510.

Ganal, S.C., Sanos, S.L., Kallfass, C., Oberle, K., Johner, C., Kirschning, C., Lienenklaus, S., Weiss, S., Staeheli, P., Aichele, P.*, et al.* (2012). Priming of natural killer cells by nonmucosal mononuclear phagocytes requires instructive signals from commensal microbiota. Immunity *37*, 171-186.

Gibson, D.L., Ma, C., Bergstrom, K.S., Huang, J.T., Man, C., and Vallance, B.A. (2008). MyD88 signalling plays a critical role in host defence by controlling pathogen burden and promoting epithelial cell homeostasis during Citrobacter rodentium-induced colitis. Cell Microbiol *10*, 618-631.

Goh, K.C., Haque, S.J., and Williams, B.R. (1999). p38 MAP kinase is required for STAT1 serine phosphorylation and transcriptional activation induced by interferons. EMBO J *18*, 5601-5608.

Gota, C., and Calabrese, L. (2003). Induction of clinical autoimmune disease by therapeutic interferon-alpha. Autoimmunity *36*, 511-518.

Gough, D.J., Messina, N.L., Clarke, C.J., Johnstone, R.W., and Levy, D.E. (2012). Constitutive type I interferon modulates homeostatic balance through tonic signaling. Immunity *36*, 166-174.

Gough, D.J., Messina, N.L., Hii, L., Gould, J.A., Sabapathy, K., Robertson, A.P., Trapani, J.A., Levy, D.E., Hertzog, P.J., Clarke, C.J.*, et al.* (2010). Functional crosstalk between type I and II interferon through the regulated expression of STAT1. PLoS Biol *8*, e1000361.

Gracias, D.T., Stelekati, E., Hope, J.L., Boesteanu, A.C., Doering, T.A., Norton, J., Mueller, Y.M., Fraietta, J.A., Wherry, E.J., Turner, M.*, et al.* (2013). The microRNA miR-155 controls CD8(+) T cell responses by regulating interferon signaling. Nat Immunol *14*, 593-602.

Graham, R.R., Hom, G., Ortmann, W., and Behrens, T.W. (2009). Review of recent genome-wide association scans in lupus. J Intern Med *265*, 680-688.

Green, D.R., and Evan, G.I. (2002). A matter of life and death. Cancer Cell *1*, 19-30.

Gregoire, I.P., Richetta, C., Meyniel-Schicklin, L., Borel, S., Pradezynski, F., Diaz, O., Deloire, A., Azocar, O., Baguet, J., Le Breton, M.*, et al.* (2011). IRGM is a common target of RNA viruses that subvert the autophagy network. PLoS Pathog *7*, e1002422.

Gross, S., and Piwnica-Worms, D. (2005). Real-time imaging of ligand-induced IKK activation in intact cells and in living mice. Nature methods *2*, 607-614.

Grundy, J.E., Trapman, J., Allan, J.E., Shellam, G.R., and Melief, C.J. (1982). Evidence for a protective role of interferon in resistance to murine cytomegalovirus and its control by non-H-2-linked genes. Infect Immun *37*, 143-150.

Gurtler, C., and Bowie, A.G. (2013). Innate immune detection of microbial nucleic acids. Trends Microbiol *21*, 413-420.

Haegebarth, A., and Clevers, H. (2009). Wnt signaling, lgr5, and stem cells in the intestine and skin. Am J Pathol *174*, 715-721.

Haldar, A.K., Saka, H.A., Piro, A.S., Dunn, J.D., Henry, S.C., Taylor, G.A., Frickel, E.M., Valdivia, R.H., and Coers, J. (2013). IRG and GBP Host Resistance Factors Target Aberrant, "Non-self" Vacuoles Characterized by the Missing of "Self" IRGM Proteins. PLoS Pathog *9*, e1003414.

Haller, O., and Kochs, G. (2011). Human MxA protein: an interferon-induced dynamin-like GTPase with broad antiviral activity. J Interferon Cytokine Res *31*, 79-87.

Harada, H., Fujita, T., Miyamoto, M., Kimura, Y., Maruyama, M., Furia, A., Miyata, T., and Taniguchi, T. (1989). Structurally similar but functionally distinct factors, IRF-1 and IRF-2, bind to the same regulatory elements of IFN and IFN-inducible genes. Cell *58*, 729-739.

Hardy, M.P., Owczarek, C.M., Jermiin, L.S., Ejdeback, M., and Hertzog, P.J. (2004). Characterization of the type I interferon locus and identification of novel genes. Genomics *84*, 331-345.

Hata, N., Sato, M., Takaoka, A., Asagiri, M., Tanaka, N., and Taniguchi, T. (2001). Constitutive IFN-alpha/beta signal for efficient IFN-alpha/beta gene induction by virus. Biochem Biophys Res Commun *285*, 518-525.

Hayman, A.R. (2008). Tartrate-resistant acid phosphatase (TRAP) and the osteoclast/immune cell dichotomy. Autoimmunity *41*, 218-223.

Heil, F., Hemmi, H., Hochrein, H., Ampenberger, F., Kirschning, C., Akira, S., Lipford, G., Wagner, H., and Bauer, S. (2004). Species-specific recognition of single-stranded RNA via toll-like receptor 7 and 8. Science *303*, 1526-1529.

Hemmi, H., Takeuchi, O., Kawai, T., Kaisho, T., Sato, S., Sanjo, H., Matsumoto, M., Hoshino, K., Wagner, H., Takeda, K.*, et al.* (2000). A Toll-like receptor recognizes bacterial DNA. Nature *408*, 740-745.

Henry, S.C., Daniell, X., Indaram, M., Whitesides, J.F., Sempowski, G.D., Howell, D., Oliver, T., and Taylor, G.A. (2007). Impaired macrophage function underscores susceptibility to Salmonella in mice lacking Irgm1 (LRG-47). J Immunol *179*, 6963-6972.

Henry, S.C., Schmidt, E.A., Fessler, M.B., and Taylor, G.A. (2014). Palmitoylation of the Immunity Related GTPase, Irgm1: Impact on Membrane Localization and Ability to Promote Mitochondrial Fission. PLoS One *9*, e95021.

Henry, S.C., Traver, M., Daniell, X., Indaram, M., Oliver, T., and Taylor, G.A. (2010). Regulation of macrophage motility by Irgm1. J Leukoc Biol *87*, 333-343.

Honaker, Y., and Piwnica-Worms, H. (2010). Casein kinase 1 functions as both penultimate and ultimate kinase in regulating Cdc25A destruction. Oncogene *29*, 3324-3334.

Honda, K., Takaoka, A., and Taniguchi, T. (2006). Type I interferon [corrected] gene induction by the interferon regulatory factor family of transcription factors. Immunity *25*, 349-360.

Huett, A., McCarroll, S.A., Daly, M.J., and Xavier, R.J. (2009). On the level: IRGM gene function is all about expression. Autophagy *5*, 96-99.

Hunn, J.P., Koenen-Waisman, S., Papic, N., Schroeder, N., Pawlowski, N., Lange, R., Kaiser, F., Zerrahn, J., Martens, S., and Howard, J.C. (2008). Regulatory interactions between IRG resistance GTPases in the cellular response to Toxoplasma gondii. EMBO J *27*, 2495-2509.

Intemann, C.D., Thye, T., Niemann, S., Browne, E.N., Amanua Chinbuah, M., Enimil, A., Gyapong, J., Osei, I., Owusu-Dabo, E., Helm, S.*, et al.* (2009). Autophagy gene variant IRGM -261T contributes to protection from tuberculosis caused by Mycobacterium tuberculosis but not by M. africanum strains. PLoS Pathog *5*, e1000577.

Ishikawa, H., and Barber, G.N. (2008). STING is an endoplasmic reticulum adaptor that facilitates innate immune signalling. Nature *455*, 674-678.

Ito, M., Yang, Z., Andl, T., Cui, C., Kim, N., Millar, S.E., and Cotsarelis, G. (2007). Wnt-dependent de novo hair follicle regeneration in adult mouse skin after wounding. Nature *447*, 316-320.

Ivashkiv, L.B., and Donlin, L.T. (2014). Regulation of type I interferon responses. Nat Rev Immunol *14*, 36-49.

Jounai, N., Takeshita, F., Kobiyama, K., Sawano, A., Miyawaki, A., Xin, K.Q., Ishii, K.J., Kawai, T., Akira, S., Suzuki, K.*, et al.* (2007). The Atg5 Atg12 conjugate associates with innate antiviral immune responses. Proc Natl Acad Sci U S A *104*, 14050-14055.

Jung, H.H., Lee, J., Kim, J.H., Ryu, K.J., Kang, S.A., Park, C., Sung, K., Nam, D.H., Kang, W.K., Park, K.*, et al.* (2005). STAT1 and Nmi are downstream targets of Ets-1 transcription factor in MCF-7 human breast cancer cell. FEBS Lett *579*, 3941-3946.

Kamphuis, E., Junt, T., Waibler, Z., Forster, R., and Kalinke, U. (2006). Type I interferons directly regulate lymphocyte recirculation and cause transient blood lymphopenia. Blood *108*, 3253-3261.

Kawai, T., Takahashi, K., Sato, S., Coban, C., Kumar, H., Kato, H., Ishii, K.J., Takeuchi, O., and Akira, S. (2005). IPS-1, an adaptor triggering RIG-I- and Mda5-mediated type I interferon induction. Nat Immunol *6*, 981-988.

Kawashima, T., Kosaka, A., Yan, H., Guo, Z., Uchiyama, R., Fukui, R., Kaneko, D., Kumagai, Y., You, D.J., Carreras, J.*, et al.* (2013). Double-stranded RNA of intestinal commensal but not pathogenic bacteria triggers production of protective interferon-beta. Immunity *38*, 1187-1197.

Kim, C.C., Nelson, C.S., Wilson, E.B., Hou, B., DeFranco, A.L., and DeRisi, J.L. (2012). Splenic red pulp macrophages produce type I interferons as early sentinels of malaria infection but are dispensable for control. PLoS One *7*, e48126.

Kim, H., and Seed, B. (2010). The transcription factor MafB antagonizes antiviral responses by blocking recruitment of coactivators to the transcription factor IRF3. Nat Immunol *11*, 743-750.

Kim, K.A., Kakitani, M., Zhao, J., Oshima, T., Tang, T., Binnerts, M., Liu, Y., Boyle, B., Park, E., Emtage, P.*, et al.* (2005). Mitogenic influence of human R-spondin1 on the intestinal epithelium. Science *309*, 1256-1259.

Kim, T., Pazhoor, S., Bao, M., Zhang, Z., Hanabuchi, S., Facchinetti, V., Bover, L., Plumas, J., Chaperot, L., Qin, J.*, et al.* (2010). Aspartate-glutamate-alanine-histidine box motif (DEAH)/RNA helicase A helicases sense microbial DNA in human plasmacytoid dendritic cells. Proc Natl Acad Sci U S A *107*, 15181-15186.

King, K.Y., Baldridge, M.T., Weksberg, D.C., Chambers, S.M., Lukov, G.L., Wu, S., Boles, N.C., Jung, S.Y., Qin, J., Liu, D.*, et al.* (2011). Irgm1 protects hematopoietic stem cells by negative regulation of IFN signaling. Blood *118*, 1525-1533.

Kirou, K.A., and Gkrouzman, E. (2013). Anti-interferon alpha treatment in SLE. Clin Immunol *148*, 303-312.

Koerner, I., Kochs, G., Kalinke, U., Weiss, S., and Staeheli, P. (2007). Protective role of beta interferon in host defense against influenza A virus. J Virol *81*, 2025-2030.

Kreit, M., Paul, S., Knoops, L., De Cock, A., Sorgeloos, F., and Michiels, T. (2014). Inefficient type I interferon-mediated antiviral protection of primary mouse neurons is associated with the lack of apolipoprotein l9 expression. J Virol *88*, 3874-3884.

Kristiansen, H., Gad, H.H., Eskildsen-Larsen, S., Despres, P., and Hartmann, R. (2011). The oligoadenylate synthetase family: an ancient protein family with multiple antiviral activities. J Interferon Cytokine Res *31*, 41-47.

Kuhnert, F., Davis, C.R., Wang, H.T., Chu, P., Lee, M., Yuan, J., Nusse, R., and Kuo, C.J. (2004). Essential requirement for Wnt signaling in proliferation of adult small intestine and colon revealed by adenoviral expression of Dickkopf-1. Proc Natl Acad Sci U S A *101*, 266-271.

Kumagai, Y., Takeuchi, O., Kato, H., Kumar, H., Matsui, K., Morii, E., Aozasa, K., Kawai, T., and Akira, S. (2007). Alveolar macrophages are the primary interferon-alpha producer in pulmonary infection with RNA viruses. Immunity *27*, 240-252.

Laguette, N., Sobhian, B., Casartelli, N., Ringeard, M., Chable-Bessia, C., Segeral, E., Yatim, A., Emiliani, S., Schwartz, O., and Benkirane, M. (2011). SAMHD1 is the dendritic- and myeloid-cell-specific HIV-1 restriction factor counteracted by Vpx. Nature *474*, 654-657.

Lai, Y., Di Nardo, A., Nakatsuji, T., Leichtle, A., Yang, Y., Cogen, A.L., Wu, Z.R., Hooper, L.V., Schmidt, R.R., von Aulock, S.*, et al.* (2009). Commensal bacteria regulate Toll-like receptor 3-dependent inflammation after skin injury. Nat Med *15*, 1377-1382.

Lausch, E., Janecke, A., Bros, M., Trojandt, S., Alanay, Y., De Laet, C., Hubner, C.A., Meinecke, P., Nishimura, G., Matsuo, M.*, et al.* (2011). Genetic deficiency of tartrate-resistant acid phosphatase associated with skeletal dysplasia, cerebral calcifications and autoimmunity. Nat Genet *43*, 132-137.

Lee, G., White, L.S., Hurov, K.E., Stappenbeck, T.S., and Piwnica-Worms, H. (2009). Response of small intestinal epithelial cells to acute disruption of cell division through CDC25 deletion. Proc Natl Acad Sci U S A *106*, 4701-4706.

Lee, M.N., Ye, C., Villani, A.C., Raj, T., Li, W., Eisenhaure, T.M., Imboywa, S.H., Chipendo, P.I., Ran, F.A., Slowikowski, K.*, et al.* (2014). Common genetic variants modulate pathogen-sensing responses in human dendritic cells. Science *343*, 1246980.

Lei, Y., Wen, H., Yu, Y., Taxman, D.J., Zhang, L., Widman, D.G., Swanson, K.V., Wen, K.W., Damania, B., Moore, C.B.*, et al.* (2012). The mitochondrial proteins NLRX1 and TUFM form a complex that regulates type I interferon and autophagy. Immunity *36*, 933-946.

Levy, D.E., Kessler, D.S., Pine, R., Reich, N., and Darnell, J.E., Jr. (1988). Interferon-induced nuclear factors that bind a shared promoter element correlate with positive and negative transcriptional control. Genes Dev *2*, 383-393.

Liao, W., Goh, F.Y., Betts, R.J., Kemeny, D.M., Tam, J., Bay, B.H., and Wong, W.S. (2011). A novel anti-apoptotic role for apolipoprotein L2 in IFN-gamma-induced cytotoxicity in human bronchial epithelial cells. J Cell Physiol *226*, 397-406.

Lichtman, E.I., Helfgott, S.M., and Kriegel, M.A. (2012). Emerging therapies for systemic lupus erythematosus--focus on targeting interferon-alpha. Clin Immunol *143*, 210-221.

Ling, Y.M., Shaw, M.H., Ayala, C., Coppens, I., Taylor, G.A., Ferguson, D.J., and Yap, G.S. (2006). Vacuolar and plasma membrane stripping and autophagic elimination of Toxoplasma gondii in primed effector macrophages. J Exp Med *203*, 2063-2071.

Liu, B., Gulati, A.S., Cantillana, V., Henry, S.C., Schmidt, E.A., Daniell, X., Grossniklaus, E., Schoenborn, A.A., Sartor, R.B., and Taylor, G.A. (2013). Irgm1-deficient mice exhibit Paneth cell abnormalities and increased susceptibility to acute intestinal inflammation. Am J Physiol Gastrointest Liver Physiol *305*, G573-584.

Liu, Z., Lu, H., Jiang, Z., Pastuszyn, A., and Hu, C.A. (2005). Apolipoprotein l6, a novel proapoptotic Bcl-2 homology 3-only protein, induces mitochondria-mediated apoptosis in cancer cells. Mol Cancer Res *3*, 21-31.

Loo, Y.M., Fornek, J., Crochet, N., Bajwa, G., Perwitasari, O., Martinez-Sobrido, L., Akira, S., Gill, M.A., Garcia-Sastre, A., Katze, M.G.*, et al.* (2008). Distinct RIG-I and MDA5 signaling by RNA viruses in innate immunity. J Virol *82*, 335-345.

Lood, C., Gullstrand, B., Truedsson, L., Olin, A.I., Alm, G.V., Ronnblom, L., Sturfelt, G., Eloranta, M.L., and Bengtsson, A.A. (2009). C1q inhibits immune complex-induced interferon-alpha production in plasmacytoid dendritic cells: a novel link between C1q deficiency and systemic lupus erythematosus pathogenesis. Arthritis Rheum *60*, 3081-3090.

Luperchio, S.A., and Schauer, D.B. (2001). Molecular pathogenesis of Citrobacter rodentium and transmissible murine colonic hyperplasia. Microbes Infect *3*, 333-340.

MacMicking, J.D., Taylor, G.A., and McKinney, J.D. (2003). Immune control of tuberculosis by IFN-gamma-inducible LRG-47. Science *302*, 654-659.

Madison, B.B., Dunbar, L., Qiao, X.T., Braunstein, K., Braunstein, E., and Gumucio, D.L. (2002). Cis elements of the villin gene control expression in restricted domains of the vertical (crypt) and horizontal (duodenum, cecum) axes of the intestine. J Biol Chem *277*, 33275-33283.

Maher, S.G., Romero-Weaver, A.L., Scarzello, A.J., and Gamero, A.M. (2007). Interferon: cellular executioner or white knight? Curr Med Chem *14*, 1279-1289.

Mahoney, Z.X., Stappenbeck, T.S., and Miner, J.H. (2008). Laminin alpha 5 influences the architecture of the mouse small intestine mucosa. J Cell Sci *121*, 2493-2502.

Malvin, N.P., Seno, H., and Stappenbeck, T.S. (2012). Colonic epithelial response to injury requires Myd88 signaling in myeloid cells. Mucosal immunology *5*, 194-206.

Marie, I., Durbin, J.E., and Levy, D.E. (1998). Differential viral induction of distinct interferon-alpha genes by positive feedback through interferon regulatory factor-7. EMBO J *17*, 6660-6669.

Martens, S., Parvanova, I., Zerrahn, J., Griffiths, G., Schell, G., Reichmann, G., and Howard, J.C. (2005). Disruption of Toxoplasma gondii parasitophorous vacuoles by the mouse p47-resistance GTPases. PLoS Pathog *1*, e24.

Martens, S., Sabel, K., Lange, R., Uthaiah, R., Wolf, E., and Howard, J.C. (2004). Mechanisms regulating the positioning of mouse p47 resistance GTPases LRG-47 and IIGP1 on cellular membranes: retargeting to plasma membrane induced by phagocytosis. J Immunol *173*, 2594-2606.

Matsuzawa, T., Kim, B.H., Shenoy, A.R., Kamitani, S., Miyake, M., and Macmicking, J.D. (2012). IFN-gamma elicits macrophage autophagy via the p38 MAPK signaling pathway. J Immunol *189*, 813-818.

McCarroll, S.A., Huett, A., Kuballa, P., Chilewski, S.D., Landry, A., Goyette, P., Zody, M.C., Hall, J.L., Brant, S.R., Cho, J.H., *et al.* (2008). Deletion polymorphism upstream of IRGM associated with altered IRGM expression and Crohn's disease. Nat Genet *40*, 1107-1112.

Mitani, Y., Takaoka, A., Kim, S.H., Kato, Y., Yokochi, T., Tanaka, N., and Taniguchi, T. (2001). Cross talk of the interferon-alpha/beta signalling complex with gp130 for effective interleukin-6 signalling. Genes Cells *6*, 631-640.

Miyoshi, H., Ajima, R., Luo, C.T., Yamaguchi, T.P., and Stappenbeck, T.S. (2012). Wnt5a potentiates TGF-beta signaling to promote colonic crypt regeneration after tissue injury. Science *338*, 108-113.

Miyoshi, H., and Stappenbeck, T.S. (2013). In vitro expansion and genetic modification of gastrointestinal stem cells in spheroid culture. Nat Protoc *8*, 2471-2482.

Moon, C., Vandussen, K.L., Miyoshi, H., and Stappenbeck, T.S. (2013). Development of a primary mouse intestinal epithelial cell monolayer culture system to evaluate factors that modulate IgA transcytosis. Mucosal Immunol.

Muller, U., Steinhoff, U., Reis, L.F., Hemmi, S., Pavlovic, J., Zinkernagel, R.M., and Aguet, M. (1994). Functional role of type I and type II interferons in antiviral defense. Science *264*, 1918-1921.

Munks, M.W., Cho, K.S., Pinto, A.K., Sierro, S., Klenerman, P., and Hill, A.B. (2006). Four distinct patterns of memory CD8 T cell responses to chronic murine cytomegalovirus infection. J Immunol *177*, 450-458.

Neumann, G., Watanabe, T., Ito, H., Watanabe, S., Goto, H., Gao, P., Hughes, M., Perez, D.R., Donis, R., Hoffmann, E., *et al.* (1999). Generation of influenza A viruses entirely from cloned cDNAs. Proceedings of the National Academy of Sciences of the United States of America *96*, 9345-9350.

Newby, C.M., Sabin, L., and Pekosz, A. (2007). The RNA binding domain of influenza A virus NS1 protein affects secretion of tumor necrosis factor alpha, interleukin-6, and interferon in primary murine tracheal epithelial cells. J Virol *81*, 9469-9480.

Nice, T.J., Strong, D.W., McCune, B.T., Pohl, C.S., and Virgin, H.W. (2013). A single-amino-acid change in murine norovirus NS1/2 is sufficient for colonic tropism and persistence. J Virol *87*, 327-334.

O'Connell, R.M., Saha, S.K., Vaidya, S.A., Bruhn, K.W., Miranda, G.A., Zarnegar, B., Perry, A.K., Nguyen, B.O., Lane, T.F., Taniguchi, T., *et al.* (2004). Type I interferon production enhances susceptibility to Listeria monocytogenes infection. J Exp Med *200*, 437-445.

Packey, C.D., and Ciorba, M.A. (2010). Microbial influences on the small intestinal response to radiation injury. Curr Opin Gastroenterol *26*, 88-94.

Parkes, M., Barrett, J.C., Prescott, N.J., Tremelling, M., Anderson, C.A., Fisher, S.A., Roberts, R.G., Nimmo, E.R., Cummings, F.R., Soars, D.*, et al.* (2007). Sequence variants in the autophagy gene IRGM and multiple other replicating loci contribute to Crohn's disease susceptibility. Nat Genet *39*, 830-832.

Pawlotsky, J.M. (2014). New hepatitis C therapies: the toolbox, strategies, and challenges. Gastroenterology *146*, 1176-1192.

Pellettieri, J., and Sanchez Alvarado, A. (2007). Cell turnover and adult tissue homeostasis: from humans to planarians. Annu Rev Genet *41*, 83-105.

Perez-Morga, D., Vanhollebeke, B., Paturiaux-Hanocq, F., Nolan, D.P., Lins, L., Homble, F., Vanhamme, L., Tebabi, P., Pays, A., Poelvoorde, P.*, et al.* (2005). Apolipoprotein L-I promotes trypanosome lysis by forming pores in lysosomal membranes. Science *309*, 469-472.

Pestka, S., Krause, C.D., and Walter, M.R. (2004). Interferons, interferon-like cytokines, and their receptors. Immunol Rev *202*, 8-32.

Petkova, D.S., Viret, C., and Faure, M. (2012). IRGM in autophagy and viral infections. Front Immunol *3*, 426.

Pfefferle, P.I., and Renz, H. (2014). The mucosal microbiome in shaping health and disease. F1000Prime Rep *6*, 11.

Platanias, L.C. (2005). Mechanisms of type-I- and type-II-interferon-mediated signalling. Nat Rev Immunol *5*, 375-386.

Pothlichet, J., Niewold, T.B., Vitour, D., Solhonne, B., Crow, M.K., and Si-Tahar, M. (2011). A loss-of-function variant of the antiviral molecule MAVS is associated with a subset of systemic lupus patients. EMBO Mol Med *3*, 142-152.

Potten, C.S. (1998). Stem cells in gastrointestinal epithelium: numbers, characteristics and death. Philos Trans R Soc Lond B Biol Sci *353*, 821-830.

Prinz, M., Schmidt, H., Mildner, A., Knobeloch, K.P., Hanisch, U.K., Raasch, J., Merkler, D., Detje, C., Gutcher, I., Mages, J.*, et al.* (2008). Distinct and nonredundant in vivo functions of IFNAR on myeloid cells limit autoimmunity in the central nervous system. Immunity *28*, 675-686.

Qiu, H., Fan, Y., Joyee, A.G., Wang, S., Han, X., Bai, H., Jiao, L., Van Rooijen, N., and Yang, X. (2008). Type I IFNs enhance susceptibility to Chlamydia muridarum lung infection by enhancing apoptosis of local macrophages. J Immunol *181*, 2092-2102.

Radtke, F., and Clevers, H. (2005). Self-renewal and cancer of the gut: two sides of a coin. Science *307*, 1904-1909.

Raff, M. (2003). Adult stem cell plasticity: fact or artifact? Annu Rev Cell Dev Biol *19*, 1-22.

Ramirez-Alcantara, V., LoGuidice, A., and Boelsterli, U.A. (2009). Protection from diclofenac-induced small intestinal injury by the JNK inhibitor SP600125 in a mouse model of NSAID-associated enteropathy. Am J Physiol Gastrointest Liver Physiol *297*, G990-998.

Rayamajhi, M., Humann, J., Kearney, S., Hill, K.K., and Lenz, L.L. (2010a). Antagonistic crosstalk between type I and II interferons and increased host susceptibility to bacterial infections. Virulence *1*, 418-422.

Rayamajhi, M., Humann, J., Penheiter, K., Andreasen, K., and Lenz, L.L. (2010b). Induction of IFN-alphabeta enables Listeria monocytogenes to suppress macrophage activation by IFN-gamma. J Exp Med *207*, 327-337.

Reed, J.C. (1999). Dysregulation of apoptosis in cancer. J Clin Oncol *17*, 2941-2953.

Reya, T., and Clevers, H. (2005). Wnt signalling in stem cells and cancer. Nature *434*, 843-850.

Rice, G., Newman, W.G., Dean, J., Patrick, T., Parmar, R., Flintoff, K., Robins, P., Harvey, S., Hollis, T., O'Hara, A.*, et al.* (2007). Heterozygous mutations in TREX1 cause familial chilblain lupus and dominant Aicardi-Goutieres syndrome. Am J Hum Genet *80*, 811-815.

Rice, G.I., Bond, J., Asipu, A., Brunette, R.L., Manfield, I.W., Carr, I.M., Fuller, J.C., Jackson, R.M., Lamb, T., Briggs, T.A.*, et al.* (2009). Mutations involved in Aicardi-Goutieres syndrome implicate SAMHD1 as regulator of the innate immune response. Nat Genet *41*, 829-832.

Rice, G.I., Del Toro Duany, Y., Jenkinson, E.M., Forte, G.M., Anderson, B.H., Ariaudo, G., Bader-Meunier, B., Baildam, E.M., Battini, R., Beresford, M.W.*, et al.* (2014a). Gain-of-function mutations in IFIH1 cause a spectrum of human disease phenotypes associated with upregulated type I interferon signaling. Nat Genet *46*, 503-509.

Rice, G.I., Del Toro Duany, Y., Jenkinson, E.M., Forte, G.M., Anderson, B.H., Ariaudo, G., Bader-Meunier, B., Baildam, E.M., Battini, R., Beresford, M.W.*, et al.* (2014b). Gain-of-function mutations in IFIH1 cause a spectrum of human disease phenotypes associated with upregulated type I interferon signaling. Nat Genet.

Rice, G.I., Kasher, P.R., Forte, G.M., Mannion, N.M., Greenwood, S.M., Szynkiewicz, M., Dickerson, J.E., Bhaskar, S.S., Zampini, M., Briggs, T.A.*, et al.* (2012). Mutations in ADAR1 cause Aicardi-Goutieres syndrome associated with a type I interferon signature. Nat Genet *44*, 1243-1248.

Richards, K.H., and Macdonald, A. (2011). Putting the brakes on the anti-viral response: negative regulators of type I interferon (IFN) production. Microbes Infect *13*, 291-302.

Rijke, R.P., Plaisier, H., Hoogeveen, A.T., Lamerton, L.F., and Galjaard, H. (1975). The effect of continuous irradiation on cell proliferation and maturation in small intestinal epithelium. Cell Tissue Kinet *8*, 441-453.

Robinson, T., Kariuki, S.N., Franek, B.S., Kumabe, M., Kumar, A.A., Badaracco, M., Mikolaitis, R.A., Guerrero, G., Utset, T.O., Drevlow, B.E.*, et al.* (2011). Autoimmune disease risk variant of

IFIH1 is associated with increased sensitivity to IFN-alpha and serologic autoimmunity in lupus patients. J Immunol *187*, 1298-1303.

Rubinfeld, H., and Seger, R. (2005). The ERK cascade: a prototype of MAPK signaling. Mol Biotechnol *31*, 151-174.

Rusinova, I., Forster, S., Yu, S., Kannan, A., Masse, M., Cumming, H., Chapman, R., and Hertzog, P.J. (2013). Interferome v2.0: an updated database of annotated interferon-regulated genes. Nucleic Acids Res *41*, D1040-1046.

Santer, D.M., Hall, B.E., George, T.C., Tangsombatvisit, S., Liu, C.L., Arkwright, P.D., and Elkon, K.B. (2010). C1q deficiency leads to the defective suppression of IFN-alpha in response to nucleoprotein containing immune complexes. J Immunol *185*, 4738-4749.

Santiago, H.C., Feng, C.G., Bafica, A., Roffe, E., Arantes, R.M., Cheever, A., Taylor, G., Vieira, L.Q., Aliberti, J., Gazzinelli, R.T.*, et al.* (2005). Mice deficient in LRG-47 display enhanced susceptibility to Trypanosoma cruzi infection associated with defective hemopoiesis and intracellular control of parasite growth. J Immunol *175*, 8165-8172.

Sarasin-Filipowicz, M., Wang, X., Yan, M., Duong, F.H., Poli, V., Hilton, D.J., Zhang, D.E., and Heim, M.H. (2009). Alpha interferon induces long-lasting refractoriness of JAK-STAT signaling in the mouse liver through induction of USP18/UBP43. Mol Cell Biol *29*, 4841-4851.

Sato, T., Onai, N., Yoshihara, H., Arai, F., Suda, T., and Ohteki, T. (2009). Interferon regulatory factor-2 protects quiescent hematopoietic stem cells from type I interferon-dependent exhaustion. Nat Med *15*, 696-700.

Scales, B.S., and Huffnagle, G.B. (2013). The microbiome in wound repair and tissue fibrosis. J Pathol *229*, 323-331.

Schoggins, J.W., and Rice, C.M. (2011). Interferon-stimulated genes and their antiviral effector functions. Curr Opin Virol *1*, 519-525.

Seno, H., Miyoshi, H., Brown, S.L., Geske, M.J., Colonna, M., and Stappenbeck, T.S. (2009). Efficient colonic mucosal wound repair requires Trem2 signaling. Proc Natl Acad Sci U S A *106*, 256-261.

Seth, R.B., Sun, L., Ea, C.K., and Chen, Z.J. (2005). Identification and characterization of MAVS, a mitochondrial antiviral signaling protein that activates NF-kappaB and IRF 3. Cell *122*, 669-682.

Sharpless, N.E., and DePinho, R.A. (2004). Telomeres, stem cells, senescence, and cancer. J Clin Invest *113*, 160-168.

Shaul, Y.D., and Seger, R. (2007). The MEK/ERK cascade: from signaling specificity to diverse functions. Biochim Biophys Acta *1773*, 1213-1226.

Shenoy, A.R., Kim, B.H., Choi, H.P., Matsuzawa, T., Tiwari, S., and MacMicking, J.D. (2007). Emerging themes in IFN-gamma-induced macrophage immunity by the p47 and p65 GTPase families. Immunobiology *212*, 771-784.

Shin, K., Fogg, V.C., and Margolis, B. (2006). Tight junctions and cell polarity. Annu Rev Cell Dev Biol *22*, 207-235.

Shinohara, M.L., Lu, L., Bu, J., Werneck, M.B., Kobayashi, K.S., Glimcher, L.H., and Cantor, H. (2006). Osteopontin expression is essential for interferon-alpha production by plasmacytoid dendritic cells. Nat Immunol *7*, 498-506.

Singh, S.B., Davis, A.S., Taylor, G.A., and Deretic, V. (2006). Human IRGM induces autophagy to eliminate intracellular mycobacteria. Science *313*, 1438-1441.

Singh, S.B., Ornatowski, W., Vergne, I., Naylor, J., Delgado, M., Roberts, E., Ponpuak, M., Master, S., Pilli, M., White, E.*, et al.* (2010). Human IRGM regulates autophagy and cell-autonomous immunity functions through mitochondria. Nat Cell Biol *12*, 1154-1165.

Smith, E.E., and Malik, H.S. (2009). The apolipoprotein L family of programmed cell death and immunity genes rapidly evolved in primates at discrete sites of host-pathogen interactions. Genome Res *19*, 850-858.

Springer, H.M., Schramm, M., Taylor, G.A., and Howard, J.C. (2013). Irgm1 (LRG-47), a Regulator of Cell-Autonomous Immunity, Does Not Localize to Mycobacterial or Listerial Phagosomes in IFN-gamma-Induced Mouse Cells. J Immunol *191*, 1765-1774.

Stanley, S.A., Johndrow, J.E., Manzanillo, P., and Cox, J.S. (2007). The Type I IFN response to infection with Mycobacterium tuberculosis requires ESX-1-mediated secretion and contributes to pathogenesis. J Immunol *178*, 3143-3152.

Stetson, D.B., Ko, J.S., Heidmann, T., and Medzhitov, R. (2008). Trex1 prevents cell-intrinsic initiation of autoimmunity. Cell *134*, 587-598.

Stetson, D.B., and Medzhitov, R. (2006). Type I interferons in host defense. Immunity *25*, 373-381.

Sun, L., Wu, J., Du, F., Chen, X., and Chen, Z.J. (2013). Cyclic GMP-AMP synthase is a cytosolic DNA sensor that activates the type I interferon pathway. Science *339*, 786-791.

Tanaka, N., Sato, M., Lamphier, M.S., Nozawa, H., Oda, E., Noguchi, S., Schreiber, R.D., Tsujimoto, Y., and Taniguchi, T. (1998). Type I interferons are essential mediators of apoptotic death in virally infected cells. Genes Cells *3*, 29-37.

Tanaka, Y., and Chen, Z.J. (2012). STING specifies IRF3 phosphorylation by TBK1 in the cytosolic DNA signaling pathway. Sci Signal *5*, ra20.

Taniguchi, T., and Takaoka, A. (2001). A weak signal for strong responses: interferon-alpha/beta revisited. Nat Rev Mol Cell Biol *2*, 378-386.

Taub, R. (2004). Liver regeneration: from myth to mechanism. Nat Rev Mol Cell Biol *5*, 836-847.

Thackray, L.B., Duan, E., Lazear, H.M., Kambal, A., Schreiber, R.D., Diamond, M.S., and Virgin, H.W. (2012). Critical role for interferon regulatory factor 3 (IRF-3) and IRF-7 in type I interferon-mediated control of murine norovirus replication. J Virol *86*, 13515-13523.

Thomas, C., Moraga, I., Levin, D., Krutzik, P.O., Podoplelova, Y., Trejo, A., Lee, C., Yarden, G., Vleck, S.E., Glenn, J.S.*, et al.* (2011). Structural linkage between ligand discrimination and receptor activation by type I interferons. Cell *146*, 621-632.

Tibbetts, S.A., Loh, J., Van Berkel, V., McClellan, J.S., Jacoby, M.A., Kapadia, S.B., Speck, S.H., and Virgin, H.W.t. (2003). Establishment and maintenance of gammaherpesvirus latency are independent of infective dose and route of infection. J Virol *77*, 7696-7701.

Tiwari, S., Choi, H.P., Matsuzawa, T., Pypaert, M., and MacMicking, J.D. (2009). Targeting of the GTPase Irgm1 to the phagosomal membrane via PtdIns(3,4)P(2) and PtdIns(3,4,5)P(3) promotes immunity to mycobacteria. Nat Immunol *10*, 907-917.

Uddin, S., Yenush, L., Sun, X.J., Sweet, M.E., White, M.F., and Platanias, L.C. (1995). Interferon-alpha engages the insulin receptor substrate-1 to associate with the phosphatidylinositol 3'-kinase. J Biol Chem *270*, 15938-15941.

Unterholzner, L., Keating, S.E., Baran, M., Horan, K.A., Jensen, S.B., Sharma, S., Sirois, C.M., Jin, T., Latz, E., Xiao, T.S.*, et al.* (2010). IFI16 is an innate immune sensor for intracellular DNA. Nat Immunol *11*, 997-1004.

Van Rooijen, N., and Sanders, A. (1994). Liposome mediated depletion of macrophages: mechanism of action, preparation of liposomes and applications. J Immunol Methods *174*, 83-93.

Vanhamme, L., Paturiaux-Hanocq, F., Poelvoorde, P., Nolan, D.P., Lins, L., Van Den Abbeele, J., Pays, A., Tebabi, P., Van Xong, H., Jacquet, A.*, et al.* (2003). Apolipoprotein L-I is the trypanosome lytic factor of human serum. Nature *422*, 83-87.

Vanhollebeke, B., and Pays, E. (2006). The function of apolipoproteins L. Cell Mol Life Sci *63*, 1937-1944.

Verweij, C.L., and Vosslamber, S. (2013). Relevance of the type I interferon signature in multiple sclerosis towards a personalized medicine approach for interferon-beta therapy. Discov Med *15*, 51-60.

Virgin, H.W. (2014). The virome in Mammalian physiology and disease. Cell *157*, 142-150.

Virgin, H.W., Wherry, E.J., and Ahmed, R. (2009). Redefining chronic viral infection. Cell *138*, 30-50.

Wan, G., Zhaorigetu, S., Liu, Z., Kaini, R., Jiang, Z., and Hu, C.A. (2008). Apolipoprotein L1, a novel Bcl-2 homology domain 3-only lipid-binding protein, induces autophagic cell death. J Biol Chem *283*, 21540-21549.

Wu, D., Lamm, A.T., and Fire, A.Z. (2011). Competition between ADAR and RNAi pathways for an extensive class of RNA targets. Nat Struct Mol Biol *18*, 1094-1101.

Wu, J., Sun, L., Chen, X., Du, F., Shi, H., Chen, C., and Chen, Z.J. (2013). Cyclic GMP-AMP is an endogenous second messenger in innate immune signaling by cytosolic DNA. Science *339*, 826-830.

Xu, H., Wu, Z.Y., Fang, F., Guo, L., Chen, D., Chen, J.X., Stern, D., Taylor, G.A., Jiang, H., and Yan, S.S. Genetic deficiency of Irgm1 (LRG-47) suppresses induction of experimental autoimmune encephalomyelitis by promoting apoptosis of activated CD4+ T cells. Faseb J *24*, 1583-1592.

Yamamoto, M., Sato, S., Mori, K., Hoshino, K., Takeuchi, O., Takeda, K., and Akira, S. (2002). Cutting edge: a novel Toll/IL-1 receptor domain-containing adapter that preferentially activates the IFN-beta promoter in the Toll-like receptor signaling. J Immunol *169*, 6668-6672.

Yang, C.H., Murti, A., Valentine, W.J., Du, Z., and Pfeffer, L.M. (2005). Interferon alpha activates NF-kappaB in JAK1-deficient cells through a TYK2-dependent pathway. J Biol Chem *280*, 25849-25853.

Yang, Y.G., Lindahl, T., and Barnes, D.E. (2007). Trex1 exonuclease degrades ssDNA to prevent chronic checkpoint activation and autoimmune disease. Cell *131*, 873-886.

Yasukawa, K., Oshiumi, H., Takeda, M., Ishihara, N., Yanagi, Y., Seya, T., Kawabata, S., and Koshiba, T. (2009). Mitofusin 2 inhibits mitochondrial antiviral signaling. Sci Signal *2*, ra47.

Yoshimura, A., Naka, T., and Kubo, M. (2007). SOCS proteins, cytokine signalling and immune regulation. Nat Rev Immunol *7*, 454-465.

Zhang, W., and Liu, H.T. (2002). MAPK signal pathways in the regulation of cell proliferation in mammalian cells. Cell Res *12*, 9-18.

Zhang, Z., Yuan, B., Bao, M., Lu, N., Kim, T., and Liu, Y.J. (2011). The helicase DDX41 senses intracellular DNA mediated by the adaptor STING in dendritic cells. Nat Immunol *12*, 959-965.

Zhao, Y.O., Konen-Waisman, S., Taylor, G.A., Martens, S., and Howard, J.C. (2010). Localisation and mislocalisation of the interferon-inducible immunity-related GTPase, Irgm1 (LRG-47) in mouse cells. PLoS One *5*, e8648.

Zhao, Y.O., Rohde, C., Lilue, J.T., Konen-Waisman, S., Khaminets, A., Hunn, J.P., and Howard, J.C. (2009). Toxoplasma gondii and the Immunity-Related GTPase (IRG) resistance system in mice: a review. Mem Inst Oswaldo Cruz *104*, 234-240.

Zhou, X.J., Lu, X.L., Lv, J.C., Yang, H.Z., Qin, L.X., Zhao, M.H., Su, Y., Li, Z.G., and Zhang, H. (2011). Genetic association of PRDM1-ATG5 intergenic region and autophagy with systemic lupus erythematosus in a Chinese population. Ann Rheum Dis *70*, 1330-1337.